THE REGULATION OF YEAST HOMOTYPIC VACUOLE FUSION BY PHOSPHATIDIC ACID AND DIACYLGLYCEROL

BY

MATTHEW STARR

DISSERTATION

Submitted in partial fulfillment of the requirements
for the degree of Doctor of Philosophy in Biochemistry
in the Graduate College of the
University of Illinois at Urbana-Champaign, 2018

Urbana, Illinois

Doctoral Committee:

Associate Professor Rutilio Fratti, Chair
Professor Robert Gennis
Assistant Professor Hong Jin
Assistant Professor Kai Zhang

ABSTRACT

Eukaryotic membrane fusion is a highly conserved process that is necessary to maintain cellular homeostasis. Ultimately, two membrane compartments are brought to each other, direct contact is established, and the bilayers and lumenal contents mix. In *Saccharomyces cerevisiae*, homotypic vacuole fusion occurs through a series of well-defined phases. SNAREs are activated by their co-chaperones Sec18 (mammalian NSF) and Sec17 (mammalian α-SNAP) in an ATP dependent priming stage. Tethering first brings two fusing compartments into contact with each other via interactions between the Rab GTPase Ypt7 and its effector HOPS complex. Once tethered, compartments are pulled into tight contact with each other through the formation of *trans*-SNARE complexes during a docking stage. The final fusion stage proceeds through a hemifusion intermediate to pore formation and lumenal content mixing.

The roles of proteins that carry out membrane fusion stages are well established, however the roles regulatory lipids at the membrane play are still unclear. Many specific regulatory lipids localize to the site of fusing vacuoles termed the "vertex ring" implying an important role for them throughout the fusion process. It has been shown that the minimal membrane lipid content necessary for fusion to occur includes ergosterol, phosphatidic acid (PA), diacylglycerol (DAG), and phosphoinositides. However, the interactions and effects each of these lipids has throughout the stages of membrane fusion has not been elucidated. This project aimed to identify specific regulatory roles for the lipids PA and DAG. Previous work identified the interconversion of the two lipids by the DAG kinase Dgk1 and PA phosphatase Pah1 may be important for vacuole fusion to effectively occur.

Pah1 conversion of PA to DAG was shown to be necessary for SNARE priming activity and localization of key protein factors. We found that Sec18, the SNARE chaperone that carries out priming, is a PA binding protein. Addition of a PA-specific binding domain blocked this binding and displaced Sec18 from vacuolar membranes. Furthermore, exogenous PA addition blocked Sec18 priming activity similarly to chemical inhibition of Pah1. Vacuoles lacking Pah1 showed decreased recruitment of Sec18 to inactive SNAREs. This recruitment defect was reversible upon the introduction of Pah1 by complementation or exogenous addition. Taken together, our data suggest a direct role for the regulation of SNARE priming at the vacuole by membrane PA.

We further investigated the effects PA has on Sec18 protein conformation by looking at effects on the protein's structure during binding. We found that PA induced a conformation change in Sec18 protomers, but active hexameric Sec18 does not readily bind PA. Sec18 binding to PA resulted in different protein interactions with 1,8 ANS and different limited proteolysis profiles suggesting changes in protein conformation. No significant changes in secondary structure were determined by circular dichroism and no shifts in intrinsic tryptophan fluorescence of Sec18 were observed in the presence of PA. Molecular dynamic simulations predicted that significant protomer conformation changes occur between the monomeric and hexameric forms of Sec18. Furthermore, simulations predicted that PA binds to Sec18 at the protein's hexamer interface. Together, our data suggest that PA may regulate Sec18 function by stabilizing its inactive monomeric form preventing formation of an active hexamer.

At the endoplasmic reticulum, Dgk1 and Pah1 have been shown to direct oppose each other in the interconversion of DAG and PA. We deleted *DGK1* and observed no reversal of vacuolar morphology from *pah1*Δ cells indicating the two enzymes do not directly offset each other at the vacuole. However, vacuoles from *dgk1*Δ cells did show enhanced fusion. This elevated fusion was attributed to an increase in the fusogenic lipid DAG at the vacuole. These vacuoles also had an increased resistance to inhibitors of the Rab GTPase Ypt7. Taken together, our results suggest a role for Dgk1 in regulating vacuole fusion by reducing membrane DAG levels and altering Ypt7 activity.

Dedicated to those who have served as great inspiration for me throughout my life.

For Lieschen, Barbara, Max, and the rest of my family

ACKNOWLEDGMENTS

Graduate school has been less of an experience and more of a lifestyle. This work is the product of many years of work which has been supported by many people. I first must thank my parents, Lieschen and Terry, for always being supportive and loving and for promoting education from the time I was very young. It was their ongoing nurturing of my curiosity that ultimately led me to continuously want to learn. My sister, Allison, has also played a part in this and has always been a role model for me to look up to.

I came to UIUC for multiple reasons, but one of the most important was so that I could work with Dr. Rutilio Fratti. My main goal coming to graduate school was to learn independently, and Rudy has always allowed me to do that. His guidance has always been valuable, and the freedom he has given me to explore interesting questions that seem random has fueled my scientific curiosity. I also thank all the committee members I've had. Drs. Gennis, Jin, Zhang, and Morrissey have provided me with valuable feedback throughout this process. I would also like to thank my past and current labmates including Surya Karunakaran, Terry Sasser, Greg Miner, Logan Hurst, Robert Sparks, and Ez Ellis. Through training, scientific conversations, and collaboration each has greatly helped me with my work.

The person I must thank more than anyone is my partner in everything, Natalie. Not only has she provided me relief from the stresses that come with graduate work, but she's been the steady foundation in both our lives since I came to Illinois. Natalie has been such a positive presence. I could never accurately express how valuable her love and support have been during this time.

TABLE OF CONTENTS

CHAPTER 1: INTRODUCTION

Eukaryotic membrane fusion is of key importance in maintaining cellular homeostasis. Cargo is specifically trafficked between organelles and the plasma membrane through the creation, movement, and fusion of transport vesicles. This process is carried out through a series of highly conserved events utilizing mechanisms that are found in all eukaryotes (Jahn and Südhof, 1999). Because of this conservation, vacuoles from *Saccharomyces cerevisiae*, organelles similar to mammalian lysosomes, serve as an ideal model for studying the mechanisms and regulation of membrane fusion. The stages of homotypic vacuole fusion are experimentally well defined and the core protein machinery necessary for the process is well known. However, the roles of key regulatory players in the process including membrane lipids remain largely underappreciated. This dissertation examines the regulatory roles of lipids during the process of yeast homotypic vacuole fusion. In this chapter, I introduce the process of membrane fusion and provide an overview of the known lipid regulation of the yeast vacuole fusion process.

The stages of homotypic vacuole fusion

Yeast vacuole fusion occurs in a series of stages that are previously well described. The process begins with a priming stage in which previously used SNAREs (soluble N-ethylmaleimide-sensitive factor attachment protein receptors) are activated in an ATP dependent process. SNAREs in complex on the same membrane (cis) are recognized by the AAA+ ATPase Sec18 and its co-chaperone Sec17. Upon ATP hydrolysis by Sec18, Sec17 and the soluble SNARE Vam7 are released from the membrane and the previously inactive SNAREs are able to participate in future rounds of fusion (Mayer et al., 1996; Boeddinghaus et al., 2002). During the next tethering stage,

membranes from separate vacuoles are connected through interactions between the Rab GTPase Ypt7 and its effector complex HOPS (homotypic fusion and vacuole protein sorting complex) (Mayer and Wickner, 1997; Seals et al., 2000). Here Vam7 associates with the vacuolar membrane through interactions with HOPS and the lipid phosphatidylinositol 3-phosphate (PI3P) (Boeddinghaus et al., 2002). SNARE complexes including one R-SNARE and three Q-SNAREs from apposing membranes form a stable complex that brings the two vacuoles in close contact (Ungermann et al., 1998). During this docking stage, the two membranes are enriched in regulatory lipids and proteins at the edge of their interface, the "vertex ring" (Fratti et al., 2004; Wang et al., 2002, 2003b). The cascade then enters the fusion stage in which the outer leaflets of the membrane bilayers mix to form a hemifusion intermediate (Jahn et al., 2003). The fusion stage ends with pore formation between the hemifused compartments and luminal content mixing (Reese and Mayer, 2005).

Lipids in membrane trafficking

Regulatory lipids serve an important role in various membrane trafficking pathways. Functions have been described in cargo sorting, membrane budding, membrane fission, actin organization, membrane transport via cytoskeletal elements, and membrane fusion (Wang et al., 2007; Ford et al., 2002; Jost et al., 1998; Karunakaran et al., 2012; Hokanson et al., 2006; Boeddinghaus et al., 2002; Fratti et al., 2004; Kato and Wickner, 2001; Mayer et al., 2000). In many of these pathways, lipids such as phosphoinositides and diacylglycerol (DAG) promote association of necessary protein factors with the membrane. Elsewhere in the cell, phosphatidic acid (PA) is required for Glut4 trafficking and mitochondrial fusion and in yeast membrane fusion during spore formation (Vicogne et al., 2006; Nakanishi et al., 2006; Choi et al., 2006; Liu et al., 2007). Both PA and

phosphoinositides promote fusion in PC12 cells (James et al., 2008). In higher eukaryotes, cholesterol has been shown to mediate SNARE protein conformation and affect the organization of the SNAREs syntaxin and SNAP-23 in biological membranes (Chang et al., 2009; Predescu et al., 2005). Because these lipids are essential for processes throughout the stages of fusion across multiple processes in eukaryotic cells, it is of critical importance to understand how they influence the other necessary factors facilitating these processes.

Lipid requirements for vacuole fusion

It was originally suggested that membrane fusion was completely catalyzed by protein factors and that membranes served no purpose beyond providing a structural scaffold. Many more recent studies have shown that the presence of specific lipids at the site of fusion are in fact necessary for the process to occur. Specific lipid requirements for fusion may differ between organelles within a cell. For optimal vacuole fusion to occur the lipids PI3P, phosphatidylinositol 4,5-bisphosphate ($PI(4,5)P_2$), ergosterol, and DAG must be present in the membrane (Fratti et al., 2004; Mayer et al., 2000; Kato and Wickner, 2001; Seeley, 2002). Addition of $PI(4,5)P_2$ ligand or phosphatase to vacuoles significantly inhibited fusion (Fratti et al., 2004; Mayer et al., 2000; Collins and Wickner, 2007). PI3P ligand and phosphatase had a similar inhibitory effect on fusion, and PI3P is known to specifically bind the PX domain of the SNARE Vam7 (Fratti et al., 2004; Collins and Wickner, 2007; Cheever et al., 2001). Ergosterol extraction from vacuoles and supplementation of the lipid both affected fusion, and later the ergosterol ligand filipin was shown to inhibit fusion (Kato and Wickner, 2001; Fratti et al., 2004). DAG is a known fusogenic lipid whose ligand also significantly inhibited vacuole fusion (Villar et al., 2000; Fratti et al., 2004). Later studies using reconstituted proteoliposomes (RPLs) and purified vacuolar protein components showed that PA and

phosphatidylethanolamine (PE) are also required for vacuole fusion to occur (Mima et al., 2008; Mima and Wickner, 2009). The minimum lipid requirements for fusion of RPLs include phosphatidylcholine (PC), PE, PA, and PI3P (Mima and Wickner, 2009). PA is necessary for full association of HOPS and Sec18 to RPL membranes, and both PA and PE are required for SNARE complex assembly (Mima and Wickner, 2009). Removing DAG, ergosterol, PI3P, or PI(4,5)P_2 from RPLs also significantly reduced their capacity for fusion confirming each as a requirement for optimal fusion to occur (Mima et al., 2008). Later work using RPLs found neutral lipids that promote non-bilayer structure formation, including DAG, PE, and ergosterol, are also a requirement for vacuole fusion to occur (Zick et al., 2014).

Fusion effects of other lipids at the vacuole

While not considered necessary for vacuole fusion to occur, other lipids found at the organelle have been shown to have potential effects on fusion. For example, addition of phosphatidylinositol 4-phosphate (PI4P) ligand to *in vitro* vacuole assays has been shown to inhibit *trans*-SNARE complex formation (Collins and Wickner, 2007). Additionally, vacuole fusion and fission processes are closely linked to the synthesis and turnover of the vacuole marker lipid phosphatidylinositol (3,5) bisphosphate (PI(3,5)P_2) (Dove et al., 1997; Bonangelino et al., 1997, 2002; Rudge et al., 2004). This regulation of the fusion and fission of vacuoles is likely tied to PI(3,5)P_2 levels directing calcium release from the vacuole lumen (Dong et al., 2010). Cardiolipin was once considered a vacuole membrane component and key lipid regulator of fusion (Zinser et al., 1991; Schneiter et al., 1999; Mima et al., 2008; Mima and Wickner, 2009). However, cardiolipin is only made in mitochondria and later work using RPLs showed it is not necessary for fusion if the tethering protein Ypt7 is present (Stroupe et al., 2009). Its inclusion in the original

vacuole lipid composition may have been due to mitochondrial contamination in vacuole isolations or from mitophagy (Wickner, 2010).

Roles of lipids in vacuole fusion

Different regulatory lipids have functions specific to the different stages of vacuole fusion. Ergosterol, PI(4,5)P_2, and PA all influence the early priming stage of the fusion cascade (Mayer et al., 2000; Kato and Wickner, 2001;see Chapter 2). PI(4,5)P_2 has also been shown to stimulate fusion of RPLs when in the presence of Sec17 and Sec18 (Xu and Wickner, 2010). During tethering and docking, PI3P serves an important role in protein factor recruitment to the membrane (Boeddinghaus et al., 2002; Cabrera et al., 2014). Interestingly, PI3P has been shown to have different functions on apposed membranes both facilitating formation of a 3Q-SNARE complex on one and promoting tethering on the other via the Vam7 PX domain (Xu and Wickner, 2010). Experiments using RPLs have shown that acidic lipids such as phosphatidylinositol and PA also assist in vacuole tethering likely through associations with the HOPS complex (Orr et al., 2015).

The lipids that help catalyze the different stages of vacuole fusion are produced and modified by a suite of enzymes that localize to biological membranes. The fusogenic lipid DAG is generated by phospholipase C activity on PI(4,5)P_2 or dephosphorylation of PA by PA phosphatases and is found at the membrane interface before the fusion stage occurs (Jun et al., 2004; Han et al., 2004, 2006; Toke et al., 1998; Fratti et al., 2004). DAG can then be converted back to PA by the CTP-dependent DAG kinase Dgk1 (Han et al., 2008a; b). Additional lipid production and turnover during vacuole fusion has been shown for PI3P, PI4P, PI(3,5)P_2, and PI(4,5)P_2 (Mayer et al., 2000; Thorngren et al., 2004). The cyclic nature of specific lipids present at the different stages of

vacuole fusion suggests they may help direct the progression of the fusion cascade from one stage to another in a regulated manner.

Regulatory Lipids at the Vertex Ring

The requirement for specific lipids throughout the vacuole fusion cascade is additionally inferred by their presence at the site of fusion. When vacuoles come into contact with each other prior to fusion, they do so with the two compartments drawn together at an interface rather than at a single point. This interface, termed the boundary membrane, resembles flattened discs and at its edge is a microdomain environment known as the "vertex ring" (Wang et al., 2002). It is at the vertex ring that vacuole fusion factors become enriched prior to vacuole fusion. Specifically, the Rab GTPase Ypt7 initiates formation of the vertex ring and in concert with the disassembly of F-actin directs the localization of SNAREs and the HOPS complex (Wang et al., 2003b). Importantly, it is not only protein factors that make up the components of the vertex ring. Additionally, many of the regulatory lipids previously mentioned have been shown to localize to the vertex ring during vacuole docking (Fratti et al., 2004). These include DAG, ergosterol, PI(4,5)P_2, and PI3P. DAG is also enriched at the boundary membrane prior to fusion. The localization of these lipid and protein factors at the site of fusion occurs in an interdependent manner. Addition of inhibitory levels of lipid ligands including those for PI3P, PI(4,5)P_2, ergosterol, and DAG results in a redistribution of lipids at the vertex ring. In the same inhibitory conditions, necessary fusion proteins including Ypt7, the HOPS protein Vps33, and vacuolar SNAREs do not enrich at the vertex ring. Together this shows that the proteins and lipids that carry out vacuole fusion work in concert with each other to properly assemble and carry out their functions. Later work showed that deletion of the PA phosphatase Pah1 also decreases the enrichment of PI3P at the vertex ring (Sasser et al., 2012).

Inhibition of Pah1 activity also affects localization of Ypt7. Together these results pointed to a role for PA or DAG in affecting the localization of other fusion factors at the vacuole vertex ring. Additional studies found a link between PI3P enrichment at the vertex and actin polymerization (discussed below) providing more evidence for lipid involvement in fusion microdomain assembly (Karunakaran et al., 2012; Sasser et al., 2013).

Regulation of actin dynamics by regulatory lipids at the vertex ring

While its direct function remains largely unknown actin has been clearly demonstrated to be present at the vertex ring of docked vacuoles (Eitzen et al., 2002). Vacuole fusion requires actin dynamics and turnover which are closely linked to the activity of two Rho GTPases, Cdc42 and Rho1 (Eitzen et al., 2001; Isgandarova et al., 2007; Jones et al., 2010). Cdc42 is activated early during *in vitro* fusion reactions and promotes the polymerization of actin while Rho1 is necessary for fusion but its exact role is unknown (Eitzen et al., 2001, 2002; Isgandarova et al., 2007). Activation of Rho1 has been linked to the generation of $PI(4,5)P_2$ and activation of Cdc42 requires ergosterol, both lipids that are enriched at the vacuole vertex ring (Logan et al., 2010; Jones et al., 2010; Fratti et al., 2004). In many membrane trafficking pathways actin polymerization depends on regulatory sterols, $PI(4,5)P_2$, and 3-phosphoinositides (Bohdanowicz et al., 2010; Rozelle et al., 2000). Experiments using vacuoles showed that ergosterol is necessary for actin enrichment at the vertex ring while increased $PI(4,5)P_2$ levels reduces this enrichment (Karunakaran et al., 2012). Interestingly, polymerizing actin with the ligand jasplakinolide leads to an increase in the vertex localization of $PI(4,5)P_2$. Furthermore, vertex localization of PI3P is decreased when actin is polymerized and increased when it is depolymerized (Karunakaran et al., 2012). Additional work using vacuoles lacking the ABC transporter Ycf1 further demonstrated a link between the

regulatory lipid PI3P and actin accumulation at the vertex ring (Sasser et al., 2013). Ycf1 directly interacts with the GTPase Rho1 and its activating nucleotide exchange factor Tus1 (Lee et al., 2011; Hall, 1998). It is thought that on *ycf1*Δ vacuoles Rho1 may be less active leading to a reduction in actin polymerization. Vacuoles lacking Ycf1 show a significant increase in PI3P vertex enrichment (Sasser et al., 2013). Taken together these results suggested that an intricate link exists between actin dynamics and regulatory lipid organization at the vacuole. It appears that a cycle of actin polymerization and depolymerization may influence the proper organization of vertex ring lipids which likely affects the downstream assembly of other fusion factors.

The interconversion of phosphatidic acid and diacylglycerol mediates vacuole fusion

In 2012, it was found that the PA phosphatase Pah1 plays a significant role in endosome to vacuole maturation and vacuole fusion (Sasser et al., 2012). Vacuoles lacking Pah1 show dramatically reduced fusion levels which can be restored by complementation. The role of Pah1 during fusion was first hypothesized and later shown to occur across two stages of the fusion cascade. First, inhibition of Pah1 activity showed an inhibitory effect on priming by altering the recruitment of the SNARE chaperone Sec18 to inactive *cis*-SNARES. Second, vacuoles lacking Pah1 showed a loss of key fusion factors from the membrane. This suggested that membrane PA or DAG help control SNARE activation and progression of the fusion cascade from priming to PI3P generation and vertex ring assembly. These ideas were further explored in later works and are discussed in more detail below. Work in other systems showed that deletion of the DAG kinase Dgk1 reversed phenotypes seen in *pah1*Δ cells (Han et al., 2008a). Surprisingly, deletion of Dgk1 does not reverse the fusion defect seen for *pah1*Δ vacuoles (see Chapter 4). Deletion of Dgk1 alone, however, does have an opposite effect on fusion compared to deletion of Pah1. Vacuoles lacking Dgk1 have a

marked increase in fusion levels. This is attributed to both an increase in the fusogenic lipid DAG in vacuole membranes and altered activity of the Rab Ypt7. These results suggest that PA and DAG levels at the vacuole must maintain a balance that is crucial for regulation of multiple fusion stages.

Regulation of SNARE priming by phosphatidic acid

Inhibiting the PA phosphatase Pah1 prevents the recruitment of Sec18 to *cis*-SNARE complexes without decreasing the protein's abundance at the vacuole membrane (Sasser et al., 2012). It was hypothesized that Pah1 could regulate the transition of Sec18 from a membrane lipid bound state to an active SNARE bound state. This hypothesis was supported by previous unrelated work that unexpectedly identified NSF, the Sec18 mammalian homolog, as a PA binding protein (Manifava et al., 2001). Further investigation showed that Sec18, like NSF, is a PA binding protein and that its regulation could be tied to PA levels at the vacuole (see Chapter 2). Additional experiments showed addition of exogenous short chain dioctanoyl PA (diC8-PA) potently inhibits vacuole fusion by inhibiting Sec18 priming activity. SNARE pulldown experiments confirmed an increase in PA levels prevents Sec18 from being efficiently recruited to inactive *cis*-SNARE complexes. Recent work showed PA binding to Sec18 leads to a conformation change that may influence the hexamerization of the protein controlling its enzymatic activity (see Chapter 3).

Regulation of the Ypt7 nucleotide exchange factor Mon1-Ccz1 by PI3P

Vacuoles lacking the PA phosphatase Pah1show decreased levels of the PI-3 kinase Vps34 and the Rab GTPase Ypt7 and its nucleotide exchange factor Mon1-Ccz1 (Sasser et al., 2012). The lack of Vps34 suggests that Pah1 activity could influence PI3P levels and thus microdomain

assembly at the vertex ring. Previous work in *C. elegans* showed the Mon1 orthologue SAND-1 is recruited to late endosomes in a PI3P dependent manner (Poteryaev et al., 2010). Later work in yeast revealed that Mon1 specifically associates with PI3P at the vacuole (Lawrence et al., 2014). This association is reversed by phosphorylation of Mon1 by the casein kinase Yck3. These results were consistent with previous studies that showed Mon1 is released from vacuole membranes in an ATP dependent manner (Wang et al., 2003a). Taken together these studies highlight a potential role for PA or DAG in regulating PI3P and its associated protein factors at the vertex ring of vacuole.

Modulation of SNARE function by regulatory lipids

The lipid regulation of SNAREs first occurs with their organization during docking. It has long been known that the soluble SNARE Vam7 associates with vacuole membranes through interactions between its PX domain and PI3P (Boeddinghaus et al., 2002). This assists in both the formation of active 3Q-SNARE complexes and in tethering apposed membranes (Xu and Wickner, 2010). More recently it was determined that a polybasic region of amino acids in the middle domain of Vam7 reduces the overall protein's affinity for PI3P (Miner et al., 2016). Mutating these basic amino acids to alanine increases binding of the protein to PI3P while also reducing its ability to catalyze fusion. Additional regulation of SNARE function occurs during the fusion stage and is tied to the fluidity of the lipid bilayers surrounding them. Non-canonical SNARE complexes containing the mutant Vam7^{Q283R} are unable to facilitate fusion leading to a buildup of hemifused intermediate compartments (Fratti et al., 2007; Karunakaran and Fratti, 2013). Addition of the small molecule chlorpromazine relieves the fusion inhibition of these compartments likely by increasing membrane fluidity and reducing the force requirement of membrane restructuring (Fang

and Iwasa, 2007; Karunakaran and Fratti, 2013). Similar experiments utilizing vacuoles containing a lipid anchored mutant version of the SNARE Vam3 also showed CPZ rescue of a predominantly hemifused intermediate (Karunakaran and Fratti, 2013). Together, these results showed that the fluidity of the vacuole membrane, which is dependent on its lipid composition, mediates the ability of SNAREs to catalyze fusion.

REFERENCES

Boeddinghaus, C., A.J. Merz, R. Laage, and C. Ungermann. 2002. A cycle of Vam7p release from and PtdIns 3-P-dependent rebinding to the yeast vacuole is required for homotypic vacuole fusion. *J. Cell Biol.* doi:10.1083/jcb.200112098.

Bohdanowicz, M., G. Cosío, J.M. Backer, and S. Grinstein. 2010. Class I and class III phosphoinositide 3-kinases are required for actin polymerization that propels phagosomes. *J. Cell Biol.* doi:10.1083/jcb.201004005.

Bonangelino, C.J., N.L. Catlett, and L.S. Weisman. 1997. Vac7p, a novel vacuolar protein, is required for normal vacuole inheritance and morphology. *Mol. Cell. Biol.* doi:10.1128/MCB.17.12.6847.

Bonangelino, C.J., J.J. Nau, J.E. Duex, M. Brinkman, A.E. Wurmser, J.D. Gary, S.D. Emr, and L.S. Weisman. 2002. Osmotic stress-induced increase of phosphatidylinositol 3,5-bisphosphate requires Vac14p, an activator of the lipid kinase Fab1p. *J. Cell Biol.* doi:10.1083/jcb.200201002.

Cabrera, M., M. Nordmann, A. Perz, D. Schmedt, A. Gerondopoulos, F. Barr, J. Piehler, S. Engelbrecht-Vandre, and C. Ungermann. 2014. The Mon1-Ccz1 GEF activates the Rab7 GTPase Ypt7 via a longin-fold-Rab interface and association with PI3P-positive membranes. *J. Cell Sci.* doi:10.1242/jcs.140921.

Chang, J., S.A. Kim, X. Lu, Z. Su, K.K. Seong, and Y.K. Shin. 2009. Fusion step-specific influence of cholesterol on SNARE-mediated membrane fusion. *Biophys. J.* doi:10.1016/j.bpj.2008.11.033.

Cheever, M.L., T.K. Sato, T. De Beer, T.G. Kutateladze, S.D. Emr, and M. Overduin. 2001.

Phox domain interaction with Ptdlns(3)P targets the Vam7 t-SNARE to vacuole membranes. *Nat. Cell Biol.* doi:10.1038/35083000.

Choi, S.Y., P. Huang, G.M. Jenkins, D.C. Chan, J. Schiller, and M.A. Frohman. 2006. A common lipid links Mfn-mediated mitochondrial fusion and SNARE-regulated exocytosis. *Nat. Cell Biol.* doi:10.1038/ncb1487.

Collins, K.M., and W.T. Wickner. 2007. trans-SNARE complex assembly and yeast vacuole membrane fusion. *Proc. Natl. Acad. Sci.* doi:10.1073/pnas.0702290104.

Dong, X., D. Shen, X. Wang, T. Dawson, X. Li, Q. Zhang, X. Cheng, Y. Zhang, L.S. Weisman, M. Delling, and H. Xu. 2010. PI(3,5)P2 controls membrane trafficking by direct activation of mucolipin Ca2+ release channels in the endolysosome. *Nat. Commun.* doi:10.1038/ncomms1037.

Dove, S.K., F.T. Cooke, M.R. Douglas, L.G. Sayers, P.J. Parker, and R.H. Michell. 1997. Osmotic stress activates phosphatidylinositol-3,5-bisphosphate synthesis. *Nature*. doi:10.1038/36613.

Eitzen, G., N. Thorngren, and W. Wickner. 2001. Rho1p and Cdc42p act after Ypt7p to regulate vacuole docking. *EMBO J.* doi:10.1093/emboj/20.20.5650.

Eitzen, G., L. Wang, N. Thorngren, and W. Wickner. 2002. Remodeling of organelle-bound actin is required for yeast vacuole fusion. *J. Cell Biol.* doi:10.1083/jcb.200204089.

Fang, J., and K.H. Iwasa. 2007. Effects of chlorpromazine and trinitrophenol on the membrane motor of outer hair cells. *Biophys. J.* doi:10.1529/biophysj.106.100834.

Ford, M.G.J., I.G. Mills, B.J. Peter, Y. Vallis, G.J.K. Praefcke, P.R. Evans, and H.T. McMahon. 2002. Curvature of clathrin-coated pits driven by epsin. *Nature*. doi:10.1038/nature01020.

Fratti, R.A., K.M. Collins, C.M. Hickey, and W. Wickner. 2007. Stringent 3Q·1R composition of

the SNARE 0-layer can be bypassed for fusion by compensatory SNARE mutation or by lipid bilayer modification. *J. Biol. Chem.* doi:10.1074/jbc.M700971200.

Fratti, R.A., Y. Jun, A.J. Merz, N. Margolis, W. Wickner, and B. Wickner. 2004. Interdependent assembly of specific regulatory lipids and membrane fusion proteins into the vertex ring domain of docked vacuoles. *J. Cell Biol.* doi:10.1083/jcb.200409068.

Hall, A. 1998. Rho GTPases and the actin cytoskeleton. *Science (80-.).* doi:10.1126/science.279.5350.509.

Han, G.S., C.N. Johnston, and G.M. Carman. 2004. Vacuole Membrane Topography of the DPP1-encoded Diacylglycerol Pyrophosphate Phosphatase Catalytic Site from Saccharomyces cerevisiae. *J. Biol. Chem.* doi:10.1074/jbc.M311779200.

Han, G.S., L. O'Hara, G.M. Carman, and S. Siniossoglou. 2008a. An unconventional diacylglycerol kinase that regulates phospholipid synthesis and nuclear membrane growth. *J. Biol. Chem.* doi:10.1074/jbc.M802903200.

Han, G.S., L. O'Hara, S. Siniossoglou, and G.M. Carman. 2008b. Characterization of the yeast DGK1-encoded CTP-dependent diacylglycerol kinase. *J. Biol. Chem.* doi:10.1074/jbc.M802866200.

Han, G.S., W.I. Wu, and G.M. Carman. 2006. The Saccharomyces cerevisiae lipin homolog is a Mg2+-dependent phosphatidate phosphatase enzyme. *J. Biol. Chem.* doi:10.1074/jbc.M600425200.

Hokanson, D.E., J.M. Laakso, T. Lin, D. Sept, and E.M. Ostap. 2006. Myo1c Binds Phosphoinositides through a Putative Pleckstrin Homology Domain. *Mol. Biol. Cell*. doi:10.1091/mbc.E06-05-0449.

Isgandarova, S., L. Jones, D. Forsberg, A. Loncar, J. Dawson, K. Tedrick, and G. Eitzen. 2007.

Stimulation of actin polymerization by vacuoles via Cdc42p-dependent signaling. *J. Biol. Chem.* doi:10.1074/jbc.M704117200.

Jahn, R., T. Lang, and T.C. Südhof. 2003. Membrane fusion. *Cell*. doi:10.1016/S0092-8674(03)00112-0.

Jahn, R., and T.C. Südhof. 1999. Membrane Fusion and Exocytosis. *Annu. Rev. Biochem.* doi:10.1146/annurev.biochem.68.1.863.

James, D.J., C. Khodthong, J.A. Kowalchyk, and T.F.J. Martin. 2008. Phosphatidylinositol 4,5-bisphosphate regulates SNARE-dependent membrane fusion. *J. Cell Biol.* doi:10.1083/jcb.200801056.

Jones, L., K. Tedrick, A. Baier, M.R. Logan, and G. Eitzen. 2010. Cdc42p is activated during vacuole membrane fusion in a sterol-dependent subreaction of priming. *J. Biol. Chem.* doi:10.1074/jbc.M109.074609.

Jost, M., F. Simpson, J.M. Kavran, M.A. Lemmon, and S.L. Schmid. 1998. Phosphatidylinositol-4,5-bisphosphate is required for endocytic coated vesicle formation. *Curr. Biol.* doi:10.1016/S0960-9822(98)00022-0.

Jun, Y., R.A. Fratti, and W. Wickner. 2004. Diacylglycerol and its formation by phospholipase C regulate Rab- and SNARE-dependent yeast vacuole fusion. *J. Biol. Chem.* doi:10.1074/jbc.M411363200.

Karunakaran, S., and R.A. Fratti. 2013. The Lipid Composition and Physical Properties of the Yeast Vacuole Affect the Hemifusion-Fusion Transition. *Traffic*. doi:10.1111/tra.12064.

Karunakaran, S., T. Sasser, S. Rajalekshmi, and R. a. Fratti. 2012. SNAREs, HOPS and regulatory lipids control the dynamics of vacuolar actin during homotypic fusion in S. cerevisiae. *J. Cell Sci.* doi:10.1242/jcs.091900.

Kato, M., and W. Wickner. 2001. Ergosterol is required for the Sec18/ATP-dependent priming step of homotypic vacuole fusion. *EMBO J.* doi:10.1093/emboj/20.15.4035.

Lawrence, G., C.C. Brown, B.A. Flood, S. Karunakaran, M. Cabrera, M. Nordmann, C. Ungermann, and R.A. Fratti. 2014. Dynamic association of the PI3P-interacting Mon1-Ccz1 GEF with vacuoles is controlled through its phosphorylation by the type 1 casein kinase Yck3. *Mol. Biol. Cell*. doi:10.1091/mbc.E13-08-0460.

Lee, M.E., K. Singh, J. Snider, A. Shenoy, C.M. Paumi, I. Stagljar, and H.O. Park. 2011. The Rho1 GTPase acts together with a vacuolar glutathione S-conjugate transporter to protect yeast cells from oxidative stress. *Genetics*. doi:10.1534/genetics.111.130724.

Liu, S., K.A. Wilson, T. Rice-stitt, A.M. Neiman, and J.A. Mcnew. 2007. In vitro fusion catalyzed by the sporulation-specific t-sNARE light-chain Spo20p is stimulated by phosphatidic acid. *Traffic*. doi:10.1111/j.1600-0854.2007.00628.x.

Logan, M.R., L. Jones, and G. Eitzen. 2010. Cdc42p and Rho1p are sequentially activated and mechanistically linked to vacuole membrane fusion. *Biochem. Biophys. Res. Commun.* doi:10.1016/j.bbrc.2010.02.102.

Manifava, M., J.W.J.F. Thuring, Z.Y. Lim, L. Packman, A.B. Holmes, and N.T. Ktistakis. 2001. Differential Binding of Traffic-related Proteins to Phosphatidic Acid- or Phosphatidylinositol (4,5)-Bisphosphate-coupled Affinity Reagents. *J. Biol. Chem.* doi:10.1074/jbc.M010308200.

Mayer, A., D. Scheglmann, S. Dove, A. Glatz, W. Wickner, and A. Haas. 2000. Phosphatidylinositol 4,5-Bisphosphate Regulates Two Steps of Homotypic Vacuole Fusion. *Mol. Biol. Cell*. doi:10.1091/mbc.11.3.807.

Mayer, A., and W. Wickner. 1997. Docking of yeast vacuoles is catalyzed by the ras-like

GTPase Ypt7p after symmetric priming by Sec18p (NSF). *J. Cell Biol.* doi:10.1083/jcb.136.2.307.

Mayer, A., W. Wickner, and A. Haas. 1996. Sec18p (NSF)-driven release of Sec17p (α-SNAP) can precede docking and fusion of yeast vacuoles. *Cell*. doi:10.1016/S0092-8674(00)81084-3.

Mima, J., C.M. Hickey, H. Xu, Y. Jun, and W. Wickner. 2008. Reconstituted membrane fusion requires regulatory lipids, SNAREs and synergistic SNARE chaperones. *EMBO J.* doi:10.1038/emboj.2008.139.

Mima, J., and W. Wickner. 2009. Complex lipid requirements for SNARE-and SNARE chaperone-dependent membrane fusion. *J. Biol. Chem.* doi:10.1074/jbc.M109.010223.

Miner, G.E., M.L. Starr, L.R. Hurst, R.P. Sparks, M. Padolina, and R.A. Fratti. 2016. The central polybasic region of the soluble snare (soluble n-ethylmaleimide-sensitive factor attachment protein receptor) Vam7 affects binding to phosphatidylinositol 3-phosphate by the PX (Phox Homology) domain. *J. Biol. Chem.* doi:10.1074/jbc.M116.725366.

Nakanishi, H., M. Morishita, C.L. Schwartz, A. Coluccio, J. Engebrecht, and A.M. Neiman. 2006. Phospholipase D and the SNARE Sso1p are necessary for vesicle fusion during sporulation in yeast. *J. Cell Sci.* doi:10.1242/jcs.02841.

Orr, A., W. Wickner, S.F. Rusin, A.N. Kettenbach, and M. Zick. 2015. Yeast vacuolar HOPS, regulated by its kinase, exploits affinities for acidic lipids and Rab:GTP for membrane binding and to catalyze tethering and fusion. *Mol. Biol. Cell*. doi:10.1091/mbc.E14-08-1298.

Poteryaev, D., S. Datta, K. Ackema, M. Zerial, and A. Spang. 2010. Identification of the switch in early-to-late endosome transition. *Cell*. doi:10.1016/j.cell.2010.03.011.

Predescu, S.A., D.N. Predescu, K. Shimizu, I.K. Klein, and A.B. Malik. 2005. Cholesterol-dependent syntaxin-4 and SNAP-23 clustering regulates caveolar fusion with the endothelial plasma membrane. *J. Biol. Chem.* doi:10.1074/jbc.M505659200.

Reese, C., and A. Mayer. 2005. Transition from hemifusion to pore opening is rate limiting for vacuole membrane fusion. *J. Cell Biol.* doi:10.1083/jcb.200510018.

Rozelle, A.L., L.M. Machesky, M. Yamamoto, M.H.E. Driessens, R.H. Insall, M.G. Roth, K. Luby-Phelps, G. Marriott, A. Hall, and H.L. Yin. 2000. Phosphatidylinositol 4,5-bisphosphate induces actin-based movement of raft-enriched vesicles through WASP-Arp2/3. *Curr. Biol.* doi:10.1016/S0960-9822(00)00384-5.

Rudge, S.A., D.M. Anderson, and S.D. Emr. 2004. Vacuole size control: regulation of PtdIns(3,5)P_2 levels by the vacuole-associated Vac14-Fig4 complex, a PtdIns(3,5)P_2-specific phosphatase. *Mol. Biol. Cell*. doi:10.1091/mbc.E03-05-0297.

Sasser, T., Q.S. Qiu, S. Karunakaran, M. Padolina, A. Reyes, B. Flood, S. Smith, C. Gonzales, and R.A. Fratti. 2012. Yeast lipin 1 orthologue Pah1p regulates vacuole homeostasis and membrane fusion. *J. Biol. Chem.* doi:10.1074/jbc.M111.317420.

Sasser, T.L., G. Lawrence, S. Karunakaran, C. Brown, and R.A. Fratti. 2013. The yeast ATP-binding cassette (ABC) transporter Ycf1p enhances the recruitment of the soluble SNARE Vam7p to vacuoles for efficient membrane fusion. *J. Biol. Chem.* doi:10.1074/jbc.M112.441089.

Schneiter, R., B. Brügger, R. Sandhoff, G. Zellnig, A. Leber, M. Lampl, K. Athenstaedt, C. Hrastnik, S. Eder, G. Daum, F. Paltauf, F.T. Wieland, and S.D. Kohlwein. 1999. Electrospray ionization tandem mass spectrometry (ESI-MS/MS) analysis of the lipid molecular species composition of yeast subcellular membranes reveals acyl chain-based

sorting/remodeling of distinct molecular species en route to the plasma membrane. *J. Cell Biol.* doi:10.1083/jcb.146.4.741.

Seals, D.F., G. Eitzen, N. Margolis, W.T. Wickner, and A. Price. 2000. A Ypt/Rab effector complex containing the Sec1 homolog Vps33p is required for homotypic vacuole fusion. *Proc. Natl. Acad. Sci.* doi:10.1073/pnas.97.17.9402.

Seeley, E.S. 2002. Genomic Analysis of Homotypic Vacuole Fusion. *Mol. Biol. Cell*. doi:10.1091/mbc.01-10-0512.

Stroupe, C., C.M. Hickey, J. Mima, A.S. Burfeind, and W. Wickner. 2009. Minimal membrane docking requirements revealed by reconstitution of Rab GTPase-dependent membrane fusion from purified components. *Proc. Natl. Acad. Sci.* doi:10.1073/pnas.0903801106.

Thorngren, N., K.M. Collins, R.A. Fratti, W. Wickner, and A.J. Merz. 2004. A soluble SNARE drives rapid docking, bypassing ATP and Sec17/18p for vacuole fusion. *EMBO J.* doi:10.1038/sj.emboj.7600286.

Toke, D.A., W.L. Bennett, J. Oshiro, W.I. Wu, D.R. Voelker, and G.M. Carman. 1998. Isolation and characterization of the Saccharomyces cerevisiae LPP1 gene encoding a Mg2+-independent phosphatidate phosphatase. *J. Biol. Chem.* doi:10.1074/jbc.273.23.14331.

Ungermann, C., K. Sato, and W. Wickner. 1998. Defining the functions of trans-SNARE pairs. *Nature*. doi:10.1038/25069.

Vicogne, J., D. Vollenweider, J.R. Smith, P. Huang, M.A. Frohman, and J.E. Pessin. 2006. Asymmetric phospholipid distribution drives in vitro reconstituted SNARE-dependent membrane fusion. *Proc. Natl. Acad. Sci. U. S. A.* doi:10.1073/pnas.0606881103.

Villar, A. V., A. Alonso, and F.M. Goni. 2000. Leaky vesicle fusion induced by phosphatidylinositol-specific phospholipase C: Observation of mixing of vesicular inner

monolayers. *Biochemistry*. doi:10.1021/bi992515c.

Wang, C.W., P.E. Stromhaug, E.J. Kauffman, L.S. Weisman, and D.J. Klionsky. 2003a. Yeast homotypic vacuole fusion requires the Ccz1-Mon1 complex during the tethering/docking stage. *J. Cell Biol.* doi:10.1083/jcb.200308071.

Wang, J., H.-Q. Sun, E. Macia, T. Kirchhausen, H. Watson, J.S. Bonifacino, and H.L. Yin. 2007. PI4P Promotes the Recruitment of the GGA Adaptor Proteins to the Trans-Golgi Network and Regulates Their Recognition of the Ubiquitin Sorting Signal. *Mol. Biol. Cell*. doi:10.1091/mbc.E06-10-0897.

Wang, L., A.J. Merz, K.M. Collins, and W. Wickner. 2003b. Hierarchy of protein assembly at the vertex ring domain for yeast vacuole docking and fusion. *J. Cell Biol.* doi:10.1083/jcb.200209095.

Wang, L., E.S. Seeley, W. Wickner, and A.J. Merz. 2002. Vacuole fusion at a ring of vertex docking sites leaves membrane fragments within the organelle. *Cell*. doi:10.1016/S0092-8674(02)00632-3.

Wickner, W. 2010. Membrane Fusion: Five Lipids, Four SNAREs, Three Chaperones, Two Nucleotides, and a Rab, All Dancing in a Ring on Yeast Vacuoles. *Annu. Rev. Cell Dev. Biol.* doi:10.1146/annurev-cellbio-100109-104131.

Xu, H., and W. Wickner. 2010. Phosphoinositides function asymmetrically for membrane fusion, promoting tethering and 3Q-SNARE subcomplex assembly. *J. Biol. Chem.* doi:10.1074/jbc.M110.183111.

Zick, M., C. Stroupe, A. Orr, D. Douville, and W.T. Wickner. 2014. Membranes linked by trans-SNARE complexes require lipids prone to non-bilayer structure for progression to fusion. *Elife*. doi:10.7554/eLife.01879.

Zinser, E., C.D.M. Sperka-Gottlieb, E. V. Fasch, S.D. Kohlwein, F. Paltauf, and G. Daum. 1991. Phospholipid synthesis and lipid composition of subcellular membranes in the unicellular eukaryote Saccharomyces cerevisiae. *J. Bacteriol.* doi:10.1128/jb.173.6.2026-2034.1991.

CHAPTER 2: PHOSPHATIDIC ACID SEQUESTERS Sec18 FROM *cis*-SNARE COMPLEXES TO INHIBIT PRIMING[1]

ABSTRACT

Yeast vacuole fusion requires the activation of *cis*-SNARE complexes through priming carried out by Sec18p/NSF and Sec17p/α-SNAP. The association of Sec18p with vacuolar *cis*-SNAREs is regulated in part by phosphatidic acid (PA) phosphatase production of diacylglycerol (DAG). Inhibition of PA phosphatase activity blocks the transfer of membrane associated Sec18p to SNAREs. Thus, we hypothesized that Sec18p associates with PA-rich membrane microdomains before transferring to *cis*-SNARE complexes upon PA phosphatase activity. Here we examined the direct binding of Sec18p to liposomes containing PA or DAG. We found that Sec18p preferentially bound to liposomes containing PA compared to those containing DAG by approximately five-fold. Additionally, using a specific PA-binding domain blocked Sec18p binding to PA-liposomes and displaced endogenous Sec18p from isolated vacuoles. Moreover, the direct addition of excess PA blocked the priming activity on isolated vacuoles in a manner similar to chemically inhibiting PA phosphatase activity. These data suggest that the conversion of PA to DAG facilitates the recruitment of Sec18p to *cis*-SNAREs. Purified vacuoles from yeast lacking the PA phosphatase Pah1p showed reduced Sec18p association with *cis*-SNAREs and

[1] This chapter appeared in its entirety in the journal *Traffic*.
Starr, M. L., Hurst, L. R., and Fratti, R. A. (2016). Phosphatidic acid sequesters Sec18p from cis-SNARE complexes to inhibit priming. Traffic *17*, 1091-1109.
This article is reprinted with permission from the publisher and is available from https://onlinelibrary.wiley.com/doi/abs/10.1111/tra.12423
DOI: 10.1111/tra.12423

complementation with plasmid-encoded *PAH1* or recombinant Pah1p restored the interaction. Taken together this demonstrates that regulating PA concentrations by Pah1p activity controls SNARE priming by Sec18p.

INTRODUCTION

Eukaryotic membrane fusion is a process vital to cellular homeostasis. Trafficking of transport vesicles among organelles and the plasma membrane is governed by of a series of events that is highly conserved in all eukaryotes from yeast to humans (Jahn and Südhof, 1999). The proteins that carry out this process are diverse, but all fusion machinery ultimately facilitates a series of membrane contact, fusion, and compartment mixing event (Jahn et al., 2003). We use vacuoles from *Saccharomyces cerevisiae* as a model to examine the regulation of the eukaryotic fusion machinery.

Yeast homotypic vacuole fusion has been well described and is characterized by a series of experimentally defined stages. The fusion cascade begins with the priming stage in which the AAA+ ATPase Sec18p (NSF) and its co-chaperone Sec17p (α-SNAP) disassemble inactive *cis*-SNARE complexes. Priming requires ATP hydrolysis by Sec18p and results in the disassociation of Sec17p and the soluble SNARE Vam7p from the membrane (Boeddinghaus et al., 2002; Mayer et al., 1996). During the tethering/docking stage, the Rab GTPase Ypt7p and its effector complex HOPS interact to bring two vacuolar compartments together (Mayer and Wickner, 1997; Seals et al., 2000). Vam7p rebinds the vacuolar membrane through interactions with HOPS and the regulatory lipid phosphatidylinositol 3-phosphate (PI3P) leading to the formation of *trans*-SNARE

pairing between apposing membranes (Boeddinghaus et al., 2002; Ungermann et al., 1998). At this stage the two membranes are closely associated and are enriched in regulatory proteins and lipids at the periphery of their interface named the "vertex ring" microdomain (Fratti et al., 2004; Wang et al., 2002, 2003). The fusion cascade proceeds through the formation of a hemifusion intermediate before pore formation and luminal content mixing occur (Jahn et al., 2003; Reese and Mayer, 2005).

Maintenance of SNARE proteins is crucial for turnover of eukaryotic membrane fusion events. Upon fusion and compartment mixing, SNAREs exist in a stable *cis*-SNARE complex in which all SNAREs reside on a single membrane rendering them unable to carry out subsequent rounds of docking. During priming, homohexameric Sec18p/NSF associates with *cis*-SNARE complexes through binding to Sec17p/SNAPs and generates the necessary force to disassociate inactive complexes into active individual SNAREs (Mayer et al., 1996). Recent evidence suggests that NSF disrupts *cis*-SNARE complexes through a "loaded-spring" mechanism (Ryu et al., 2015; Zhao et al., 2015). In this model, NSF ATPase activity leads to large conformational changes in the NSF N-terminal and D1 domains, which exert enough force on SNAPs to disassemble the SNAREs. Direct regulation of this Sec18p/NSF priming activity remains mostly unknown, although protein kinase C has been implicated in negative regulation of NSF association with *cis*-SNARE complexes (Matveeva et al., 2001). Of interest, NSF has been found to bind phosphatidic acid (PA), a regulatory lipid required for vacuole fusion; however, the effects of Sec18p/NSF lipid association are still not well understood (Manifava et al., 2001; Mima and Wickner, 2009; Sasser et al., 2012).

Regulatory phospholipids on the cytosolic face of the vacuolar membrane serve as key regulators of the fusion machinery. A presence of phosphatidylcholine (PC), phosphatidylethanolamine (PE), PA, diacylglycerol (DAG), and PI3P is essential for vacuolar fusion to occur and serve as the minimal lipid requirements of the fusion reaction (Mima and Wickner, 2009). Additional lipids including PI4P, PI(4,5)P_2 and ergosterol are also required for optimal homotypic vacuolar fusion(Fratti et al., 2004; Karunakaran and Fratti, 2013; Kato and Wickner, 2001; Mayer et al., 2000). Specific lipid head groups provide a scaffold for the binding and recruitment of proteins that actively carry out the stages of fusion. This function relies on direct protein-lipid interactions between the membrane and protein machinery as exemplified by the binding of PI3P by the Vam7p PX domain (Cheever et al., 2001). Specific lipids also affect the fusion machinery physically through changes to membrane dynamics. This role is demonstrated by the dependence of SNARE function on lipid microdomain formation and potential allosteric effects exerted on the transmembrane domains of SNARE proteins (Fratti et al., 2004; Karunakaran et al., 2012). Reversible changes to the concentration of specific lipids within microdomains also mediate protein-lipid interactions at the vertex ring and dynamics of vacuole associated actin.

The interconversion of regulatory lipids is catalyzed by a variety of lipid modifying proteins. These enzymes respond to varied growth conditions through coordination of genetic and biochemical mechanisms. The yeast PA phosphatase Pah1p plays an important role in the regulation of lipid synthesis. Pah1p has been shown to have a role in mediation of the transcription of the lipid synthesis genes *INO1, INO2* and *OPI3* through its phosphatase activity (Han et al., 2007; O'Hara et al., 2006). This is critical for organelle replication for daughter cells during mitosis as the nuclear envelope and endoplasmic reticulum must expand. Unphosphorylated Pah1p generates DAG,

which is involved in the synthesis of triacylglycerol, PC, and PE (Karanasios et al., 2010; Choi et al., 2011). Recently, it was shown that Pah1p localizes to the nuclear vacuole junction at the diauxic shift during acute glucose starvation (Barbosa et al., 2015).

A number of lipid modifying enzymes have been implicated in vacuole fusion or fission events and display abnormal morphologies or other observable defects when deleted or mutated. Both PA and DAG are essential lipids for vacuole fusion and have been implicated in organelle transport and fusion activities. For instance DAG plays a role in Golgi to ER transport and the formation of COPI vesicles (Fernandez-Ulibarri et al., 2007), where as PA is important for sporulation and stimulating the fusion activity of the SNARE Spo20p (Liu et al., 2007; Nakanishi et al., 2006). In addition, the PA phosphatase activity of Pah1p is necessary for endolysosomal maturation and vacuole homotypic fusion (Sasser et al., 2012). Deletion of *PAH1* leads to the fragmentation of immature vacuoles and severely abrogates fusion activity. This phenotype is proposed to come from two defects involving the fusion machinery. First, vacuoles harvested from *pah1*Δ yeast contain strikingly reduced levels of factors involved in regulating vacuole fusion including the PI-3 kinase Vps34p and its product PI3P, Ypt7p and its guanine exchange factor Mon1p-Ccz1p, as well as the HOPS subunit Vps39p (Sasser et al., 2012; Lawrence et al., 2014). Second, deletion of *PAH1* or inhibition of PA phosphatase activity led to a measurable decrease in priming and SNARE-associated Sec18p. Importantly, neither *PAH1* deletion nor chemical inhibition of PA phosphatase activity alters the total levels of Sec18p associated with vacuoles. Thus, we posit that inactive (*i.e.* SNARE-free) Sec18p remains associated with vacuoles through interactions with PA and that modification of PA releases Sec18p to *cis*-SNAREs to enable priming. In this study, we examined the interactions of Sec18p and PA in the regulation of priming. We report that like its

mammalian orthologue NSF, Sec18p specifically binds to PA. Additionally, both increased levels of PA and the absence of Pah1p on the vacuole inhibited Sec18p-dependent priming and prevent recruitment of Sec18p to *cis*-SNARE complexes.

MATERIALS AND METHODS

Reagents

All reagents were diluted in PS buffer (20 mM PIPES-KOH pH 6.8, 200 mM sorbitol) to a working concentration before use in experiments. Antibodies against Sec17p (Haas and Wickner, 1996) and Sec18p have been described previously. *N*-ethylmaleimide (NEM), propranolol hydrochloride, and ATPγS were purchased from Sigma Aldrich and dissolved in PS buffer. The lipids used in this study: POPA (1-palmitoyl-2-oleoyl-sn-glycero-3-phosphate), POPC (1-palmitoyl-2-oleoyl-sn-glycero-3-phosphatidylcholine), POPE (1-palmitoyl-2-oleoyl-sn-glycero-3-phosphatidylethanolamine), POG/DAG (1-palmitoyl-2-oleoyl-sn-glycerol), diC8-PA (1,2-dioctanoyl-*sn*-glycero-3-phosphate), and diC8-DAG (1,2-dioctanoyl-*sn*-glycerol) were purchased from Avanti Polar Lipids as chloroform stock solutions and stored at -20ºC.

Recombinant proteins

Recombinant His_6-Sec18p was purified from *Escherichia coli* as previously described (Steel et al., 1999). Briefly, PQE9-His_6-Sec18p plasmid was transformed into Rosetta-2 (DE3) pLysS (EMD Biosciences) competent cells and plated on LB agar plates containing 100 μg/ml ampicillin and 35 μg/ml chloramphenicol. Transformed cells were grown for 14 h in 100 ml LB at 37ºC. Culture flasks containing 1 liter Terrific Broth were inoculated with 50 ml of the pre-culture and grown at

37ºC to A_{600} = 0.6. Cells were induced with 1 mM 1-thio-β-D-galactopyranoside at 16ºC for 14 h before being collected by centrifugation and washed with lysis buffer (10 mM HEPES-KOH pH 7.0, 500 mM KCl, 5 mM ATP, 5 mM $MgCl_2$, 2 mM β-mercaptoethanol, 1 mM PMSF and protease inhibitor cocktail). Cells were lysed with four passes through a French pressure cell. Lysates were cleared by centrifugation (200,000 x *g*, 30 min, 4ºC), and the cleared lysate was loaded onto a Ni-NTA agarose column (Thermo Scientific) equilibrated with lysis buffer. The resin was washed with 20 column volumes of lysis buffer containing 10% glycerol and 50 mM Imidazole. His_6-Sec18p was eluted from with lysis buffer containing 10% glycerol and 350 mM Imidazole. The eluted protein was further purified by gel filtration in GF buffer (20 mM PIPES-KOH pH 6.8, 200 mM Sorbitol, 125 mM KCl, 5 mM $MgCl_2$, 2 mM ATP, 2 mM DTT and 10% glycerol) and 1 ml fractions were collected. Sec18p elutes from the column as three distinct peaks: the hexameric pool with a molecular mass of 640 kDa elutes early (approximately 50 ml post injection), and dimer and monomeric pools each elute later (approximately 90 and 105 ml post-injection, respectively). The hexameric pool of Sec18p was used in all experiments. The recombinant His_6-SUMO-Pah1p construct used was created for this study. The *PAH1* gene was cloned from BJ3505 genomic DNA via PCR amplification using the primers: Forward 5' – TACTTCCAATCCAATGCAATGCAGTACGTAGGAA – 3' and Reverse 5' – TTATCCACTTCCAATGTTATTATTAATCTTCGAATTCATCTTCG – 3'. The amplified gene was inserted into pET His6 Sumo TEV LIC cloning vector (2S-T) (Addgene plasmid #29711) using the restriction enzyme SspI and the LIC method previously described to create the plasmid pSP1 (Aslanidis and de Jong, 1990). Three liters of Rosetta2(DE3)pLysS (EMD Millipore) cells transformed with pSP1 were grown in auto-inducing media supplemented with 2 mM $MgSO_4$ at 37^{o}C to an OD_{600} of 4.0, and cells were harvested by centrifugation (Studier, 2005). Cells were

lysed by freeze-thaw and sonication in buffer containing 50 mM Tris-HCl, pH 7.5, 300 mM NaCl, 2 mM $MgCl_2$, 10 mM imidazole, and 1mM phenylmethanesulfonyl fluoride (PMSF). Lysates were centrifuged for 1 hour at 140,000 x *g*, and the supernatant was applied to Ni-NTA agarose resin (Invitrogen). The resin was washed with lysis buffer supplemented with 25 mM imidazole and 0.5 mM ATP, and bound proteins were eluted with lysis buffer supplemented with 300 mM imidazole. Eluted protein was dialyzed into PS buffer containing 125 mM KCl. Recombinant GST-DEP, GST-C1b, GST-ENTH and GST-Vam7p were purified as described and dialyzed into PS buffer containing 125 mM KCl (Capelluto et al., 2014; Johnson et al., 2000; Rosenthal et al., 1999; Fratti et al., 2007). The plasmid for GST-DEP expression was a gift from Dr. D. Capelluto (Virginia Tech University).

Strains

BJ3505 (*MATα pep4::HIS3 prb1-Δ1.6R his3-200 lys2-801 trp1Δ101(gal3) ura3-52 gal2 can1*) and DKY6281 (*MATα leu2-3 leu2-112 ura3-52 his3-Δ200 trpΔ1-901 lys 2-801*) were used for standard vacuole fusion assays (Haas et al., 1994). BJ3505-CBP-Vam3p vacuoles were used for the isolation of Sec18p-SNARE complexes (Collins and Wickner, 2007). *PAH1* deleted strains RFY17 and RFY18 and WT Pah1p plasmid complemented strain RFY19, RFY20 have previously been described (Sasser et al., 2012).

Vacuole Isolation and in vitro vacuole fusion assay

Vacuoles were isolated from yeast strains by density gradient floatation as previously described (Haas et al., 1994). Fusion reactions (30 µl) contained 3 µg each of vacuoles from BJ3505 (*pep4Δ PHO8)* and DK6281 (*PEP4 pho8Δ),* fusion assay buffer (125 mM KCl, 5 mM $MgCl_2$, 20 mM

PIPES-KOH pH 6.8, 200 mM sorbitol), ATP regenerating system (1 mM ATP, 29 mM creatine phosphate, 0.1 mg/ml creatine kinase), 10 μM CoA, and 283 nM Pbi2p. Reactions were incubated at 27°C for 90 min and the Pho8p activity was measured in 250 mM Tris-Cl PH 8.5, 0.4% Triton X-100, 10 mM $MgCl_2$, 1 mM *p*-nitrophenyl phosphate. Fusion-dependent alkaline phosphatase maturation was measured by the amount of *p*-nitrophenylate produced. *p*-Nitrophenylate absorbance was measured at 400 nm.

Liposome Preparation and Co-Floatation Assay

Small unilamellar liposomes containing various lipid compositions were prepared using the sonication method (Mima and Wickner, 2009). Briefly, stock lipids in chloroform were mixed to produce a lipid mixture with the desired lipid mole percentages of 2.6 μmoles of total phospholipids. The lipid mixture was dried under a gentle stream of nitrogen and dried in a speed-vacuum for an additional 60 min. The tubes were placed under vacuum in a desiccator for an additional 14 h. To the dried lipids, 2.6 ml of 1X PBS solution was added. Tubes were covered with parafilm and incubated at room temperature for 1 h. The lipids were resuspended with vortexing and disrupted in a water bath sonicator for 30 min. To measure protein binding to the liposomes we used a floatation assay as described (Matsuoka et al., 1998). Briefly, 40 μl of lipid binding domain/PBS mixture was incubated with 150 μl of the 1 mM liposome suspension for 5 minutes at 30ºC before 20 μg of recombinant His_6-Sec18p was added. Samples were incubated for an additional 10 min at 30ºC and 630 μl of 1.65 M sucrose (PBS) was added. Samples were loaded into the bottom of a centrifuge tube and layered with 840 μl of 0.75 M sucrose (PBS), and 1X PBS to the top of the tube. Samples were centrifuged (200,000 x *g,* 90 min, 4ºC) and 200 μl of floated liposomes were recovered from the top of the 0.75 M sucrose layer. The bottom 100 μl fraction

was recovered and SDS sample buffer was added to sample unbound protein levels. Liposomes were resuspended in 1 ml of 1X PBS and isolated by centrifugation (16,000 x *g*, 10 min, 4ºC). SDS sample buffer was added to the final liposome pellet and bound proteins were resolved by SDS-PAGE. The proteins were transferred to nitrocellulose and probed by Western blotting. Images were acquired using a ChemiDoc MP Imaging System (Bio-Rad).

Vacuole Competition Binding Assay

Vacuoles were harvested from DKY6281. Each sample contained 12 μg of vacuoles suspended in binding assay buffer (125 mM KCl, 5 mM $MgCl_2$, 20 mM PIPES-KOH pH 6.8, 200 mM sorbitol) to a final volume of 60 μl. Recombinant GST-DEP, GST-C1b, or GST-ENTH in binding assay buffer was added to the indicated concentrations and samples were incubated at 4ºC for 10 min. Whole vacuole samples with no added lipid binding domain were saved for input controls. Supernatant and pellet fractions were isolated by centrifugation (16,000 x *g*, 5 min, 4ºC) and suspended in 1X SDS sample buffer. Samples were heated at 95ºC for 5 min, resolved by SDS-PAGE, and transferred to nitrocellulose. Presence of Sec18p in the input controls and supernatant fractions was probed by Western blot.

Priming Assay

Priming activity of Sec18p was assayed as previously described (Mayer et al., 1996). Briefly, vacuoles were harvested from BJ3505. The equivalent of two standard fusion reactions was incubated at 27ºC with buffer, NEM, diC8-PA, or diC8-DAG. At the indicated times, vacuoles were removed by centrifugation (16,000 x *g*, 5 min, 4ºC) and SDS sample buffer was added to the

supernatants. Samples were heated at 95ºC for 5 min, resolved by SDS-PAGE, transferred to nitrocellulose, and probed by Western blot.

Sec18p-SNARE Complex Detection using CBP-Vam3p Pull-down

Analysis of the formation of Sec18p-*cis*-SNARE complexes was assayed as previously described (Sasser et al., 2012). Briefly, vacuoles used were isolated from BJ3505-CBP-Vam3p. Isolation of Sec18p-*cis*-SNARE complexes was performed in large-scale fusion reactions (480 µl) using 96 µg of vacuoles. Reactions were incubated at 27ºC for the indicated time and treated with buffer or propranolol. Reactions treated with ATPγS were treated with buffer and ATP regenerating system containing ATPγS in place of ATP. Separate reactions were kept on ice as 0 min samples and without ATP regenerating added as No ATP samples. After incubation, samples were placed on ice for 5 min and 30 µl samples were withdrawn to assay fusion activity. Remaining samples were centrifuged (13,000 x *g*, 15 min, 4ºC) and supernatant fractions were removed. The membrane fractions were gently resuspended in ice-cold solubilization buffer (20 mM Tris-Cl, pH 7.5, 150 mM NaCl, 1 mM $MgCl_2$, 0.5% Nonidet P-40 alternative, 10% glycerol) with protease inhibitors (0.46 µg/ml leupeptin, 3.5 µg/ml pepstatin, 2.4 µg/ml Pefabloc-SC, 1 mM PMSF). Solubilization buffer was added to a final volume of 600 µl and samples were mixed by nutation (20 min, 4ºC). Insoluble debris was removed by centrifugation (16,000 x *g*, 15 min, 4ºC) and supernatants were transferred to fresh tubes. A 60 µl sample was withdrawn for input samples. The remaining extracts were brought to 2 mM $CaCl_2$ and incubated with 50 µl of equilibrated calmodulin-Sepharose 4B (GE Healthcare) (4°C, 14 h, nutating). Beads were collected by centrifugation (4,000 *g*, 2 min, 4 °C) and washed 4 times in solubilization buffer. Bound proteins were eluted with SDS sample buffer containing 5 mM EGTA and heated at 95ºC for 5 min. The samples were resolved using SDS-PAGE, transferred to nitrocellulose, and probed by Western blot.

Sec18p-SNARE Complex Detection using GST-Vam7p Pull-down

Analysis of the formation of Sec18p-*cis*-SNARE complexes in mutant strains was assayed essentially the same as in CBP-Vam3p containing strains with some modifications. Vacuoles were isolated from *pah1*Δ strains (RFY17 and RFY18) or p*PAH1*-complemented strains (RFY19 and RFY20). Large-scale reactions were used (480 μl) using 96 μg of vacuoles. Recombinant GST-Vam7p was added to reactions (200 nM) prior to addition of ATP regenerating system and incubated at 27ºC for 30 min. ATP regenerating system was then added to samples and incubated for the indicated times at 27ºC. Fusion assay buffer was added in place of ATP regenerating system in the "no-ATP" sample. The 0 min sample was kept on ice throughout the duration of the incubation step. Solubilization buffer differed from the CBP-Vam3p solubilization buffer (20 mM HEPES-KOH, 100 mM NaCl, 2mM EDTA, 0.5% Nonidet P-40 alternative, 1 mM DTT, 20% glycerol, 1 mM PMSF, 0.46 μg/ml leupeptin, 3.5 μg/ml pepstatin, and 2.4 μg/ml Pefabloc-SC) and Glutathione Sepharose 4B resin (GE Healthcare) was used for the pull-down of complexes. The same method was used for Sec18p-SNARE complex detection in diC8-PA and diC8-DAG treated samples using vacuoles isolated from BJ3505.

Statistical analysis

All statistical analysis was calculated using one-way ANOVA. *P* values of ≤ 0.05 were considered significant. Half-times for the gain of resistance fusion assay were calculated using first-order exponential decay fitting with weights and errors (OriginPro 9.1 software).

RESULTS

Sec18p binds preferentially to membranes containing phosphatidic acid

The yeast PA phosphatase Pah1p regulates endolysosomal maturation leading to impaired homotypic vacuolar fusion (Sasser et al., 2012). Inhibition of PA phosphatase activity with the small molecule propranolol suggested that phosphatidic acid potentially had a specific role in mediating the priming activity of the SNARE chaperone. Treatment with propranolol blocked the binding of Sec18p to *cis*-SNARE complexes, while the total levels of vacuole associated Sec18p remained constant. Importantly, vacuoles from *pah1*Δ cells harbor wild type levels of Sec18p. Thus, we hypothesized that the conversion of PA to DAG led to a transition of Sec18p from a PA bound state to a *cis*-SNARE bound state. The Sec18p mammalian orthologue NSF was previously shown to specifically bind resin-conjugated PA, but the purpose of this binding remained unknown (Manifava et al., 2001). Here we asked if Sec18p also binds PA, a relationship that could be controlled by PA phosphatase activity. To test this we used a liposome-binding assay to detect Sec18p binding to membranes of different lipid compositions. Recombinant Sec18p was incubated with liposomes containing mixtures of the lipids PC, PE, PA, and DAG. Liposome-bound Sec18p was separated from unbound protein by floatation. Sec18p showed light binding to PC:PE liposomes alone, however this binding was significantly weaker compared to liposomes containing PA (Figure 2.1A). Liposomes containing DAG also showed little Sec18p binding relative to liposomes containing PA. This stark difference in binding between PA and DAG containing membranes is consistent with a requirement for Pah1p activity in regulating Sec18p recruitment from the membrane to *cis*-SNARE complexes. Next, we tested to see if the concentration of PA or DAG specifically had an effect on Sec18p binding to liposomes. Similar liposome floatation

assays were carried out but included liposomes of increasing PA or DAG concentrations. Membrane-bound Sec18p was present at higher levels in liposomes that contained elevated levels of PA (Figure 2.1B). Strikingly, an increase in the concentration of DAG in the liposomes had a significant negative effect on the level of Sec18p membrane association (Figure 2.1B). These data suggest that Sec18p binds preferentially to membranes containing PA and that the presence of DAG may promote the release of Sec18p from binding to membrane lipids directly. Taken together, this suggests that the conversion of PA to DAG may affect Sec18p membrane localization dynamics and Pah1p may specifically play a role in controlling the state Sec18p membrane lipid association.

We next tested whether the specificity of Sec18p binding to membranes extends beyond a nonspecific electrostatic interaction. The cytosolic face of the yeast vacuolar membrane contains a wide array of regulatory anionic phospholipids (Li and Kane, 2009). Because of this we asked if Sec18p would show preferential binding to PA or if it would also bind to other vacuolar membrane lipids carrying a negative charge. We performed liposome-binding assays with liposomes that contained PS, an anionic phospholipid that, like PA, localizes to the outer leaflet of the yeast vacuolar membrane. We again observed preferential Sec18p binding to liposomes of increasing PA concentration (Figure 2.1C). Sec18p binding to liposomes containing PS showed no significant binding suggesting that Sec18p lipid binding has specificity for PA and not anionic lipids in general. It is also important to note that the absence of liposomes in our binding assays gave no signal and detection of liposome-associated Sec18p was non-random (Figure 2.1D). These results highlight a specific binding interaction between Sec18p and PA that is likely present at the yeast vacuolar membrane.

To further probe Sec18p binding to specific membrane lipids, we performed binding competition assays in the presence of the PA-specific binding domain GST-DEP from the mouse protein Dvl2 (Capelluto et al., 2014). The addition of GST-DEP was expected to disrupt Sec18p binding to liposomes containing PA by occupying potential binding sites on the membrane. The addition of GST-DEP showed no significant effect on the level of Sec18p bound to PC:PE liposomes, but severely affected the ability of Sec18p to bind liposomes containing PA (Figure 2.2A, $P<0.005$). This suggests that the observed membrane binding of Sec18p was specifically dependent on the presence of PA. Surprisingly, the addition of GST-DEP also lowered the level of Sec18p binding to membranes containing DAG ($P<0.05$). We suspect that GST-DEP has some non-negligible amount of binding to DAG as many characterized PA-binding domains contain essential hydrophobic residues that embed in membranes(Kooijman et al., 2007). The absence of a large headgroup on DAG could allow for GST-DEP to sit very close to the acyl chain region within the bilayer promoting hydrophobic residue interactions with DAG or adjacent lipids. Considering this and the significant increase in binding to membranes containing PA when compared to those containing DAG, the data suggest that Sec18p membrane lipid binding is dependent on the presence of PA. To further characterize this interaction, we performed a binding competition assay that utilized PA-containing liposomes and the addition of increasing concentrations of GST-DEP. In the absence of competitor, significant binding of Sec18p to the liposomes was observed, and this binding was perturbed by the addition of GST-DEP in a dose-dependent manner (Figure 2.2B). These data further indicate that Sec18p has specific binding to PA.

To probe for specific Sec18p-lipid interactions on vacuole membranes, we used a binding competition assay that contained purified vacuoles in place of liposomes. Vacuoles were harvested from yeast and incubated on ice with the lipid-specific binding domains GST-DEP, GST-C1b (protein kinase C βII), and GST-ENTH (rat epsin 1) to bind to PA, DAG, and PI(4,5)P_2 respectively and displace vacuolar proteins bound to each (Johnson et al., 2000; Rosenthal et al., 1999). C1b and ENTH have been previously shown to cause the release of HOPS and Vam7p from vacuoles (Fratti et al., 2004; Stroupe et al., 2006). Samples were separated into bound and unbound fractions by centrifugation and Sec18p levels were assayed by Western blot. The percentage of Sec18p in the unbound fraction significantly increased with the addition of GST-DEP in a dose dependent manner when compared to the control similar to what was seen in the liposome-binding assays described above (Figure 2.2C). Addition of GST-C1b showed a slight increase in the proportion of unbound Sec18p from the untreated control condition however this release was independent of the concentration added and was statistically insignificant. Addition of GST-ENTH led to an increase of Sec18p release at the highest concentration used; however, the amount of released Sec18p was not statistically significant. Taken together, these data suggest that disruption of Sec18p binding to membrane lipids is most affected when PA is specifically occupied. This further supports the notion that Sec18p binding to vacuolar membranes occurs in a PA dependent manner. From this experiment we cannot rule out potential interactions between Sec18p and vacuolar DAG or PI(4,5)P_2. However, considering the lack of dose independent effect using GST-C1b along with our previous observations, the direct binding of Sec18p to DAG seems unlikely. Sec18p interactions with PI(4,5)P_2 are an interesting possibility that were not further investigated. However, it is not difficult to envision Sec18p having specific interactions with multiple regulatory phospholipids at different points of regulation or perhaps even during a single binding event. It is

important to note that ENTH and C1b disrupt vertex microdomain organization (Fratti et al., 2004), thus the limited release of Sec18p caused by binding $PI(4,5)P_2$ and DAG here could be due to the redistribution of PA on vacuoles.

Phosphatidic acid inhibits vacuolar fusion during the priming stage

Sec18p, like its mammalian orthologue NSF, performs the necessary priming activity within the membrane fusion cascade. During this priming step, Sec18p hydrolyzes ATP to disassemble inactive *cis*-SNARE complexes and reactivate them for additional rounds of SNARE-pairing and fusion. Sec18p priming activity is necessary for membrane fusion to occur within the cell, and its importance to organelle trafficking and maintenance is highlighted by the fact that its null mutant strains are inviable. Because its function is vital for fusion activity and cell survival, we believe Sec18p is a target for a key regulation point within the vacuolar fusion cascade. This combined with the PA-specific binding previously seen and the regulatory role of Pah1p has in membrane fusion led us to investigate whether the lipids PA and DAG had an effect on Sec18p activity and vacuolar fusion.

To measure vacuolar fusion we employed the well-characterized proPho8p maturation vacuole content mixing assay as previously described (Haas et al., 1994). To test the effects of specific lipids on fusion, we used dioctanoyl-PA (diC8-PA) and diC8-DAG (Dong et al., 2010; Siddiqui et al., 1995). We first assayed if the addition of diC8-PA or diC8-DAG showed a significant effect on overall vacuolar fusion activity. Addition of diC8-PA led to potent inhibition of vacuolar content mixing in a dose-dependent manner (Figure 2.3A), whereas adding the same concentrations of diC8-DAG did not affect fusion (Figure 2.3B). Importantly, inhibition by diC8-

PA could be reversed by the addition of recombinant Sec18p suggesting a direct interaction between the protein and lipid (Figure 2.3C). We then wanted to test if sequestering PA with the PA-specific binding domain GST-DEP would have a measureable effect on fusion activity. Addition GST-DEP had a minimal effect on fusion except at the highest concentration tested (10 μM), which reduced fusion by approximately 50% (Figure 2.3D). Higher concentrations were not used due to buffer interference with the fusion assay. The inhibition of fusion by GST-DEP is in keeping with the vacuole competition binding assay in Figure 2.2C where GST-DEP at ≥10 μM significantly displaced Sec18p from the membrane. We reason that fusion inhibition caused by addition of GST-DEP may occur at higher concentrations because of a decrease of the overall Sec18p level on the membrane to below a threshold required for priming activity to occur. Alternatively, this inhibition may be due to general crowding on the membrane and not from an inaccessibility of PA to the fusion machinery. Taken together the data suggest that increased concentrations of PA within the vacuolar membrane have an inhibitory effect on membrane fusion activities but increased concentrations of DAG do not.

Previous work suggested that Pah1p activity regulates Sec18p priming activity through its control of PA concentrations in the vacuolar membrane (Sasser et al., 2012). Because we observed Sec18p-PA binding and the inhibition of fusion by excess PA, we expected that this lipid could be potentially blocking the priming stage of the fusion cascade. To test this, we wanted to use an inhibitor that would block Sec18p activity for comparison. NEM is a known inhibitor of NSF priming activity however its effects on Sec18p-mediated priming activity have not been fully investigated. Because NEM is known to alkylate NSF we reasoned that a similar modification could take place with Sec18p and perturb priming activity. We found that NEM potently inhibited

fusion at ≥1 mM suggesting that NEM might modify and inhibit Sec18p (Figure 2.3E). To test whether diC8-PA, dic8-DAG, or NEM had priming specific inhibition we employed a variant of the content mixing assay that utilizes a Vam7p bypass of priming. Previous work has shown that priming-specific inhibition with an inhibitor such as α-Sec17p IgG can be rescued by the addition of recombinant Vam7p, a soluble SNARE protein (Fratti and Wickner, 2007; Fratti et al., 2007). We expected that a priming-specific defect caused by addition of diC8-PA or NEM should also be rescued in this manner. Surprisingly, a Vam7p bypass did not rescue fusion activity in the presence of diC8-PA or NEM (Figure 2.3F). These data suggest that diC8-PA and NEM could additionally be affecting stages downstream of priming in the fusion cascade. It should be noted that Vam7p function is related to the presence of the ABC transporter Ycf1p that contains multiple free Cys required for its activity (Sasser et al., 2013; Wei et al., 2014). Thus, alkylating Ycf1p could prevent Vam7p bypass of the effect of NEM on Sec18p. To probe whether diC8-PA or NEM could be inhibiting a later fusion stage we performed a temporal acquisition of resistance assay in which inhibitors were added at different time points throughout the fusion reaction (Mayer et al., 1996; Haas et al., 1995). Here fusion reactions gain resistance to an inhibitor once enough time had passed for its target to carry out its relevant activity. Therefore, fusion would recover at earlier time points for inhibitors that specifically target machinery early in the fusion reaction (*e.g.* α-Sec17p IgG) while inhibitors targeting later stages would gain resistance later in the reaction (*e.g.* GDI). We compared diC8-PA inhibition kinetics to that of α-Sec17p IgG, propranolol, NEM, and GDI through calculated gain of resistance half-times using first-order exponential decay fitting (Figure 2.3G) (Mayer et al., 1996; Sasser et al., 2012). Interestingly, diC8-PA showed similar recovery of fusion to that of the tethering stage inhibitor GDI (Figure 2.3H). This suggests that PA could be inhibiting fusion during a stage downstream of priming, independent of Sec18p, however

we cannot rule out that diC8-PA may be blocking additional rounds of fusion. It is important to note that these results can only point to the last stage of fusion that is targeted by an inhibitor and that PA may be regulating multiple fusion stages including priming. NEM showed early recovery of fusion similar to that of α-Sec17p IgG and propranolol suggesting that it likely has an inhibitory effect on priming activity.

Next we determined if increased levels of PA had a noticeable effect on Sec18p activity during the priming stage. To do this we examined the release of Sec17p upon Sec18p-mediated priming (Mayer et al., 1996). Sec17p associates with the membrane through binding to *cis*-SNARE complexes, which recruits Sec18p to stimulate its priming activity. Upon recruitment Sec18p hydrolyzes ATP to disassemble the *cis*-SNAREs leading to Sec17p dissociation from the membrane. Here we monitored Sec17p release by fractionating soluble and membrane-bound proteins followed by Western blotting. Vacuolar fusion assays were carried out in the presence of diC8-PA, diC8-DAG, or NEM after which we monitored the release of Sec17p from vacuolar membranes as a measure of priming. We found that NEM potently reduced Sec17p release relative to the untreated control condition, suggesting that Sec18p activity was blocked by NEM in a similar fashion to what is seen with NSF (Figure 2.4A). When diC8-PA was tested, we found that Sec17p release was severely inhibited. This is in keeping with the notion that diC8-PA inhibits priming by sequestering Sec18p. In contrast, diC8-DAG had no effect as predicted based on the content mixing assays. A previous study showed that NEM did not have an effect on Sec18p ATPase activity, however priming activity was not specifically examined (Steel et al., 1999). It is possible that Sec18p alkylation by NEM may affect its ability to disassemble *cis*-SNARE complexes in a manner independent of its ATPase activity. It is clear that in the presence of the

full fusion machinery Sec18p priming activity is inhibited by NEM. We then tested Sec18p activity on *pah1*Δ deletion vacuoles using the same priming assay to further examine the effect of increased PA on priming. As expected, vacuoles lacking *pah1*Δ showed significantly decreased levels of Sec17p release when compared to the wild type control (Figure 2.4B). Taken together, these data illustrate that priming activity is blocked by an increase in PA at the vacuole and that this inhibition is specific.

Phosphatidic acid regulates Sec18p recruitment to *cis*-SNARE complexes

Thus far we have found that *cis*-SNARE priming by Sec18p is blocked by the presence of increased PA while unaffected by the presence of increased DAG. This relationship supports the idea that the conversion of PA to DAG through PA phosphatase activity may have a regulatory role in the priming stage of fusion. Previous work showed that the PA phosphatase Pah1p had a regulatory role in endolysosomal maturation and was also proposed to regulate the localization of Sec18p on the membrane (Sasser et al., 2012). Sec18p has been shown to stay associated with the membrane throughout priming while its co-chaperone Sec17p is released (Mayer et al., 1996). This suggests that Sec18p stays attached to the membrane independently of Sec17p and SNAREs. Given our previous observations we identified PA as an alternate Sec18p membrane-binding site and asked if shifting dynamic membrane PA and DAG levels would also affect the association of Sec18p to SNAREs. To address this question, we utilized *cis*-SNARE pulldown assays in which recombinant GST-tagged Vam7p was introduced to fusion reactions in the absence of ATP to allow the formation of *cis*-SNARE complexes with free cognate SNAREs (Thorngren et al., 2004). It was previously shown that all vacuole-associated Vam7p is bound in *cis*-SNARE complexes suggesting SNARE complexes formed were appropriate Sec18p priming targets (Collins et al.,

2005). The fusion reactions were then started with the addition of ATP and pulldowns of the GST-Vam7p containing *cis*-SNARE complexes were performed across various time points. The level of Sec18p associated with the newly formed *cis*-SNARE complexes was analyzed by Western blot. To further test the effect of altering the PA:DAG ratio on priming we harvested vacuoles from *pah1*Δ strains to remove PA phosphatase activity relevant to fusion. The recruitment of Sec18p to *cis*-SNARE complexes was severely inhibited on *pah1*Δ vacuoles compared to wild type vacuoles across at each time point tested (Figure 2.5A-B). To confirm that the effect on Sec18p was only due to the lack of Pah1p, we used vacuoles from *pah1*Δ yeast complemented with plasmid-encoded *PAH1* (Sasser et al., 2012). Complementation fully reversed Sec18p recruitment to *cis*-SNARE complexes (Figure 2.5C). Addition of recombinant Pah1p also fully reversed the recruitment defect seen on *pah1*Δ vacuoles (Figure 2.5D). Taken together these data suggest that PA levels in the membrane play a significant role in the regulation of Sec18p recruitment to *cis*-SNARE complexes for priming.

To further examine the potential role PA could have in Sec18p recruitment to *cis*-SNAREs we employed a similar pulldown approach but included the addition of the small molecule inhibitor propranolol. Here we reasoned that the addition of propranolol, a known inhibitor of PA phosphatase activity, should lead to similar Sec18p-*cis*-SNARE association levels as our *pah1*Δ vacuoles. Because propranolol inhibition of vacuolar fusion can be rescued by the addition of exogenous Vam7p we instead carried out pulldowns using vacuoles that harbor the syntaxin orthologue Vam3p containing an internal calmodulin-binding domain (CBP-Vam3p) (Collins and Wickner, 2007). As expected, inhibition of Pah1p activity by the addition of propranolol significantly decreased the levels of Sec18p associated with *cis*-SNARE complexes relative to

control levels (Figure 2.6A). This is consistent with the effect seen in *pah1*Δ vacuoles and further supports a role for PA in the regulation of SNARE priming.

A previous study showed that mammalian NSF bound PA in a nucleotide-dependent fashion wherein the ADP bound state of the protein had greater binding to PA than the ATP bound state (Manifava et al., 2001). We asked if the nucleotide-bound state might also play a role in Sec18p binding to PA and ultimately its recruitment to *cis*-SNARE complexes. We reasoned that if ATP is replaced with the slowly hydrolyzable analog ATPγS, then PA binding by Sec18p could be lessened and a larger pool would be available to bind to *cis*-SNARE complexes. Sec18p is known to bind to the *cis*-SNAREs in an ATP-bound state so we expected levels associated with *cis*-SNARE complexes to be at wild type levels or greater. Using either our GST-Vam7p (not shown) or CBP-Vam3p pulldown assays, we tested the effect of ATPγS on Sec18p recruitment to *cis*-SNARE complexes. Sec18p association to SNAREs was similar to control conditions with ATP (Figure 2.6B). We next tested Sec18p interactions with PA directly using a liposome floatation assay in the presence of Mg^{2+}, EDTA, or ATPγS to assay the dependence of the nucleotide-bound state (Figure 2.6C). We observed no significant difference between the nucleotide states tested suggesting that unlike NSF, binding of Sec18p to PA was independent of such effects.

Phosphatidic acid blocks the recruitment of Sec18p to *cis*-SNARE complexes

We next wanted to determine if Pah1p could regulate Sec18p association with *cis*-SNAREs through its maintenance of membrane PA and DAG levels. The absence of Pah1p from the membrane likely increased the level of PA present, allowing the lipid to bind to Sec18p and sequester it from *cis*-SNAREs ultimately stalling its priming activity. To test this, we utilized the

GST-Vam7p pulldowns of *cis*-SNAREs as mentioned above, in the presence of inhibitory concentrations of diC8-PA or the equivalent concentration of diC8-DAG. Addition of diC8-PA abolished Sec18p association with *cis*-SNARE complexes when compared to the untreated vacuoles (Figure 2.7A). The total level of membrane-bound Sec18p was not affected. Addition of the same concentration of diC8-DAG did not significantly affect the level of Sec18p associated to *cis*-SNARE complexes compared to the control (Figure 2.7B). These findings support the idea that Pah1p could regulate Sec18p recruitment to *cis*-SNARE complexes through its maintenance of PA and DAG levels on the membrane. By controlling the dynamic levels of PA and DAG present in the vacuolar membrane, Pah1p could regulate the priming stage by affecting the localization of Sec18p.

DISCUSSION

The protein machinery involved in the regulation of membrane fusion has been well characterized, however the regulatory effects of phospholipids on these proteins are still not well understood. The dynamic changes that these lipids undergo throughout the fusion cascade are only beginning to be explored. Yeast homotypic vacuole fusion utilizes a set of regulatory lipids that helps mediate each stage in a series of defined events. Lipids likely fulfill multiple roles during membrane fusion events including controlling the physical properties of the membrane, and providing a scaffold for the protein fusion machinery to bind, and organization of proteins into microdomains where fusion occurs. These lipids are currently known to include ergosterol, phosphoinositides, DAG, and PA, which are maintained and modified by a diverse group of kinases, phosphatases, and lipases.

PA has a regulatory role in multiple fusion pathways including Glut4 trafficking, mitochondrial fusion, and prospore membrane fusion (Nakanishi et al., 2006; Vicogne et al., 2006; Choi et al., 2006). Additionally, PA has been identified as one of the minimum lipid requirements required for SNARE-dependent fusion of reconstituted proteoliposomes (RPLs) and promotes the association of Sec18p and HOPS with vacuolar SNARE RPLs (Mima and Wickner, 2009). However, it remains uncertain whether PA directly interacts with these proteins or if it participates in establishing a conducive environment for optimal protein function. PA is converted to DAG during the fusion cascade and inhibition of PA phosphatase activity blocks fusion at the priming stage. The importance of DAG in vacuole fusion is demonstrated in part by the effect of the DAG-binding domain C1b, which disrupts the organization of the vertex microdomain resulting in the potent inhibition of fusion (Fratti et al., 2004; Jun et al., 2004). DAG is a fusogenic lipid due to its negative curvature and ability to disrupt lipid bilayers (Das and Rand, 1984; Seddon, 1990). These features also allow DAG to trigger the fusion of protein-free liposomes (Sánchez-Migallón et al., 1995; Villar et al., 2000). While the potential importance of PA and DAG to vacuole fusion has been highlighted, no specific regulatory mechanisms have been described. Previously, it was found that the yeast PA phosphatase Pah1p has a significant regulatory role in the vacuolar fusion cascade suggesting that the balance of PA and DAG at the site of fusion is critical in mediating fusion related events (Sasser et al., 2012; Lawrence et al., 2014).

Our earlier studies suggested that Pah1p regulated fusion in part by triggering the priming stage of the fusion cascade (Sasser et al., 2012). We theorized that prior to engaging *cis*-SNARE complexes Sec18p resided as part of a resting pool of protein bound to the membrane in a PA-dependent manner. Pah1p activity would convert PA to DAG leading to the release of Sec18p from the

membrane facilitating its recruitment to *cis*-SNARE bundles bound to Sec17p. In keeping with this model this study showed that deletion of *PAH1* or chemical inactivation of its phosphatase activity led to the retention of Sec18p bound to the PA enriched membrane and blocking its translocation to Sec17p-bound *cis*-SNAREs. This is further bolstered by our findings that Sec18p binds preferentially to liposome membranes that contain PA. This interaction is specific as replacement of PA with other acidic or small head group lipids abolishes Sec18p binding. PA is a unique phospholipid in that it is both anionic and promotes negative membrane curvature, a property favorable for protein insertion at the head group region of the membrane bilayer (Kooijman and Burger, 2009). It is likely that a Sec18p lipid-binding site would interact with the vacuolar membrane in a way dependent on both electrostatic forces and curvature effects, however we did not detect significant binding of the protein to membranes that contained DAG, another lipid that promotes negative curvature. Considering this and the finding that Sec18p does not bind other anionic phospholipids we expect that the lipid association we observed is specific for PA. These results parallel previous work that showed the Sec18p mammalian orthologue NSF is also a PA binding protein (Manifava et al., 2001). While no sequence orthologue has been described for PA binding regions, most that have been described contain a combination of adjacent basic and hydrophobic amino acids (Kooijman and Burger, 2009). The basic residues in PA binding domains are able to preferentially bind the lipid phosphomonoester head group through hydrogen bonding as described by the electrostatic-hydrogen bond switch model (Kooijman et al., 2007). The presence of hydrophobic residues often allows for PA binding proteins to insert into the membrane and interact with adjacent lipid acyl chains (Van Den Brink-Van Der Laan et al., 2004). Based on our data, we propose that Sec18p association with PA requires electrostatic interactions between a lipid-binding region on the protein and the phosphomonoester head group of PA. This binding

is likely enhanced by surrounding hydrophobic interactions but these interactions alone are not strong enough to support the entire binding event. We propose that upon Pah1p-dependent conversion of PA to DAG, crucial electrostatic interactions between Sec18p and PA are interrupted and Sec18p is released from the membrane.

Specific lipids have been shown to be of crucial importance in regulating the different stages of membrane fusion (Boeddinghaus et al., 2002; Fratti et al., 2004; Sasser et al., 2012; Karunakaran and Fratti, 2013; Karunakaran et al., 2012; Lawrence et al., 2014; Stroupe et al., 2006; Jun et al., 2004). In this study, we show that PA has an inhibitory effect during the priming stage of fusion while DAG does not. Previous studies have shown that addition of ergosterol ligands or antibody against PI(4,5)P_2 also potently inhibit Sec18p priming activity (Kato and Wickner, 2001; Mayer et al., 2000). Interestingly, mammalian NSF does not bind PI(4,5)P_2 alone (Manifava et al., 2001). It is possible that Sec18p and NSF have distinct lipid interactions, however it is also important to consider the roles of both ergosterol and PI(4,5)P_2 at the site of fusion. Each of these lipids is a requirement for functional microdomain formation at the vertex ring (Fratti et al., 2004). Disruption of these microdomains with exogenous ligands may compromise the organization of necessary protein and lipid machinery at the site of fusion ultimately resulting in a priming defect. We have demonstrated direct physical interaction between Sec18p and PA, and we believe this association accounts for PA-specific priming inhibition.

There are two primary ways that we considered PA could inhibit the priming activity of Sec18p directly. First, PA could decrease the ability of Sec18p to disassociate *cis*-SNARE complexes through allosteric effects. Alternatively, PA could act to sequester Sec18p away from *cis*-SNARE

complexes effectively stalling priming. In this study, we provide evidence in accord with the latter possibility. We observed a decrease in recruitment of Sec18p to *cis*-SNAREs on vacuoles from a *pah1*Δ deletion strain, as well as by inhibition of PA phosphatase activity with propranolol, and upon addition of exogenous PA. Taken together, we propose that dynamic PA and DAG levels mediate Sec18p localization on the vacuolar membrane and recruitment to *cis*-SNARE complexes.

The stark contrast in effects that PA and DAG have on priming activity frame Pah1p as a potential initiator of the fusion cascade. Reactivation of SNAREs and turnover of fusion may be controlled by Pah1p through its modulation of local PA concentrations at the vertex ring. We propose a model in which Sec18p is initially recruited to the vacuolar membrane through binding to organized PA pools (Figure 2.8). Once recruited, Sec18p remains bound to PA pools where it is unable to access SNAREs during non-priming stages of fusion. Upon completion of compartment fusion and generation of *cis*-SNAREs, Pah1p converts pools of PA to DAG effectively lowering local PA concentrations. Sec18p is freed from the membrane and is able to be recruited to *cis*-SNARE complexes for priming. It is possible that conversion of PA to other regulatory phospholipids through a CDP-DAG intermediate may also serve as an initiator of priming. Under this model, PA could serve as a global regulator of Sec18p localization in the cell. However, previous work has shown that Sec18p levels at the vacuole are not increased in *pah1*Δ cells (Sasser et al., 2012). It is possible that there is an upper limit to PA dependent membrane association of Sec18p, or there may be compensatory enzymatic activity of other lipid modifiers such as Phospholipase D. Further work is needed to investigate these possibilities and probe organelle specificity of Sec18p regulation by PA.

While the PA binding region of Sec18p/NSF is not clear, the potential effects of this lipid interaction are interesting to consider. The role of each of the three domains in Sec18p/NSF has been previously described, and binding of any of these to PA could have inhibitory effects on its overall function. The nucleotide binding domains of Sec18p/NSF (D1 and D2) are responsible for ATPase activity and formation of a homohexamer respectively (Whiteheart et al., 1994; Hanson et al., 1997). It is possible that PA binds to the D1 domain and disrupts the ability of Sec18p to hydrolyze ATP making it unable to generate the necessary force for *cis*-SNARE complex disruption. It is also possible that PA binds to the D2 domain and blocks the formation of the active Sec18p homohexamer. This could force Sec18p into a monomeric state preventing it from effectively associating with *cis*-SNARE complexes. The N-terminal domain of Sec18p is responsible for association with Sec17p and *cis*-SNARE complexes (Babor and Fass, 1999). Binding of the N-terminal domain to PA could block the basic groove needed for Sec17p binding preventing recruitment of Sec18p to *cis*-SNARE complexes. This potential association of the N-terminal domain to PA is consistent with our observations and model, however additional work is necessary to identify the specific PA binding region of Sec18p to understand the mechanism of this regulation.

It is clear that phosphatidic acid can modulate membrane fusion through its control of Sec18p priming activity at the vacuole. Additional work is needed to identify the PA-binding region on Sec18p. Also of interest will be determining the upstream regulation of PA content on the vacuole. PA is produced from DAG by Dgk1p, from PC by Spo14p, and from PE by PE-PLD making all of these enzymes potential regulators of SNARE priming (Han et al., 2008; Sreenivas et al., 1998; Waksman et al., 1997). Sec18p regulation by phosphatidic acid provides another example of the

highly organized interplay between protein and lipid machinery that helps to carry out membrane fusion and trafficking events.

FIGURES

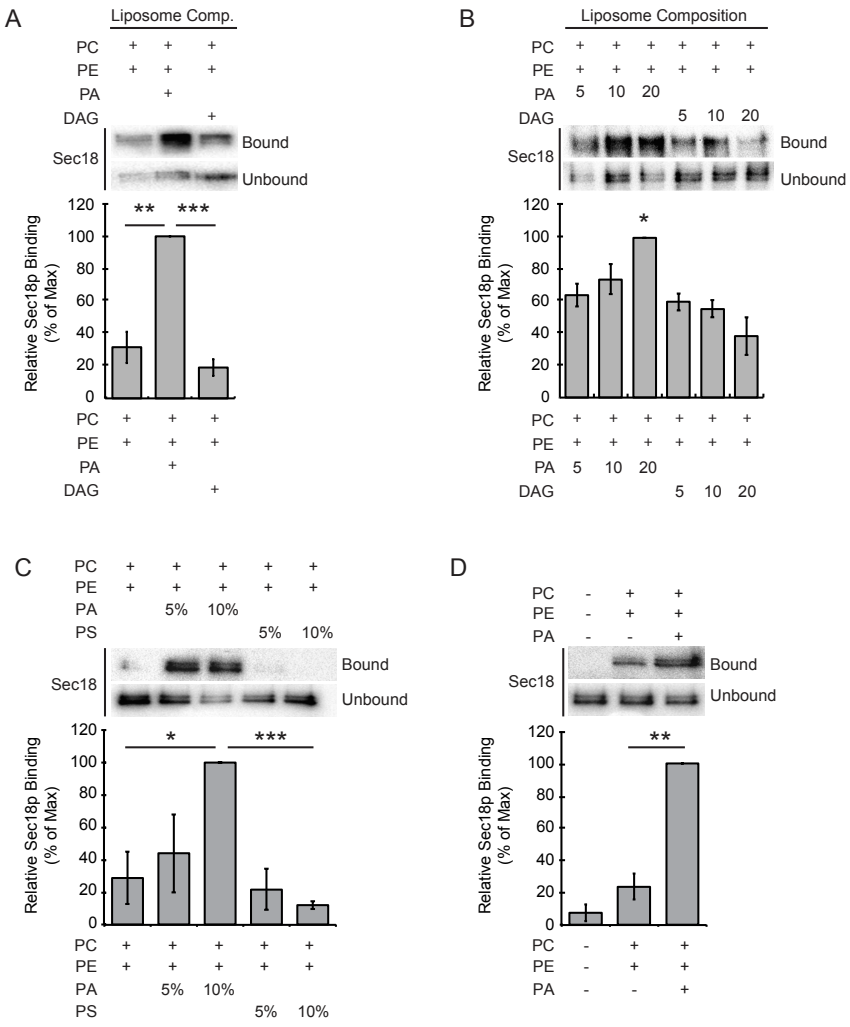

Figure 2.1. Sec18p preferentially binds to liposomes containing phosphatidic acid. Recombinant His_6-Sec18p (2 μg) was incubated with liposomes of the indicated compositions for 10 min at 30°C. Liposomes were isolated by centrifugation and washed with 1X PBS before bound proteins were resolved by SDS-PAGE. Bar graphs show average normalized densitometry values measured for 3 separate experiments. Binding was observed in liposomes with PA or DAG (A), with increasing concentrations of PA or DAG (B), with increasing concentrations of PA or PS (C), and with no liposomes (D). * P<0.05; ** P<0.001; *** P<0.0001

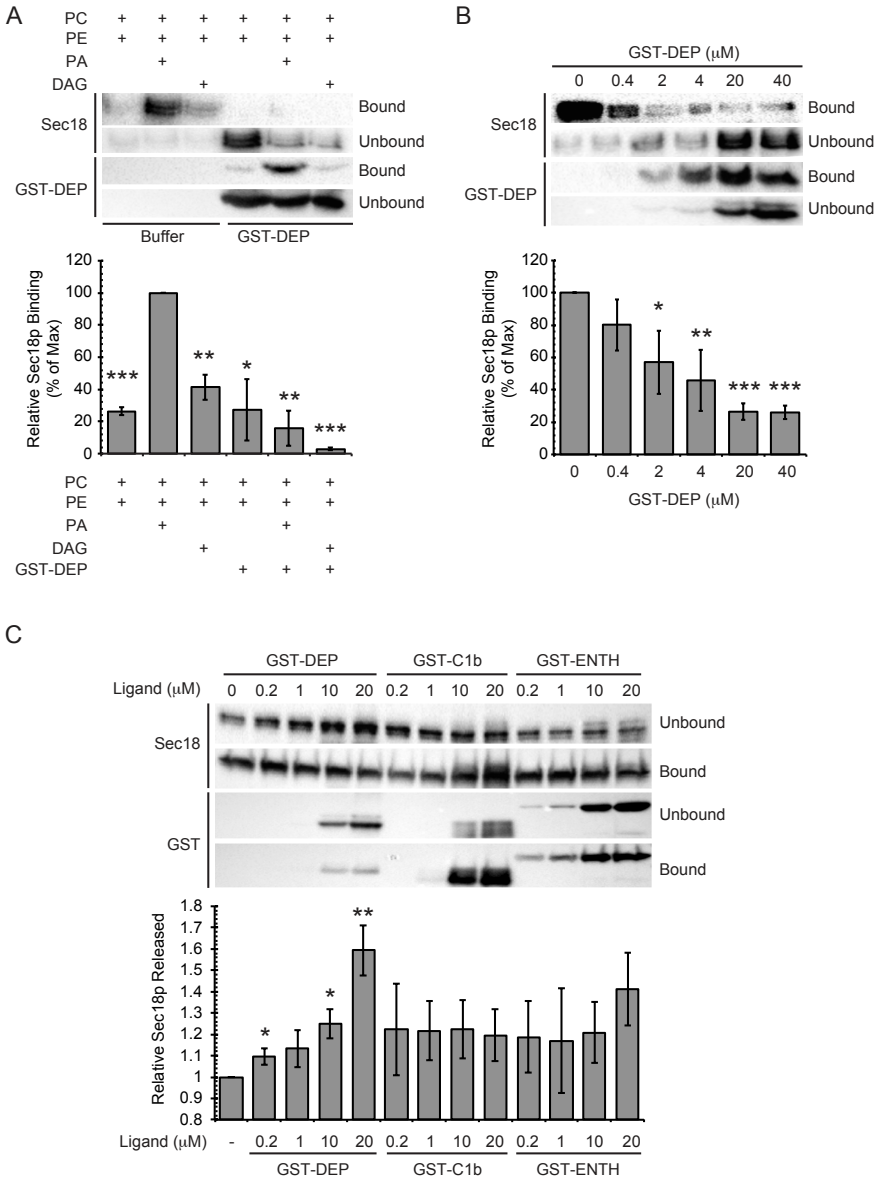

Figure 2.2. The PA-binding domain DEP reduces Sec18p binding to membranes. (A) Liposomes of the indicated compositions were incubated without Dvl2-DEP or with 20 μM Dvl2-DEP for 5 min at 30°C. Recombinant His_6-Sec18p (2 μg) was added to the sample and incubated for 10 min at 30°C. (B) GST-DEP titration and Sec18p binding to liposomes was performed as described above in the presence of the indicated concentrations of GST-DEP. (C) Vacuoles were harvested from wild type DKY6281 and incubated with GST-DEP, GST-C1b domain, or GST-ENTH domain. Bound and unbound fractions were separated by centrifugation and resolved by SDS PAGE. Bar graphs show the percentage of unbound Sec18p in each sample normalized to wild type control. * P<0.05; ** P<0.001; *** P<0.0001.

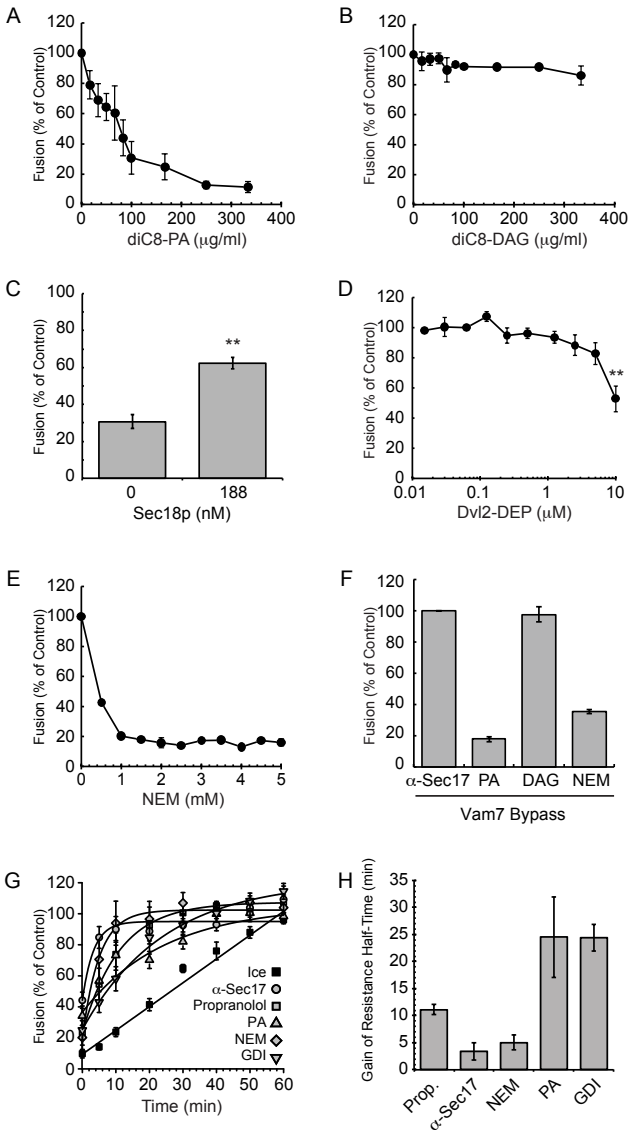

Figure 2.3. Addition of exogenous phosphatidic acid or *N*-ethylmaleimide causes a severe membrane fusion defect. Vacuoles were harvested from wild type BJ3505 and DKY6281 and tested for fusion by luminal mixing and proPho8p maturation. Fusion reactions containing 3 μg of each vacuole type were incubated in the presence of diC8-PA (A), or diC8-DAG (B) at the indicated concentrations. (C) Fusion reactions containing 100 μg/ml diC8-PA were incubated in the presence of 188 nM recombinant Sec18p. Fusion reactions containing 3 μg of each vacuole type were incubated in the presence of GST-DEP (D) or NEM (E) at the indicated concentrations. Fusion results were normalized to untreated wild type vacuoles at standard conditions. (F) Exogenous recombinant Vam7p (200 nM) was used to bypass fusion inhibitors. (G) Gain of resistance kinetics assays were performed in the presence of 140 μg/ml α-Sec17p IgG, 2 mM propranolol, 300 μM diC8-PA, 1 mM NEM, or PS buffer. Data was fit using first-order exponential decay with weights and errors. (H) Calculated half-times from first-order exponential decay fit. ** P<0.001.

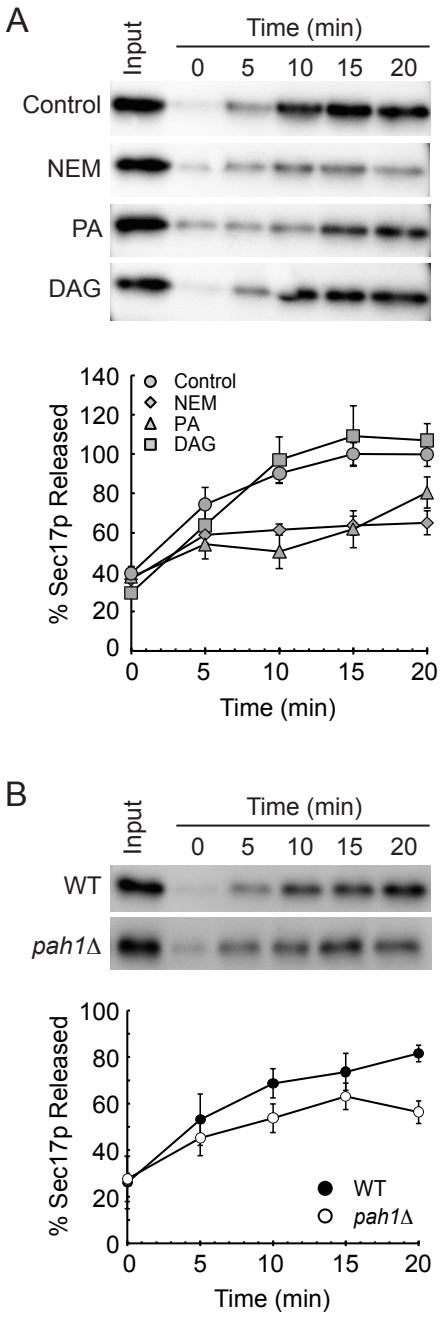

Figure 2.4. Addition of exogenous phosphatidic acid but not diacylglycerol inhibits the priming activity of Sec18p. (A) Vacuoles from BJ3505 yeast were assayed for priming activity as detected by the release of Sec17p from the membrane fraction. Fusion reactions of 3 μg of vacuoles were incubated in the presence of buffer, 1 mM NEM, 300 μM diC8-PA, or 300 μM diC8-DAG. Vacuoles were pelleted by centrifugation at the indicated times and proteins in the supernatant fraction were resolved by SDS-PAGE and imaged by Western blot. Densitometry values were normalized against input sample for each condition. Graphs show the normalized averages (n=3). (B) Vacuoles from BJ3505 and *pah1*Δ yeast were assayed for priming activity as described in (A). Graph shows the normalized averages (n=3).

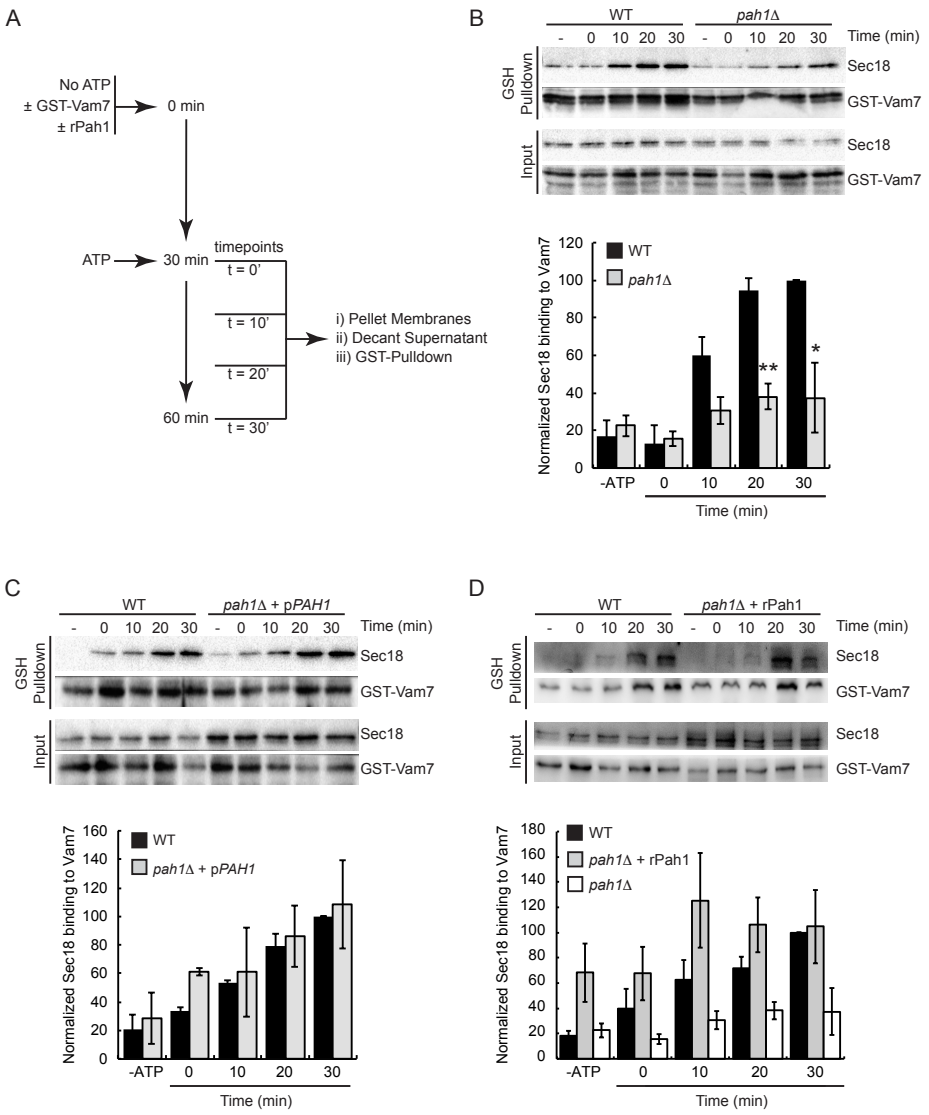

Figure 2.5. Vacuoles from a *pah1*Δ deletion strain have a decrease in the level of Sec18p bound to *cis*-SNARE complexes. Vacuoles were harvested from BJ3505, RFY17 (BJ3505 *pah1*Δ), and RFY19 (BJ3505 *pah1*Δ, p*PAH1*) strains and assayed for Sec18p binding to *cis*-SNARE complexes. (A) Recombinant GST-Vam7p was added to fusion reactions and incubated at 27°C for 30 min in the absence of ATP to allow formation of *cis*-SNARE complexes containing GST-Vam7p. Next, ATP regenerating system was added and the samples were incubated at 27°C for the indicated times before vacuoles were isolated by centrifugation and solubilized. Glutathione Sepharose was used to pull down GST-Vam7p and attached proteins were resolved by SDS-PAGE and imaged by Western blot. (B) WT versus *pah1*Δ vacuoles. (C) WT versus *pah1*Δ + p*PAH1* vacuoles. (D) WT versus *pah1*Δ vacuoles + 200 µg/ml rPah1p. Densitometry values for Sec18p pull down were normalized against the corresponding pull down Vam7p value. Graph shows the normalized average ratios (n=3). The white bars represent the *pah1*Δ pulldown data from panel B. This is to facilitate visualization of the effect of adding recombinant Pah1. * $P<0.05$; ** $P<0.001$.

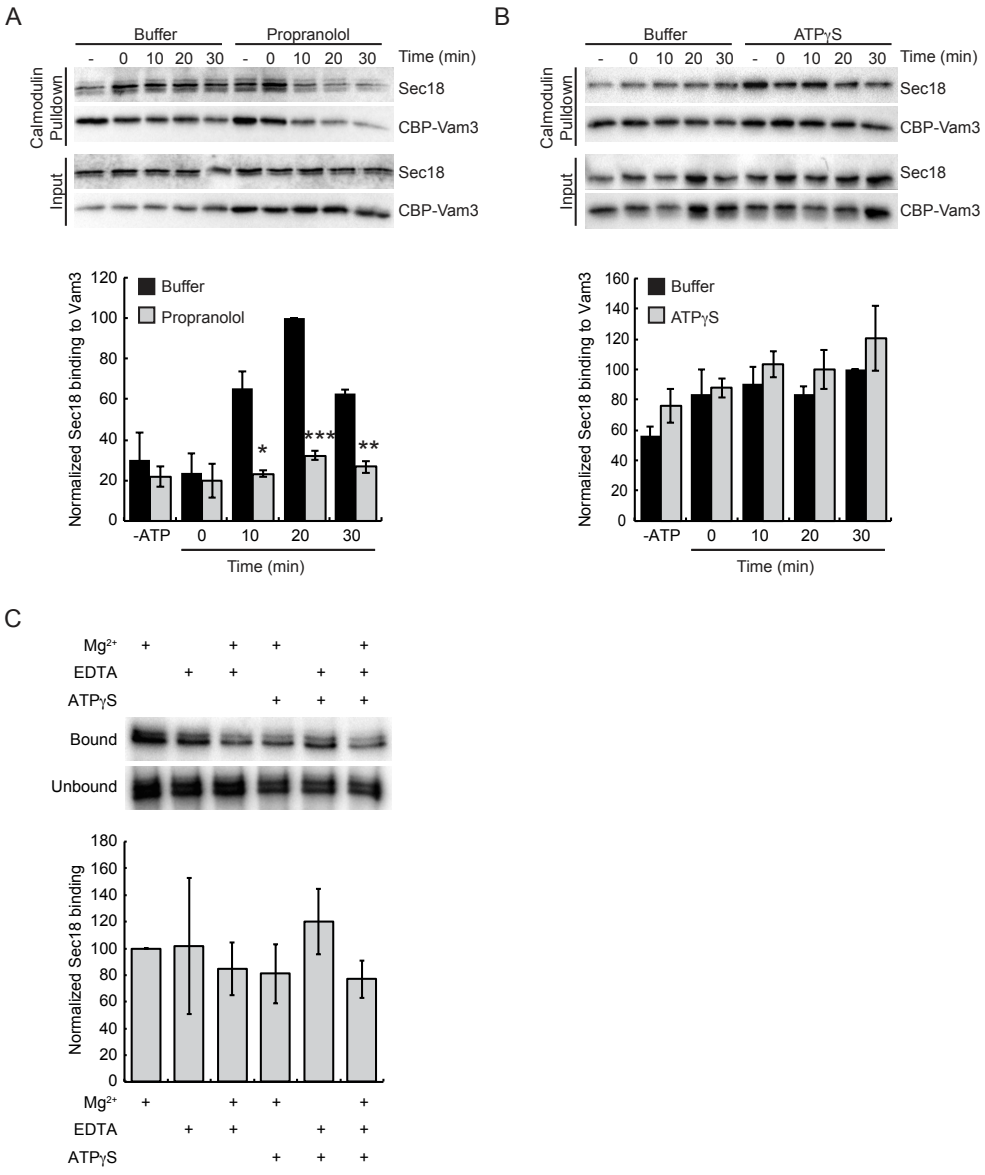

Figure 2.6. Vacuoles treated with the Pah1p inhibitor propranolol have a decreased level of Sec18p bound to *cis*-SNARE complexes. Vacuoles were harvested from BJ3505 yeast expressing CBP-Vam3p and assayed for Sec18p binding to *cis*-SNARE complexes. Fusion reactions were incubated at 27°C for the indicated times in the presence of propranolol or ATPγS or fusion buffer. At the indicated times, vacuoles were isolated by centrifugation and solubilized. Calmodulin agarose was used to pull down CBP-Vam3p and attached proteins were resolved by SDS-PAGE and imaged by immunoblotting. Fusion reactions were treated with PS buffer, 2 mM propranolol (A) or 1 mM ATPγS (B). (C) Liposome binding and effect of the nucleotide-binding state of Sec18p was tested using liposomes containing 10% PA. His_6-Sec18p (2 μg) was incubated with PA liposomes in binding buffer alone or in the presence of 1 mM Mg^{2+}, 1 mM EDTA, or 1 mM ATPγS. Densitometry values for Sec18p pull down were normalized against the

Figure 2.6 (cont.)
corresponding pull down Vam7p value. Graph shows the normalized average ratios (n=3). * $P<0.05$; ** $P<0.001$; *** $P<0.0001$.

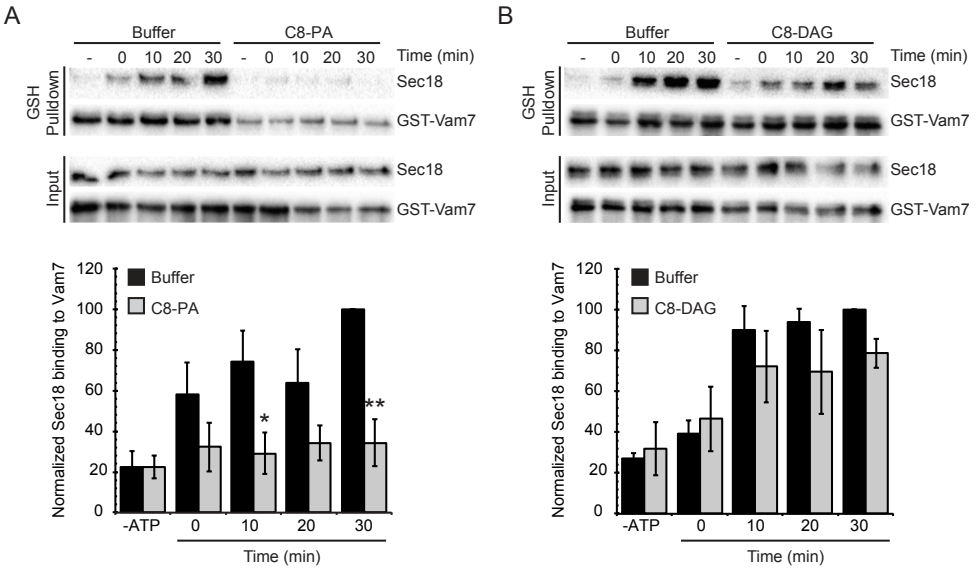

Figure 2.7. Vacuoles treated with diC8-PA have a decrease in the level of Sec18p bound to *cis*-SNARE complexes. Vacuoles were harvested from BJ3505 and assayed for Sec18p binding to *cis*-SNARE complexes. Recombinant GST-Vam7p was added to fusion reactions and incubated at 27°C for 30 min in the absence of ATP to allow formation of *cis*-SNARE complexes containing GST-Vam7p. Next, ATP regenerating system was added and the samples were incubated at 27°C for the indicated times before vacuoles were isolated by centrifugation and solubilized. Glutathione Sepharose was used to pull down GST-Vam7p and protein complexes were resolved by SDS-PAGE and examined by Western blot. Fusion reactions were treated with PS buffer, 300 μM diC8-PA (A) or 300 μM diC8-DAG (B). Densitometry values for Sec18p pull down were normalized against the corresponding pull down Vam7p value. Graph shows the normalized average ratios (n=3). * $P<0.05$; ** $P<0.001$.

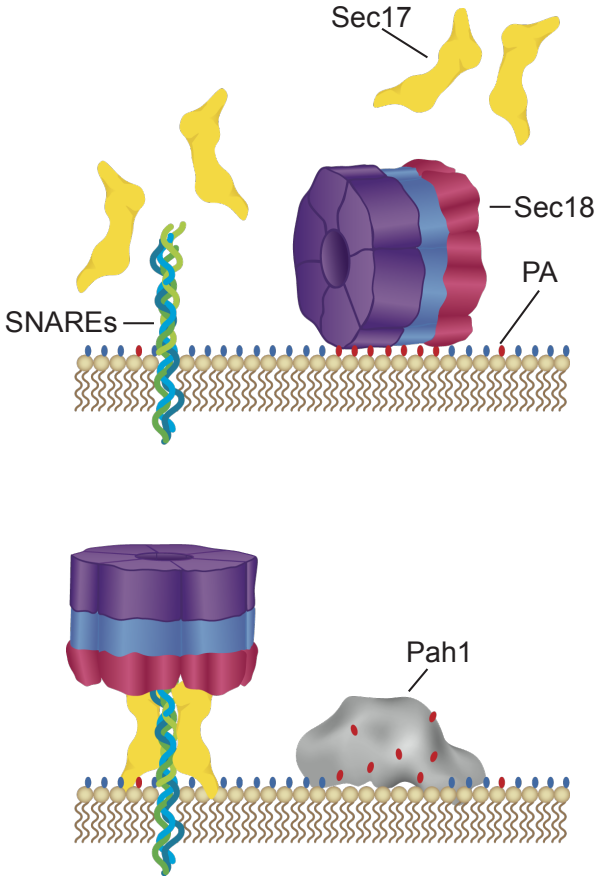

Figure 2.8. Working model of Sec18p regulation by PA. Sec18p associates with vacuole membranes through direct interactions with PA. Upon PA hydrolysis by Pah1p, Sec18p is no longer sequestered on the membrane away from *cis*-SNAREs and is recruited to them to carry out priming activity. Red ovals depict PA's phosphate head group. Blue ovals depict generic lipid head groups.

REFERENCES

Aslanidis, C., and P.J. de Jong. 1990. Ligation-independent cloning of PCR products (LIC-PCR). *Nucleic Acids Res.* doi:10.1093/nar/18.20.6069.

Babor, S.M., and D. Fass. 1999. Crystal structure of the Sec18p N-terminal domain. *Proc. Natl. Acad. Sci. U. S. A.* doi:10.1073/pnas.96.26.14759.

Barbosa, A.D., H. Sembongi, W.-M. Su, S. Abreu, F. Reggiori, G.M. Carman, and S. Siniossoglou. 2015. Lipid partitioning at the nuclear envelope controls membrane biogenesis. *Mol. Biol. Cell*. doi:10.1091/mbc.E15-03-0173.

Boeddinghaus, C., A.J. Merz, R. Laage, and C. Ungermann. 2002. A cycle of Vam7p release from and PtdIns 3-P-dependent rebinding to the yeast vacuole is required for homotypic vacuole fusion. *J. Cell Biol.* doi:10.1083/jcb.200112098.

Capelluto, D.G.S., X. Zhao, A. Lucas, J.A. Lemkul, S. Xiao, X. Fu, F. Sun, D.R. Bevan, and C. V. Finkielstein. 2014. Biophysical and molecular-dynamics studies of phosphatidic acid binding by the Dvl-2 DEP domain. *Biophys. J.* doi:10.1016/j.bpj.2014.01.032.

Cheever, M.L., T.K. Sato, T. De Beer, T.G. Kutateladze, S.D. Emr, and M. Overduin. 2001. Phox domain interaction with Ptdlns(3)P targets the Vam7 t-SNARE to vacuole membranes. *Nat. Cell Biol.* doi:10.1038/35083000.

Choi, H.S., W.M. Su, J.M. Morgan, G.S. Han, Z. Xu, E. Karanasios, S. Siniossoglou, and G.M. Carman. 2011. Phosphorylation of phosphatidate phosphatase regulates its membrane association and physiological functions in Saccharomyces cerevisiae: Identification of SER602, THR723, and SER744as the sites phosphorylated by CDC28 (CDK1)-encoded cyclin-dependent kinas. *J. Biol. Chem.* doi:10.1074/jbc.M110.155598.

Choi, S.Y., P. Huang, G.M. Jenkins, D.C. Chan, J. Schiller, and M.A. Frohman. 2006. A common lipid links Mfn-mediated mitochondrial fusion and SNARE-regulated exocytosis. *Nat. Cell Biol.* doi:10.1038/ncb1487.

Collins, K.M., N.L. Thorngren, R.A. Fratti, and W.T. Wickner. 2005. Sec17p and HOPS, in distinct SNARE complexes, mediate SNARE complex disruption or assembly for fusion. *EMBO J.* doi:10.1038/sj.emboj.7600658.

Collins, K.M., and W.T. Wickner. 2007. trans-SNARE complex assembly and yeast vacuole membrane fusion. *Proc. Natl. Acad. Sci.* doi:10.1073/pnas.0702290104.

Das, S., and R.P. Rand. 1984. Diacylglycerol causes major structural transitions in phospholipid bilayer membranes. *Biochem. Biophys. Res. Commun.* doi:10.1021/bi00358a022.

Dong, X., D. Shen, X. Wang, T. Dawson, X. Li, Q. Zhang, X. Cheng, Y. Zhang, L.S. Weisman, M. Delling, and H. Xu. 2010. PI(3,5)P2 controls membrane trafficking by direct activation of mucolipin Ca2+ release channels in the endolysosome. *Nat. Commun.* doi:10.1038/ncomms1037.

Fernández-Ulibarri, I., M. Vilella, F. Lázaro-Diéguez, E. Sarri, S.E. Martínez, N. Jiménez, E. Claro, I. Mérida, K.N.J. Burger, and G. Egea. 2007. Diacylglycerol Is Required for the Formation of COPI Vesicles in the Golgi-to-ER Transport Pathway. *Mol. Biol. Cell.* doi:10.1091/mbc.E07.

Fratti, R.A., K.M. Collins, C.M. Hickey, and W. Wickner. 2007. Stringent 3Q·1R composition of the SNARE 0-layer can be bypassed for fusion by compensatory SNARE mutation or by lipid bilayer modification. *J. Biol. Chem.* doi:10.1074/jbc.M700971200.

Fratti, R.A., Y. Jun, A.J. Merz, N. Margolis, W. Wickner, and B. Wickner. 2004. Interdependent assembly of specific regulatory lipids and membrane fusion proteins into the vertex ring

domain of docked vacuoles. *J. Cell Biol.* doi:10.1083/jcb.200409068.

Fratti, R.A., and W. Wickner. 2007. Distinct targeting and fusion functions of the PX and SNARE domains of yeast vacuolar Vam7p. *J. Biol. Chem.* doi:10.1074/jbc.M700584200.

Haas, a, and W. Wickner. 1996. Homotypic vacuole fusion requires Sec17p (yeast alpha-SNAP) and Sec18p (yeast NSF). *EMBO J.*

Haas, A., B. Conradt, and W. Wickner. 1994. G-protein ligands inhibit in vitro reactions of vacuole inheritance. *J. Cell Biol.* doi:10.1083/jcb.126.1.87.

Haas, A., D. Scheglmann, T. Lazar, D. Gallwitz, and W. Wickner. 1995. The GTPase Ypt7p of Saccharomyces cerevisiae is required on both partner vacuoles for the homotypic fusion step of vacuole inheritance. *EMBO J.*

Han, G.S., L. O'Hara, G.M. Carman, and S. Siniossoglou. 2008. An unconventional diacylglycerol kinase that regulates phospholipid synthesis and nuclear membrane growth. *J. Biol. Chem.* doi:10.1074/jbc.M802903200.

Han, G.S., S. Siniossoglou, and G.M. Carman. 2007. The cellular functions of the yeast lipin homolog Pah1p are dependent on its phosphatidate phosphatase activity. *J. Biol. Chem.* doi:10.1074/jbc.M705777200.

Hanson, P.I., R. Roth, H. Morisaki, R. Jahn, and J.E. Heuser. 1997. Structure and conformational changes in NSF and its membrane receptor complexes visualized by quick-freeze/deep-etch electron microscopy. *Cell*. doi:10.1016/S0092-8674(00)80512-7.

Jahn, R., T. Lang, and T.C. Südhof. 2003. Membrane fusion. *Cell*. doi:10.1016/S0092-8674(03)00112-0.

Jahn, R., and T.C. Südhof. 1999. Membrane Fusion and Exocytosis. *Annu. Rev. Biochem.* doi:10.1146/annurev.biochem.68.1.863.

Johnson, J.E., J. Giorgione, and A.C. Newton. 2000. The C1 and C2 domains of protein kinase C are independent membrane targeting modules, with specificity for phosphatidylserine conferred by the C1 domain. *Biochemistry*. doi:10.1021/bi000902c.

Jun, Y., R.A. Fratti, and W. Wickner. 2004. Diacylglycerol and its formation by phospholipase C regulate Rab- and SNARE-dependent yeast vacuole fusion. *J. Biol. Chem.* doi:10.1074/jbc.M411363200.

Karanasios, E., G.-S. Han, Z. Xu, G.M. Carman, and S. Siniossoglou. 2010. A phosphorylation-regulated amphipathic helix controls the membrane translocation and function of the yeast phosphatidate phosphatase. *Proc. Natl. Acad. Sci.* doi:10.1073/pnas.1007974107.

Karunakaran, S., and R.A. Fratti. 2013. The Lipid Composition and Physical Properties of the Yeast Vacuole Affect the Hemifusion-Fusion Transition. *Traffic*. doi:10.1111/tra.12064.

Karunakaran, S., T. Sasser, S. Rajalekshmi, and R. a. Fratti. 2012. SNAREs, HOPS and regulatory lipids control the dynamics of vacuolar actin during homotypic fusion in S. cerevisiae. *J. Cell Sci.* doi:10.1242/jcs.091900.

Kato, M., and W. Wickner. 2001. Ergosterol is required for the Sec18/ATP-dependent priming step of homotypic vacuole fusion. *EMBO J.* doi:10.1093/emboj/20.15.4035.

Kooijman, E.E., and K.N.J. Burger. 2009. Biophysics and function of phosphatidic acid: a molecular perspective. *Biochim Biophys Acta*. doi:S1388-1981(09)00093-6 [pii]\r10.1016/j.bbalip.2009.04.001.

Kooijman, E.E., D.P. Tieleman, C. Testerink, T. Munnik, D.T.S. Rijkers, K.N.J. Burger, and B. De Kruijff. 2007. An electrostatic/hydrogen bond switch as the basis for the specific interaction of phosphatidic acid with proteins. *J. Biol. Chem.* doi:10.1074/jbc.M609737200.

Lawrence, G., C.C. Brown, B.A. Flood, S. Karunakaran, M. Cabrera, M. Nordmann, C.

Ungermann, and R.A. Fratti. 2014. Dynamic association of the PI3P-interacting Mon1-Ccz1 GEF with vacuoles is controlled through its phosphorylation by the type 1 casein kinase Yck3. *Mol. Biol. Cell*. doi:10.1091/mbc.E13-08-0460.

Li, S.C., and P.M. Kane. 2009. The yeast lysosome-like vacuole: Endpoint and crossroads. *Biochim. Biophys. Acta - Mol. Cell Res.* doi:10.1016/j.bbamcr.2008.08.003.

Liu, S., K.A. Wilson, T. Rice-stitt, A.M. Neiman, and J.A. Mcnew. 2007. In vitro fusion catalyzed by the sporulation-specific t-sNARE light-chain Spo20p is stimulated by phosphatidic acid. *Traffic*. doi:10.1111/j.1600-0854.2007.00628.x.

Manifava, M., J.W.J.F. Thuring, Z.Y. Lim, L. Packman, A.B. Holmes, and N.T. Ktistakis. 2001. Differential Binding of Traffic-related Proteins to Phosphatidic Acid- or Phosphatidylinositol (4,5)-Bisphosphate-coupled Affinity Reagents. *J. Biol. Chem.* doi:10.1074/jbc.M010308200.

Matsuoka, K., Y. Morimitsu, K. Uchida, and R. Schekman. 1998. Coat assembly directs v-SNARE concentration into synthetic COPII vesicles. *Mol. Cell*. doi:10.1016/S1097-2765(00)80168-9.

Matveeva, E.A., S.W. Whiteheart, T.C. Vanaman, and J.T. Slevin. 2001. Phosphorylation of the N-Ethylmaleimide-sensitive Factor Is Associated with Depolarization-dependent Neurotransmitter Release from Synaptosomes. *J. Biol. Chem.* doi:10.1074/jbc.M007394200.

Mayer, A., D. Scheglmann, S. Dove, A. Glatz, W. Wickner, and A. Haas. 2000. Phosphatidylinositol 4,5-Bisphosphate Regulates Two Steps of Homotypic Vacuole Fusion. *Mol. Biol. Cell*. doi:10.1091/mbc.11.3.807.

Mayer, A., and W. Wickner. 1997. Docking of yeast vacuoles is catalyzed by the ras-like

GTPase Ypt7p after symmetric priming by Sec18p (NSF). *J. Cell Biol.* doi:10.1083/jcb.136.2.307.

Mayer, A., W. Wickner, and A. Haas. 1996. Sec18p (NSF)-driven release of Sec17p (α-SNAP) can precede docking and fusion of yeast vacuoles. *Cell*. doi:10.1016/S0092-8674(00)81084-3.

Mima, J., and W. Wickner. 2009. Complex lipid requirements for SNARE-and SNARE chaperone-dependent membrane fusion. *J. Biol. Chem.* doi:10.1074/jbc.M109.010223.

Nakanishi, H., M. Morishita, C.L. Schwartz, A. Coluccio, J. Engebrecht, and A.M. Neiman. 2006. Phospholipase D and the SNARE Sso1p are necessary for vesicle fusion during sporulation in yeast. *J. Cell Sci.* doi:10.1242/jcs.02841.

O'Hara, L., G.S. Han, P.C. Sew, N. Grimsey, G.M. Carman, and S. Siniossoglou. 2006. Control of phospholipid synthesis by phosphorylation of the yeast lipin Pah1p/Smp2p Mg2+-dependent phosphatidate phosphatase. *J. Biol. Chem.* doi:10.1074/jbc.M606654200.

Reese, C., and A. Mayer. 2005. Transition from hemifusion to pore opening is rate limiting for vacuole membrane fusion. *J. Cell Biol.* doi:10.1083/jcb.200510018.

Rosenthal, J.A., H. Chen, V.I. Slepnev, L. Pellegrini, A.E. Salcini, P.P. Di Fiore, and P. De Camilli. 1999. The epsins define a family of proteins that interact with components of the clathrin coat and contain a new protein module. *J. Biol. Chem.* doi:10.1074/jbc.274.48.33959.

Ryu, J.K., D. Min, S.H. Rah, S.J. Kim, Y. Park, H. Kim, C. Hyeon, H.M. Kim, R. Jahn, and T.Y. Yoon. 2015. Spring-loaded unraveling of a single SNARE complex by NSF in one round of ATP turnover. *Science (80-.).* doi:10.1126/science.aaa5267.

Sánchez-Migallón, M.P., F.J. Aranda, and J.C. Gómez-Fernández. 1995. The dissimilar effect of

diacylglycerols on Ca(2+)-induced phosphatidylserine vesicle fusion. *Biophys. J.* 68:558–566. doi:10.1016/S0006-3495(95)80217-1.

Sasser, T., Q.S. Qiu, S. Karunakaran, M. Padolina, A. Reyes, B. Flood, S. Smith, C. Gonzales, and R.A. Fratti. 2012. Yeast lipin 1 orthologue Pah1p regulates vacuole homeostasis and membrane fusion. *J. Biol. Chem.* doi:10.1074/jbc.M111.317420.

Sasser, T.L., G. Lawrence, S. Karunakaran, C. Brown, and R.A. Fratti. 2013. The yeast ATP-binding cassette (ABC) transporter Ycf1p enhances the recruitment of the soluble SNARE Vam7p to vacuoles for efficient membrane fusion. *J. Biol. Chem.* doi:10.1074/jbc.M112.441089.

Seals, D.F., G. Eitzen, N. Margolis, W.T. Wickner, and A. Price. 2000. A Ypt/Rab effector complex containing the Sec1 homolog Vps33p is required for homotypic vacuole fusion. *Proc. Natl. Acad. Sci.* doi:10.1073/pnas.97.17.9402.

Seddon, J.M. 1990. An Inverse Face-Centered Cubic Phase Formed by Diacylglycerol-Phosphatidylcholine Mixtures. *Biochemistry*. doi:10.1021/bi00486a031.

Siddiqui, R.A., D. English, K. Harvey, Y. Cui, M.I. Martin, J. Wentland, L. Akard, J. Jansen, J. Thompson, and J.G.N. Garcia. 1995. Phorbol ester-induced priming of superoxide generation by phosphatidic acid-stimulated neutrophils and granule-free neutrophil cytoplasts. *J. Leukoc. Biol.* doi:10.1002/jlb.58.2.189.

Sreenivas, A., J.L. Patton-Vogt, V. Bruno, P. Griac, and S.A. Henry. 1998. A role for phospholipase D (Pld1p) in growth, secretion, and regulation of membrane lipid synthesis in yeast. *J. Biol. Chem.* doi:10.1074/jbc.273.27.16635.

Steel, G.J., A.J. Laude, A. Boojawan, D.J. Harvey, and A. Morgan. 1999. Biochemical analysis of the Saccharomyces cerevisiae SEC18 gene product: implications for the molecular

mechanism of membrane fusion. *Biochemistry*. doi:10.1021/bi990315v.

Stroupe, C., K.M. Collins, R.A. Fratti, and W. Wickner. 2006. Purification of active HOPS complex reveals its affinities for phosphoinositides and the SNARE Vam7p. *EMBO J.* doi:10.1038/sj.emboj.7601051.

Studier, F.W. 2005. Protein production by auto-induction in high-density shaking cultures. *Protein Expr. Purif.* doi:10.1016/j.pep.2005.01.016.

Thorngren, N., K.M. Collins, R.A. Fratti, W. Wickner, and A.J. Merz. 2004. A soluble SNARE drives rapid docking, bypassing ATP and Sec17/18p for vacuole fusion. *EMBO J.* doi:10.1038/sj.emboj.7600286.

Ungermann, C., K. Sato, and W. Wickner. 1998. Defining the functions of trans-SNARE pairs. *Nature*. doi:10.1038/25069.

Van Den Brink-Van Der Laan, E., V. Chupin, J.A. Killian, and B. De Kruijff. 2004. Small alcohols destabilize the KcsA tetramer via their effect on the membrane lateral pressure. *Biochemistry*. doi:10.1021/bi0496079.

Vicogne, J., D. Vollenweider, J.R. Smith, P. Huang, M.A. Frohman, and J.E. Pessin. 2006. Asymmetric phospholipid distribution drives in vitro reconstituted SNARE-dependent membrane fusion. *Proc. Natl. Acad. Sci. U. S. A.* doi:10.1073/pnas.0606881103.

Villar, A. V., A. Alonso, and F.M. Goni. 2000. Leaky vesicle fusion induced by phosphatidylinositol-specific phospholipase C: Observation of mixing of vesicular inner monolayers. *Biochemistry*. doi:10.1021/bi992515c.

Waksman, M., X. Tang, Y. Eli, J.E. Gerst, and M. Liscovitch. 1997. Identification of a novel Ca2+-dependent, phosphatidylethanolamine- hydrolyzing phospholipase D in yeast bearing a disruption in PLD1. *J. Biol. Chem.* doi:10.1074/jbc.272.1.36.

Wang, L., A.J. Merz, K.M. Collins, and W. Wickner. 2003. Hierarchy of protein assembly at the vertex ring domain for yeast vacuole docking and fusion. *J. Cell Biol.* doi:10.1083/jcb.200209095.

Wang, L., E.S. Seeley, W. Wickner, and A.J. Merz. 2002. Vacuole fusion at a ring of vertex docking sites leaves membrane fragments within the organelle. *Cell*. doi:10.1016/S0092-8674(02)00632-3.

Wei, W., N. Smith, X. Wu, H. Kim, J. Seravalli, O. Khalimonchuk, and J. Lee. 2014. YCF1-Mediated Cadmium Resistance in Yeast Is Dependent on Copper Metabolism and Antioxidant Enzymes. *Antioxid. Redox Signal.* doi:10.1089/ars.2013.5436.

Whiteheart, S.W., K. Rossnagel, S.A. Buhrow, M. Brunner, R. Jaenicke, and J.E. Rothman. 1994. N-ethylmaleimide-sensitive fusion protein: A trimeric ATPase whose hydrolysis of ATP is required for membrane fusion. *J. Cell Biol.* doi:10.1083/jcb.126.4.945.

Zhao, M., S. Wu, Q. Zhou, S. Vivona, D.J. Cipriano, Y. Cheng, and A.T. Brunger. 2015. Mechanistic insights into the recycling machine of the SNARE complex. *Nature*. doi:10.1038/nature14148.

CHAPTER 3: PHOSPHATIDIC ACID INHIBITS SNARE PRIMING BY INDUCING CONFORMATIONAL CHANGES IN Sec18 PROTOMERS

ABSTRACT

Eukaryotic homeostasis relies on membrane fusion catalyzed by SNARE proteins. Inactive SNARE bundles are re-activated by Sec18/NSF driven disassembly to enable a new round of fusion. We previously found that phosphatidic acid (PA) binds Sec18 to sequester it from SNAREs. Dephosphorylation of PA dissociates Sec18 from the membrane allowing it to engage SNARE complexes. We now report that PA induces conformational changes in Sec18 protomers, while hexameric Sec18 cannot bind PA membranes. The association of Sec18 with PA was shown to be sensitive to membrane curvature, suggesting that regulation could vary on different organelles in a curvature dependent manner. Molecular dynamics showed that PA binding sites exist on the D1 and D2 domains of Sec18 and that residues needed for binding were masked in the hexameric form of the protein. Together these data indicate that PA regulates Sec18 function through altering protein architecture and stabilizing membrane-bound protomers.

INTRODUCTION

Membrane fusion is necessary for all eukaryotes to effectively transport cellular components between organelles. Vesicle trafficking is carried out through a series of events that are highly conserved across eukarya (Jahn and Südhof, 1999). Many proteins that drive the process differ between eukaryotic species, but all perform similar roles allowing compartment contact, bilayer fusion, and luminal content mixing (Jahn et al., 2003). The final stage of membrane fusion, and luminal content mixing, is catalyzed by SNARE proteins. Each participating membrane contributes either an R-SNARE or three Q-SNARE coils that wrap around each other to form a parallel four-helical *trans*-SNARE complex that brings membranes into close apposition. The formation of such complexes releases free energy that is transmitted to the membranes to trigger fusion. Once fusion occurs and membranes are merged, the four helical SNARE bundle, now a *cis*-SNARE complex, is inactive and requires reactivation in order to undergo a new round of fusion.

The activation *cis*-SNAREs, also known as *Priming*, is carried out by the AAA+ protein Sec18/NSF and its adaptor protein Sec17/α-SNAP (Mayer et al., 1996). Current models suggest that NSF primes *cis*-SNAREs through a "loaded-spring" mechanism triggered by *cis*-SNARE recognition and ATP hydrolysis (Ryu et al., 2015). NSF binds to *cis*-SNAREs with the help of α-SNAP to form what is known as the 20S complex (Chang et al., 2012; Söllner et al., 1993; Wilson et al., 1992; Zhao et al., 2015). In its active form, NSF forms a homohexamer which surrounds the *cis*-SNAREs and α-SNAP proteins to form the 20S particle (Fleming et al., 1998). Association with *cis*-SNARE-α-SNAP complexes triggers ATP hydrolysis which leads to a large

conformational change in the protein. This generates enough force to disrupt the 20S complex and separate the individual SNAREs from each other effectively reactivating them.

Previous work identified that both NSF and Sec18 bind to the regulatory glycerophospholipid phosphatidic acid (PA) (Manifava et al., 2001; see Chapter 2). PA has been shown to have regulatory effects in multiple vesicular trafficking pathways including sporulation, regulated exocytosis, lysosomal maturation, and homotypic vacuole fusion (Liu et al., 2007; Nakanishi et al., 2006; Rogasevskaia and Coorssen, 2015; Sasser et al., 2012; see Chapter 2). In the case of Sec18, increased PA levels lead to reduced priming activity likely due to a decrease in recruitment to *cis*-SNAREs (see Chapter 2). On yeast vacuoles, PA is converted to diacylglycerol (DAG) by the PA phosphatase Pah1, an ortholog of mammalian Lipin1. In the absence of Pah1 activity, PA levels remain intact and sequester Sec18 from *cis*-SNARE complexes to prevent priming and arrest the fusion pathway (Sasser et al., 2012). DAG can be converted to PA through the action of the DAG kinase Dgk1, whose inactivation leads to elevated DAG concentrations that enhance fusion through modulating the activity of the Rab GTPase Ypt7 (see Chapter 4). Thus, the interconversion of PA and DAG serves as a regulatory switch to control vacuole fusion.

Here we asked what effects PA-binding has on the overall architectural dynamics of Sec18/NSF that could lead to a decrease in its priming activity. To do so, we measured binding of monomeric and hexameric Sec18 to different forms of PA. We report that monomeric Sec18 has significantly stronger binding than the hexameric form to all forms of PA. We probed changes to the architecture of Sec18 when bound to short-chain PA and found that the protein exists in a significantly different conformation in its PA-bound state, without significant changes to its secondary structure. To

study the mechanism of Sec18 binding to PA, molecular dynamics simulations were performed using the mammalian version of Sec18, namely NSF. NSF was used as it has high identity to Sec18 and has more structural information available at the protein data bank (PDB ID: 3J94) (Zhao and Brunger, 2016). The molecular dynamic simulations performed suggest NSF binds to PA at regions of the protein that are only exposed in the monomeric state of the protein. Taken together, we propose that PA regulates the priming activity of NSF/Sec18 by limiting the formation of its active hexamer.

MATERIALS AND METHODS

Reagents

POPA (1-palmitoyl-2-oleoyl-sn-glycero-3-phosphate), POPC (1-palmitoyl-2-oleoyl-sn-glycero-3-phosphatidylcholine), POPE (1-palmitoyl-2-oleoyl-sn-glycero-3-phosphatidylethanolamine), C8-PA (1,2-dioctanoyl-*sn*-glycero-3-phosphate), C8-DAG (1,2-dioctanoyl-*sn*-glycerol), and C8-PS (1,2-dioctanoyl-*sn*-glycero-3-phospho-L-serine) were purchased from Avanti Polar Lipids (Alabaster, AL, USA) as chloroform stock solutions and stored at -20°C. CM7 and Ni-NTA (Standard and S series) sensor chips, and Regeneration buffers (Glycine pH 1-3) were procured from GE Healthcare (Buckinghamshire UK). Ni-NTA Atto 488 dye was procured from Sigma-Aldrich Corp. (St. Louis Missouri). Monolith NT.115 standard treated capillaries for thermophoresis were purchased from Nanotemper (München Germany).

Plasmid construction

Plasmid for expression of $Sec18_{His8}$ was created by amplification of *SEC18* by PCR from genomic DNA of the yeast strain DKY6281 using primers containing NdeI and XhoI restriction cut sites (Forward: 5'-ACGTACGTCATATGTTCAAGATACCTGGTTTTGG-3', Reverse: 5'-ATCGAATGCTCGAGT-GCGGATTGGGTCAT CAACT-3'). PCR Product was inserted into pET42a using NdeI and XhoI in frame with a C-terminal 8xHis tag sequence under the control of a T7 promoter to create pSec18H8.

Plasmid for expression of GST-Sec18 was created using primers containing EcoRI and XhoI restriction cut sites (Forward: 5'-ATGCAATGGAATTCATGTTCAAGATACCTGGTTTTGG-3', Reverse: 5'-ATCGAATGCTC GAGTTATGCGGATTGGGTCATCAACT-3'). PCR product was inserted into pParallel GST using EcoRI and XhoI to create pGSTSec18. Plasmid for expression of GST-N terminal domain was created in the same way using a different reverse primer (Forward: 5'-ATGCAATGGAATTCATGTTCAAGATACCTGGTTTTGG-3', Reverse: 5'-ATCGAATGCTCGAGTCTTCCTTTGAAAAAATTAATTTGTGTTTGTTT-3') to create pGSTN.

Protein purification

For purification, pSec18His8 was transformed into Rosetta 2 (DE3) pLysS Competent Cells (Novagen) and $Sec18_{His8}$ expression was carried out using auto-inducing medium (AIM) (Studier, 2014). Cells were grown in AIM until reaching stationary phase (37°C, 18 hours, shaking) and harvested by centrifugation. Cells were resuspended in lysis buffer (20 mM HEPES pH=6.8, 300 mM NaCl, 0.1% Triton-100, 2 mM 2-mercaptoethanol, 20 mM imidazole, 10% glycerol, 1 mM

ATP, 1 mM PMSF, and 1X cOmplete Protease Inhibitor Cocktail (Roche)) and lysed by French press. Lysates were cleared by centrifugation (50,000 *x g*, 20 min, 4°C) and incubated with Ni-NTA resin (Invitrogen) overnight at 4°C. Resin was washed with 100 bed volumes of wash buffer (lysis buffer with 50 mM imidazole) before protein was eluted in 1 ml fractions (lysis buffer with 250 mM imidazole). Protein was concentrated before being run through gel filtration (Superose 6) using size exclusion buffer (20 mM HEPES pH 6.8, 300mM NaCl, 1 mM 2-mercaptoethanol, 10% glycerol). $Sec18_{His8}$ elutes in two peaks corresponding to monomeric and hexameric pools. Each pool was collected and concentrated before use. For circular dichroism experiments, $Sec18_{His8}$ was purified using the same approach with different buffer compositions. CD lysis buffer (50 mM phosphate buffer pH 6.8, 20 mM imidazole, 1mM PMSF), CD wash buffer (50 mM phosphate buffer pH 6.8, 50 mM imidazole), CD elution buffer (50 mM phosphate buffer pH 6.8, 250 mM imidazole), and CD SEC buffer (50 mM phosphate buffer pH 6.8) were used. GST-Sec18 was purified similarly using Rosetta 2 (DE3) pLysS Competent Cells transformed with pGSTSec18 but with the following changes. GST lysis buffer (50 mM Tris pH 8.0, 150 mM NaCl, 5 mM EDTA, 1 mM ATP, 1 mM PMSF, and 1X cOmplete Protease Inhibitor Cocktail) was used through the lysis and chromatography wash steps. Protein was eluted with GST elution buffer (20 mM HEPES pH 7.2, 150 mM NaCl, 10 mM reduced glutathione) and dialyzed against 1X HBS pH 7.2 before being aliquoted and stored at -80°C. GST-N was purified in the same way using cells transformed with pGST-N. The DEP PA binding domain from murine Dvl2 was purified as a GST-fusion as described (Capelluto et al., 2014). Membrane scaffold protein 1D1 (MSP1D1-His) was prepared as described (Denisov et al., 2004).

Nanodisc Preparation

Lipid composition of PA nanodiscs consisting of 3.023 µmol POPC diC16, .098 µmol PA diC16, and .78 µmol POPE and PC nanodiscs consisting of 3.121 µmol POPC diC16 and .78 µmol POPE were combined, dried, and desiccated overnight. Lipids were then dissolved in 20 mM sodium deoxycholate in TBS (50 mM Tris-HCl, pH 7.4, 150 mM NaCl, and .02% NaN_3) and sonicated. MSP1D1 membrane scaffold protein (MSP) was then added in a ratio of 70:1 lipid to protein and detergent removed with Bio-Beads® SM-2 (Bio-Rad). Nanodiscs were isolated using size exclusion chromatograph and quantified using a NanoDrop and the extinction coefficient of 21,000 L mol^{-1} cm^{-1} for MSP1D1 (24.66 kD), and the resultant mg/mL divided by two because there are two MSP proteins per nanodisc (Sparks et al., 2016).

Surface Plasmon Resonance

Surface plasmon resonance (SPR) measurements were performed on a Biacore T200 instrument equipped with an Ni-NTA chip. Approximately 2000 RU of 5% PA nanodiscs were immobilized non-covalently using 100 mM NiSO4 flowed at 10 µL/s followed by a blank buffer injection of HEPES pH 7.4, 150 mM NaCl (HBS Buffer). Injections were performed in HBS buffer at a flow rate of 30 µl/min with an association time of 90 sec, dissociation time of 300 sec., and binding was measured in relative response units (RU) as described (Sparks et al., 2016). Regeneration with EDTA was performed at flow rate 30 µL/s for 120 s using 100 µM EDTA buffer. Proteins were injected using 1:1 dilutions from highest concentration and steady state was obtained using GE BIAcore T200 evaluation software version 3.0 (BIAevaluate). Proteins were injected using 1:1 dilutions for Sec 18 monomer (3.64 µM, 1,82 µM, 911 nM, and 455 nM), DEP PA binding domain (57.5 µM, 28.8 µM, 14.4 µM, 7.2 µM, 3.6 µM, 5.8 µM), and N domain from Sec18 (84.3 µM, 8.4

μM, 4.2 μM, 1.1 μM, 527 nM, and 1.69 μM) with one concentration from each titration run in duplicate. Steady state data was fitted and exported using BiaEvaluate software into GraphPad Prism 7.00 for Windows, GraphPad Software (La Jolla, CA).

Microscale thermophoresis

Thermophoresis measurements were performed using a Monolith NT.115 labeled thermophoresis machine. $Sec18_{His8}$ was labeled with Ni-NTA Atto 488 according to the manufacturer's protocol. M.O. Control software was used for operation of MST. Target protein concentrations were 50 nM for all His-tag labeled proteins Sec 18 monomer, Sec18 hexamer, PA nanodiscs, and PC nanodiscs. LED excitation power was set to 90% and MST set to high allowing 3 seconds prior to MST on to check for initial fluorescence differences, 25 s for thermophoresis, and 3 s for regeneration after MST off. Analysis was performed using M.O. Affinity Analysis Software as the difference between initial fluorescence measure in the first 5 s as compared with thermophoresis at 15 s. All measurements were performed in PBS buffer (137 mM NaCl, 2.7 mM KCl, 8 mM Na2HPO4, and 2 mM KH2PO4, pH 7.4) without Tween except for Sec18 Hexamer, which was performed in 50% PBS buffer and 50% Storage buffer (20 mM HEPES pH=6.8 300 mM NaCl 1 mM beta-mercaptoethanol 10% glycerol) and binding affinity was generated using Graphpad Sigmoidal 4PL fit from points exported from M.O. Affinity Analysis software using K_D Model with target concentration fixed at 50 nM generating bound and unbound, and fraction bound data exported to Graphpad to generate Figures using standard curve Sigmoidal for final K_D.

Limited Proteolysis

Cleavage reactions were carried out in proteolysis buffer (20 mM HEPES pH 7.2, 150 mM NaCl, 2 mM ATP, 2 mM $MgCl_2$). $Sec18_{His8}$ (2 μM) was added to proteolysis buffer and incubated with indicated lipid concentration on ice for 5 min. Trypsin or thrombin diluted in 1X HBS was added to assay tubes at indicated concentrations and incubated at 25°C for 30 min. Cleavage reactions were stopped with the addition of SDS sample buffer containing 1 mM PMSF. Samples were resolved with SDS-PAGE and gels were stained using Coomassie Blue. Gels were destained with methanol/acetic acid solution (50%/7%) and imaged using a ChemiDoc MP Imaging System (Bio-Rad).

Tryptophan Fluorescence Spectroscopy

$Sec18_{His8}$ (500 nM) was incubated with the indicated concentrations of C8-PA in fluorescence assay buffer (20 mM HEPES pH 7.2, 150 mM NaCl, 1 mM $MgCl_2$, 1 mM ATP). Lipid dilutions were first prepared in assay buffer and measured for background fluorescence before $Sec18_{His8}$ was added and incubated at 25°C. Intrinsic tryptophan fluorescence measurements were made using a fluorimeter with Peltier temperature control (Agilent Technologies). Samples were excited at 295 nm and the emission spectra were collected from 300-400 nm. Samples were measured in a 100 μL cuvette (Starna Cells). Initial background fluorescence spectra for each lipid concentration were subtracted from final measurements.

1,8-ANS Fluorescence Spectroscopy

ANS binding experiments were carried out in fluorescence assay buffer with 5 μM 1-anilino-8-naphthalenesulfonate (ANS) (Cayman Chemical). Initial spectra were taken without $Sec18_{His8}$ to

measure any background fluorescence from buffer or added lipids (ex. 350 nm, em. 390-620 nm). $Sec18_{His8}$ diluted in assay conditions was then added to the assay to the indicated concentration and incubated at 25°C for 5 min before spectra were obtained. Initial background fluorescence spectra for each lipid concentration were subtracted from final measurements.

Circular Dichroism

Monomeric $Sec18_{His8}$ purified in phosphate buffer was incubated with and without C8-PA to equilibrium (25°C, 15 min). Protein concentration used was 5 μM and lipid concentration used was 100 μM. Circular dichroism was measured using a spectropolarimeter (JASCO). All spectra were recorded from 260 nm to 200 nm at 50 nm min^{-1} and measurements were taken in a 1 mm pathlength cuvette.

Differential Scanning Fluorimetry

Sec18 (2.75 mg/mL) was diluted to a final concentration of 0.11 mg/mL in phosphate buffer containing 1 mM ATP, 1 mM $MgCl_2$, and 4X SYPRO orange dye. Next, 22.5 μL of this mix was added to a white hard-shell 96-well PCR plate (Bio-Rad) which contained 2.5 μL of serial dilutions of C8-PA in phosphate buffer. The plates were then sealed with Microseal 'B' film (Bio-Rad), and samples were allowed to equilibrate at room temperature for 30 min before beginning the assay. Melting curves were performed using a Bio-Rad CFX Connect real-time detection system. The melt curve protocol was 25°C for 3 min followed by a 25-90°C gradient with 0.5°C increments. Each temperature was held for 10 seconds and the fluorescence intensity was measured (Ex = 490

nm, Em = 560 nm). The first derivative of the fluorescence readings was used to determine the melting temperature(s) for each condition.

Preparation of D1-D2 monomer and hexamer models

The D1-D2 monomer model (residues 215-737) was derived from an Cryo-EM structure of ATP-bound NSF complex (PDB 3J94 - chain A) (Zhao et al., 2015). Missing residues [335-346, 458-478 in PDB 3J94 (chain A)] were built via homology modeling using the crystal structure of the homologous N-D1 domain of p97 (PDB 1E32) as a template by MODELLER 9.19 (Blundell et al., 1993). The complete D1-D2 hexamer model was prepared (Jo et al., 2014) using the same PDB 3J94 as the monomer. Missing loops in each monomer were modeled in CHARMM GUI to ensure that no clashes or topological errors exist in the complex structure. Cis-peptide bonds in both monomer and hexamer structures were examined and fixed manually using Cispeptide plugin in VMD (Schreiner et al., 2011). A further refinement of loops built in the hexamer was performed via MDFF (Trabuco et al., 2008).

Equilibrium MD simulations of D1-D2 monomer and D1-D2 hexamer

The MD simulations were performed with NAMD 2.12 using CHARMM36m force field (Phillips et al., 2005; Huang et al., 2017). Langevin dynamics and Langevin piston Nosé−Hoover methods were used to maintain constant temperature at 310.15 K and pressure at 1 atm (Feller et al., 1995; Martyna et al., 1994). The long-range electrostatic forces were evaluated using the particle mesh Ewald (PME) method with a 1 Å grid spacing (Darden et al., 1993; Essmann et al., 1995). The van der Waals interactions were calculated with a cutoff of 12 Å and a force-based switching scheme after 10 Å. Integration time step was set at 2 fs with SETTLE algorithm applied (Miyamoto and

Kollman, 1992). VMD 1.9.3 was used for MD trajectory visualization and analysis (Humphrey et al., 1996). The D1-D2 monomer model was first equilibrated for 20 ns with harmonic restraints (0.05 kcal/mol/Å^2) on protein Cα atoms except modelled loops, then followed by 200 ns equilibration without restraints.

PA lipids flooding simulations of D1-D2 monomer and D1-D2 hexamer

All the structures of D1-D2 monomer and hexamer were combined with a lipid grid of 5 x 5 x 5 short-chain PA lipids consisting of protein, solvent, and lipid with overlapping lipids on protein removed. The flooding box was then solvated and ionized with the SOLVATE and AUTOIONIZE plugins within VMD [PMID: 8744570] with a final NaCl concentration of 150 mM. The constructed D1-D2 monomer (ATP-bound and ATP-free) and D1-D2 hexamer (ATP-bound) were simulated in a short-chain PA solution for 120 ns each for monomer and 166 ns for hexamer, termed Fl_{on}^{ATP}, $Fl_{Mon}^{ATP-free}$ and Fl_{Hex}^{ATP}. Final simulation systems include for monomer ~80 mM PA lipids in water and for hexamer short-chain PA solution (120 mM, 223 PA molecules in a 188 Å x 187 Å x 133 Å water box) for $Fl_{Mon,}^{ATP}$ Fl_{Hex}^{ATP}, and $Fl_{Mon}^{ATP-free}$. Harmonic restraints were applied on protein C_α atoms except modelled loops throughout the simulation, to preserve protein secondary structure.

Binding Site Simulations on NSF for PA

To characterize C8-PA and D1-D2 monomer interactions, molecular ensemble docking of PA was done on D1-D2 monomer using AutoDock Vina (Pande et al., 2010). The previously mentioned equilibrium simulation of D1-D2 was used to fully sample the dynamics of D1-D2 for molecular docking, where snapshots were taken every 100 ps of the 200 ns trajectory. For each snapshot, an

80Å by 94Å by 108Å grid box was used to fully sample the entire structure. Each snapshot was docked with an exhaustiveness of 10, yielding a total of 2000 PA docked poses, with the affinities of each poses obtained from the resultant log files. These poses where then clustered using a hybrid K-centers and K-medoids clustering algorithm using root-mean-square deviation (RMSD) method, for which three main clusters where identified (Beauchamp et al., 2011). These clusters where then compared to SiteMap (Halgren, 2009). Schrodinger SiteMap was used on equilibrated D1-D2 NSF monomer indicating top potential ligand binding regions of NSF D1-D2 monomer including shallow binding sites.

Statistics

Results are expressed as the mean ± S.E. where n = number of replicates. SPR experiments were analyzed using GE BIAevaluation Software, MST experiments were analyzed using M.O. Affinity Analysis software and GraphPad Prism was utilized for statistical approaches.

RESULTS

Sec18 monomer binds to PA with higher affinity than the hexameric form

Our previous work showed that Sec18 preferentially bound to liposomes containing phosphatidylcholine (PC), phosphatidylethanolamine (PE) and PA relative to those composed of only PC and PE, or ones where PA was replaced with DAG (see Chapter 2). This was in keeping with older findings showing that mammalian NSF bound to resin-linked PA (Manifava et al., 2001). Here our studies were extended to further define how Sec18 binds to PA. To start we used microscale thermophoresis (MST) to acquire binding affinities to dioctonyl PA (C8-PA), which prevents Sec18 from binding *cis*-SNARE complexes, consequently precluding priming from occurring (see Chapter 2). We used both monomeric and hexameric Sec18 with a range of C8-PA. The C-terminal 8xHistidine tag of Sec18 was labeled with Ni-NTA Atto 488. As shown in Figure 3.1A, monomeric Sec18 (mSec18) bound to C8-PA with a K_D of 1.4±0.68 μM (blue circles), whereas the hexameric form (hSec18) had a K_D of 29±8.6 μM (red squares). This suggested that either hSec18 has residues occluded for PA binding or is in an inappropriate conformation to bind C8-PA in hexameric form. It is possible that a small soluble C8-PA could access a binding site on Sec18 that is obscured in the hexamer, where membrane contained PA is unable to reach PA binding regions on Sec18 when Sec18 is hexamerized, especially regions contained in the hexamerization interface of Sec18 hexamer.

Due to the difference in binding affinities to C8-PA, we next asked if limiting the mobility of PA to two dimensions would show a similar disparity between the monomer and hexamer. To this aim we used sonicated liposomes as previously reported as well as extruded 0.8 μm diameter liposomes

to approximate the diameter of yeasts vacuoles. We found that mSec18 bound sonicated PA liposomes with a K_D of 9.3±1.32 μM (red circles) and 0.8 μm PA liposomes with a K_D of 97.7±10.9 μM (blue triangles) (Figure 3.1B). In both cases, mSec18 bound with a lower affinity relative to C8-PA, supporting the notion that membranous PA is limited in its interactions with Sec18. As a control for PA specificity we tested sonicated liposomes containing only PC and PE (purple squares), and found that Sec18 did not appreciably bind, which is in keeping with our previous study. Importantly, we found that hSec18 did not bind 0.8 μm PA liposomes (orange diamonds) or 0.1 μM PA liposomes (not shown). This data is indicative of two major conclusions. First, it is apparent that membrane curvature affects Sec18 binding to PA, similar to other PA binders (Putta et al., 2016). Second, and more importantly, is that the hexameric Sec18 lacks the ability to bind PA, potentially by masking a binding site or by restricting conformational changes needed to bind PA.

Membrane curvature affects Sec18 binding to PA

To further test the role of membrane curvature we generated PA liposomes using extrusion with diameters of 0.1, 0.4 and 0.8 μm. These were used in parallel to sonicated liposomes with an average diameter of 30-50 nm (Lapinski et al., 2007). MST experiments showed that the affinity for PA was reduced as the diameter of membranes increased. Sonicated PA liposomes bound mSec18 with a K_D of 9.3±1.32 μM, while the K_D values of 0.1 μm, 0.4 μm and 0.8 μm liposomes were 45.1±11.8 μM, 56.8±15.6 μM, and 97.7±10.9 μM, respectively (Figure 3.1C). Although not a linear effect, it is clear that membrane curvature alters the ability of Sec18 to bind PA. This also suggests that the effect of PA on Sec18 mediated SNARE priming could vary depending on the local curvature of an organelle.

ATP can reduce PA binding by Sec18

Sec18/NSF like many other AAA+ proteins contains two nucleotide binding domains (NBD) each residing in a one of the domains that make up the rings of the hexameric protein. The D1 ring of Sec18 hydrolyses ATP to generate the mechanical force needed to disrupt *cis*-SNARE bundles whereas the D2 ring binds ATP to stabilize the hexameric form of the protein. This is reflected in the different affinities for ATP found between the two NBDs. In NSF the D1 NBD binds ATP with a K_D of 15-20 μM, while the D2 NBD binds with a K_D of 30-40 nM (Matveeva et al., 1997). Here we asked ATP binding, which is linked to large conformational changes during SNARE priming, would affect PA binding. First we determined the affinity of mSec18 for ATP using MST and found that mSec18 had a K_D of 56±16 μM, which likely reflects the low-affinity binding site in D1 (Figure 3.1D). We were unable to detect the high affinity binding to be expected of the D2 NBD. We then tested if ATP binding altered PA binding. mSec18 was pre-incubated with 0.8 μm PA liposomes, then introduced to 100 nM ATP, 100 μM ATP, or buffer alone (no ATP). This showed that in the presence of 100 nM ATP, a saturating concentration for the D2 NBD (not shown), there was no effect on PA binding as the curve overlapped with the no ATP control (Figure 3.1E, blue circles vs red squares, respectively). Both conditions bound to PA with a K_D of approximately 100 μM. In contrast, saturating both NBDs with 100 μM ATP completely blocked binding to PA liposomes (green diamonds). As a negative control we incubated hSec18 with PA liposomes in the absence of ATP, which showed no binding at concentrations of PA liposomes tested (purple squares).

Sec18 binds PA with similar affinity to DEP PA binding domain

In our previous study we competed Sec18 binding to PA liposomes with GST-DEP, a well characterized PA binding domain from the murine protein Dvl2 (Capelluto et al., 2014). Here we compared the binding affinity of DEP to mSec18. Because we previously used GST-DEP, we measured its binding in comparison to GST-Sec18. We also wanted to verify our MST data with surface plasmon resonance (SPR) and PA nanodiscs (PA-ND), which were linked to Ni-NTA SPR chips through the 6xHis tags of the ND scaffold proteins. These experiments showed that GST-Sec18 bound to PA-ND with a K_D of 2.7±2 μM (Figure 3.2A), whereas GST-DEP had a K_D of 18±2 μM (Figure 3.2B), indicating that Sec18 binds PA with a higher affinity relative to the *bona fide* PA-binding domain DEP. This was also seen using MST, where GST-Sec18 bound to PA-ND with a K_D of 0.6±.096 μM whereas GST-DEP had a higher K_D of 2.4±0.42 μM, and N Domain had a K_d of 8.5±14.4 μM. The increased affinity for PA nanodiscs is possibly due to the fact that nanodiscs as opposed to liposomes are quantified by actual number of nanodiscs and not total lipid concentration as in C8-PA and liposome measurements respectively. Alternatively, increased affinity of PA binding in comparison to the values in Figure 3.1 are attributed to the effect of GST dimerization or GST stabilization of conformation, which could contribute to an increase in avidity relative to His-tagged mSec18, similar what was seen with the protease inhibitor cystatin (Tudyka and Skerra, 1997).

Due to the PA inhibition of Sec18 binding to *cis*-SNARE complexes, we asked if the Sec18 N-terminal domain could bind to PA by itself. This notion is supported by the crystal structure of the NSF N-terminal domain showing the presence of a positive polybasic surface adjacent-to and

lining the α-SNAP binding groove (Yu et al., 1999). SPR measurements of GST-N-domain from Sec18 binding to PA-ND showed a K_D of 31.8±3.7 μM (Figure 3.2C). Interestingly, the N-domain bound ND containing only PC and PE with a K_D of 11±1.6 μM (Figure 3.2D), suggesting that the N-domain has no lipid-binding specificity. Because full length Sec18 binds to PA and not PC, we conclude that the N-domain does not contribute to the regulatory association with PA. This is further supported by our MST data showing that mSec18 binds to PA-ND with an affinity that is nearly two orders of magnitude higher relative to the N-domain alone (Figure 3.2E, blue circles vs red triangles).

Phosphatidic acid alters the conformation of Sec18

Our data thus far suggests that Sec18 undergoes conformational changes that allow mSec18 to bind PA while hSec18 lacks the ability to bind the lipid. To further probe for conformational changes to Sec18 we tested whether PA significantly alters binding of 8-Anilino-1-naphthalenesulfonic acid (ANS) to Sec18. ANS is a dye that has been extensively used to test lipid-binding proteins because it associates with solution exposed hydrophobic motifs (Heyduk and Lee, 1989; Roberts et al., 1999). Binding of ANS to a protein results in an increase in fluorescence yield and a blue-shifted emission. Because we have previously seen PA binding to mSec18 we expected ANS to also bind the protein in our assay. As expected, we observed ANS binding to mSec18 in a dose-dependent fashion (Figure 3.3A-B). We next wanted to test for any conformational changes upon PA binding that altered ANS binding to Sec18. To do this, we titrated increasing amounts of C8-PA into our assay and measured changes in the ANS fluorescence spectra. Because C8-PA is partially hydrophobic, ANS was first incubated with each lipid concentration to obtain a background spectrum before protein was then added to the assay,

and fluorescence was again measured. The difference spectra from these measurements shows that addition of C8-PA increases the binding of ANS to Sec18 (Figure 3.3C and F). To verify that the changes in ANS fluorescence were specific to PA binding, we tested the addition of DAG, the product of Pah1 activity on PA. No change in ANS fluorescence was detected in the presence of C8-DAG, which is consistent with inability of Sec18 to bind to DAG (Figure 3.3D and F). We also tested the anionic lipid phosphatidylserine (PS). Similar to what we observed with DAG, the addition of C8-PS had no effect on ANS fluorescence (Figure 3.3E and F). *In toto* these data suggest that C8-PA binding to Sec18 results in a conformational change in the protein that exposes additional hydrophobic pockets to solution. Such a change may account for the differences previously seen in Sec18 priming activity and *cis*-SNARE association (see Chapter 2).

To further probe for conformational changes to Sec18 induced by PA we utilized a limited proteolysis assay. Proteins can exhibit differences in their proteolytic cleavage profiles when bound to a ligand that significantly changes their overall architecture (Heyduk and Lee, 1989). Because we observed an increase in solution exposed regions of Sec18 in the presence of PA, *i.e.* increased ANS fluorescence, we expected to also see an increased sensitivity to protease degradation in the same conditions. To measure this, mSec18 was incubated with increasing concentrations of trypsin with and without C8-PA addition. As expected, mSec18 sensitivity to trypsin degradation increased in the presence of C8-PA, whereas the presence of DAG had no effect (Figure 3.4A-B).

Additionally, we performed the same limited proteolysis assay using thrombin in place of trypsin. Thrombin displays much higher specificity than trypsin and should only cleave proteins at specific

recognition sites. Incubation of Sec18 with thrombin alone showed no proteolytic degradation of the protein indicating that no recognition sites were accessible to the protease. However, upon addition of C8-PA thrombin was able to cleave Sec18 (Figure 3.4C-D). Once again, inclusion of C8-DAG did not show a similar effect indicating once again that the observed conformation change was PA specific. Finally, we titrated C8-PA into a thrombin cleavage assay keeping the concentration of the protease constant. Cleavage of Sec18 by thrombin showed dose dependence for C8-PA (Figure 3.4E-F). These data illustrate that C8-PA binding to Sec18 alters the conformation of the protein allowing for the exposure of an otherwise shielded thrombin recognition site. Sec18 has one predicted thrombin recognition site (after R638) which is located in the D2 domain of the protein [exPASy]. The D2 domain is responsible for the multimerization of Sec18 to its active hexamer when it is in a nucleotide bound state (Lenzen et al., 1998; Yu et al., 1999). This further suggests that PA alters the conformation of the Sec18 D2 domain, or potentially the conformation of D2 with respect to D1 allowing binding to PA. Changes to the D2 domain structure could alter nucleotide binding or disrupt key interactions between protomers thereby decreasing Sec18 hexamer formation. Sec18 is known to associate with *cis*-SNAREs in its active hexameric form, so inhibition of hexamer formation could decrease its ability to properly recruit to inactive SNARE complexes. This idea is consistent with previous observations that showed increased PA at the vacuole led to decreased recruitment of Sec18 to *cis*-SNARE complexes (see Chapter 2).

Phosphatidic acid has no significant effect on the secondary structure of Sec18

Because we observed significant changes in the conformation of Sec18 upon binding to C8-PA we next wanted to monitor changes in the secondary structure of the protein when bound to the lipid.

To do this we observed the α-helix and β-sheet content of Sec18 in the presence of PA using circular dichroism (CD). CD spectra of mSec18 were obtained in the absence and presence of C8-PA to determine if the protein's secondary structure was significantly affected by binding the lipid. The spectrum obtained for mSec18 alone showed that the protein was well folded (Figure 3.5A). Upon addition of C8-PA, no significant changes were seen in the spectrum suggesting the lipid binding does not alter secondary structure features within the protein.

To rule out any denaturation caused by binding of C8-PA to Sec18, intrinsic tryptophan fluorescence was measured with and without lipid addition. Sec18 contains three tryptophan residues (W88, W91, and W632) in its N and D2 domains. Upon denaturation of Sec18 with SDS, Trp fluorescence was red-shifted and showed decreased intensity (Figure 3.5B). Upon incubation with C8-PA, no shift or intensity change was observed. This suggests that PA binding to Sec18 did not lead to denaturation, *i.e.* causing a conformational change large enough to alter the local environment of any of the Trp residues found in the protein.

Finally, to test whether binding PA altered the thermal stability of Sec18, we used differential scanning fluorimetry (DSF) (Miner et al., 2016). Sec18 was labeled with SYPRO orange dye, incubated with different concentrations of C8-PA in separate wells, and equilibrated prior to starting a melting curve. Fluorescence was scanned across a temperature gradient of 20 to 95°C and the first derivative of the fluorescence data was be used to determine the T_m for each condition. DSF has the ability to show multiple melting transitions (Hew et al., 2015; Vollrath et al., 2014). Our data show that mSec18 has three melting transitions. The first mSec18 transition (T_{M1}) occurred at ~45°C, while T_{M2} and T_{M3} were at 60°C and 64°C, respectively (Figure 3.5C). The

addition of C8-PA had no effect on T_{M2} and T_{M3}, as the curves overlapped with the that of apo-Sec18. That said, C8-PA has a striking effect at T_{M1} where we observed a dose-dependent increase in fluorescence. This likely mirrors the conformational changes seen with limited proteolysis and ANS fluorescence. Taken together these observations lead us to conclude that PA binding to Sec18 induces a significant change to the architecture of the protein but does not denature the protein nonspecifically.

NSF D1-D2 undergoes large conformational change during transition between hexameric and monomeric forms

To examine the Sec18 conformational changes we observed previously at a more detailed level, atomic molecular dynamics (MD) simulations were performed using NSF, the mammalian homolog of Sec18. The NSF D1-D2 monomer extracted from the cryo-EM structure of an ATP-bound NSF complex (pdb 3J94) after removing bound ATPs was equilibrated with restraints for 20 ns and then relaxed for 200 ns. Based on the overall alpha carbon (C*α)* RMSD, the monomer undergoes conformational changes up to 15 Å apart from the form originally adopted in the hexamer (Figure 3.6A). Calculation on the secondary structure components showed that only the modeled loop region from residue 458 to 478 transitioned from helix during the relaxation to turn and coil (data not shown). This is expected as the loop was poorly resolved in cryo-EM and was only stabilized by interactions with the N-domain in the template crystal structure (the N-D1 domain of p97) used in homology modeling. The stable secondary structure observed in D1 and D2 domains indicated that the large deviation did not come from secondary structural changes, further verifying CD experiments. Instead, we observed that the conformational change was accompanied by an opening-up process of D1 and D2 domains during the relaxation (Figure 3.6A).

The observation was in agreement with the hypothesis that NSF hexamerization might require certain conformations of D1-D2 monomer and that the conformation required could be further stabilized at the hexamer interface.

Residues of NSF shown to bind to C8PA are not available for PA binding when it is in the hexameric form

Computational flooding studies were performed for both monomeric and hexameric form of the NSF D1-D2 domains, based on the structural information of mammalian NSF (Figure 3.6B). Analysis of binding was performed using percent bound as determined by proximity (H-bond distance between phosphate oxygens of PA and between a basic amino acid residue) of PA against time PA ligands were in set proximity. Residues determined to have highest percent bound were determined for both monomeric and hexameric forms of D1-D2. Our flooding simulations of NSF hexamer showed that residues having the highest percent bound PA in the monomer (Figure 3.6C) were shielded to block lipid binding in the hexameric NSF D1-D2 construct (Figure 3.6D). This suggests that PA binding specificity lies somewhere within the hexameric interface.

Binding Prediction and Clustering Analysis of PA Binding Regions of NSF

Ensemble molecular docking of C8-PA to NSF monomer was performed using the aforementioned D1-D2 equilibrium simulation (Trott and Olson, 2010). Snapshots from the equilibrium trajectory were utilized for molecular docking every 100 ps to fully sample conformational dynamics. The resulting docked C8-PA poses were clustered and an average affinity (ΔG) was determined for binding clusters of monomeric NSF showing similar affinity for C8-PA (~-5 kcal) approximating

the MST binding measurements of mSec18 to C8-PA, which is within a ± 2 kcal error prediction ratio used for many docking software programs such as Schrodinger Glide (Figure 3.7A) (Beauchamp et al., 2011; Friesner et al., 2006). To verify cluster analysis, SiteMap was used and the top 5 site scores taken (Figure 3.7B). Figure 7B depicts SiteMap site 1 corresponding to the largest cluster obtained from the ensemble docking (Figure 3.7A), which lies in the hexamerization interface illustrated in Figures 3.7C-D demonstrating the potential importance of this region for PA binding specificity.

DISCUSSION

Membrane fusion is a necessary process for all eukaryotes, and Sec18/NSF is the only known protein responsible for utilizing energy from ATP to prime SNAREs (Mayer et al., 1996; Zhao et al., 2015; Ryu et al., 2015). To achieve compartmental specificity, unique SNARE combinations are utilized by defined organelles as well as smaller transport vesicles budding from such organelles (Jahn and Scheller, 2006). Each organelle varies in both size and function, and must contain its own unique combination of protein and lipid factors to allow for specificity in trafficking and membrane fusion events. Regulation of Sec18/NSF is of special significance due its direct role in maintenance of fusion and compartmentalization throughout the eukaryotic cell. Therefore, it is important to understand the role that regulatory factors have on ubiquitous fusion machinery such as Sec18/NSF to adequately model how specificity and efficiency are balanced and maintained at different locations in the cell.

Protein function can be regulated directly through posttranslational modifications or through their interactions with other molecules, including lipids. The vacuole fusion pathway is regulated at

various stages by distinct lipids such as phosphoinositides, ergosterol, DAG and PA (Boeddinghaus et al., 2002; Fratti et al., 2004; Jun et al., 2004; Kato and Wickner, 2001; Karunakaran et al., 2012; Karunakaran and Fratti, 2013; Mayer et al., 2000; Miner et al., 2016; Sasser et al., 2012; Stroupe et al., 2006; see Chapter 2; see Chapter 4). The priming stage requires the presence of ergosterol, $PI(4,5)P_2$, as well as the conversion of PA to DAG (Kato and Wickner, 2001; Mayer et al., 2000; Sasser et al., 2012; see Chapter 2).

Previously we found that vacuolar PA sequestered Sec18 from *cis*-SNAREs and that the PA phosphatase Pah1/Lipin1 was required to convert PA to DAG to allow Sec18 dissociation from the membrane and recruitment to SNARE complexes (see Chapter 2). Although PA turnover is needed for priming, the presence of the lipid is also required downstream for mechanisms that remain to be characterized. Deletion of *PAH1* or the DAG kinase *DGK1* alters the balance of PA and DAG on vacuole to dramatically affect membrane fusion (Sasser et al., 2012; see Chapter 4). We thus postulate that enzymatic changes that alter PA levels can in turn shift the equilibrium of Sec18 from a lipid-bound to a to a SNARE-associated state. Such changes would likely have significant effects on SNARE activation and the overall progression of the membrane fusion cascade.

In this study, we demonstrated that Sec18 directly binds PA with high affinity on par with a known PA-binding domain. Moreover, only monomeric Sec18 could bind both PA membranes and soluble C8-PA, whereas hexameric was only able to bind C8-PA. This signifies that C8-PA could access PA-binding residues that are blocked in the hexamer to prevent membrane association. Sec18/NSF exists as both a monomer (non-enzymatic) and a hexamer (enzymatic). Our findings

indicate that Sec18 exists in both a monomeric lipid-bound pool and SNARE-bound hexamers. Because ATP is required for Sec18 hexamerization, we tested PA liposome binding at two concentrations of ATP. The D1 domain of NSF has K_D of ~20 μM for ATP, while the D2 hexamerization domain has a K_D of ~40 nM. PA binding was unaffected 100 nM ATP that should predominantly bind D2; however, at 100 μM ATP mSec18 binding to PA was abolished. This suggests that the nucleotide bound state of the D1 domain is important in specific PA binding of Sec18/NSF, likely due to conformational changes in the ATP bound state. Alternatively, the higher ATP concentration may shift the monomeric pool of Sec18 used to a predominantly hexameric pool decreasing its affinity for PA.

During priming, Sec17/ α-Snap is recognized by Sec18/NSF in an ATP bound state at D1 before subsequent ATPase activity occurs. We posit that Sec18 exists in both lipid-bound and SNARE-bound states and that the presence of ATP at the D1 NBD may determine the state in which the protein primarily exists. Membrane PA may prevent the association of ATP with the D1 NBD locking the protein in an inactive lipid-bound state preventing recruitment to inactive SNARE complexes. This is in line with our data in this study and with observations from previous work (see Chapter 2).

The fact that Sec18 monomer binding to PA liposomes was inhibited at a saturating ATP concentration for the D1 NBD could indicate that the PA binding site for Sec18 lies near the D1 ATP binding site. Alternatively, it is possible the conformation of Sec18 in its ATP bound state shields the protein's unique PA binding site. The idea that Sec18 binding to PA may not specifically depend on the D1 ATP binding site was supported by computational flooding

experiments performed on both hexamer and monomer in the presence and absence of ATP. Flooding experiments allowed for C8-PA to equilibrate with NSF monomer, and binding was measured using the length of time a PA molecule resided near a given residue of NSF. Many of the long term amino acid residues sharing the longest contact time to PA were predictably basic residues, especially lysine and arginine. However, dramatic differences in these residues were not noticed between the ATP and non-ATP simulations. Furthermore, many of the residues with longer PA binding time were not of importance for PA binding in the hexamer simulation. This result is in corroboration with the high binding affinity of Sec18 monomers to PA liposomes vs the hexameric form. This further indicates that the Sec18 monomer and hexamer are differentially regulated. Furthermore, it suggests that PA may influence the formation of the active hexamer by controlling the availability of its inactive monomer at membranes.

We propose that Sec18/NSF PA regulation is achieved by sequestration of Sec18/NSF monomer on PA containing membranes blocking its ability to form active hexamer. This sequestration regulates the ability of Sec18 to perform its enzymatic function of activating SNAREs. Additionally, it is possible that PA at the site of priming could increase localization of Sec18/NSF to the membrane in preparation of SNARE priming. Additional factors, such as the PA phosphatase Pah1/Lipin, could serve to activate Sec18/NSF once the fusion cascade was required to proceed (Sasser et al., 2012; see Chapter 2). In this way, PA could serve as a temporal regulator of SNARE priming activity and of the membrane fusion process as a whole.

Two additional modes of regulation are suggested by our data. First, PA membrane concentrations may play either a local or organelle-dependent role for the regulation of Sec18/NSF by lipid

binding. Depending on the concentration and localization of PA at a given membrane Sec18 sequestration by PA could either play a larger or less prominent role in regulating the priming of SNAREs. Second, we have found that curvature plays a role in Sec18 regulation by PA. Therefore, Sec18 regulation by PA could be differentially managed in the cell based on vesicle or organelle size.

This work has shown that Sec18/NSF binds to membranes containing PA with high affinity and that this lipid binding is greater to the monomeric version of the protein. Upon binding PA, Sec18/NSF undergoes a significant conformational change that coincides with a reduction in the protein's SNARE priming activity. Molecular dynamics simulations show that monomeric Sec18/NSF has greater conformational flexibility than hexamer. Equilibrium simulations indicate a large scale conformational change when NSF hexamer is converted to monomer (Figure 3.6B). We propose that binding to PA by Sec18/NSF may serve a regulatory role in preventing the formation of the active hexamer thereby throttling the priming of SNAREs. There are two main reasons we think this form of regulation is needed: 1) To keep NSF from freely priming any *cis*-SNARE complex around, and 2) To keep NSF nearby without allowing priming (Yavuz et al., 2018).

We have identified regions of NSF that are potential high PA binders (Figure 3.7A-B). Additionally, we have identified residues of NSF that show potential PA binding in monomeric form that are not capable of binding PA in hexameric form (Figure 3.6B). In order for Sec18 to form hexamer, according to our model, Sec18 would have to be removed from the membrane, and we have previously shown that the only PA phosphatase that plays a role in membrane fusion is

Pah1 (Sasser et al., 2012). It is possible that an additional chaperone may be involved in alleviating the transition of Sec18 monomer towards hexamerization.

Based on our computational studies, it appears that there are numerous candidate residues that might contribute to Sec18 PA binding. HMMM simulations have been performed (data not shown); however, due to the size and flexibility of Sec18 monomer, long time scales in the micro second range may be required to show final binding events sequestering Sec18 to a PA containing membrane. We plan to further probe this binding event using HMMM at a longer time scale to capture the exact binding event of Sec18 to a PA membrane, and to specifically identify the numerous residues that may be involved.

FIGURES

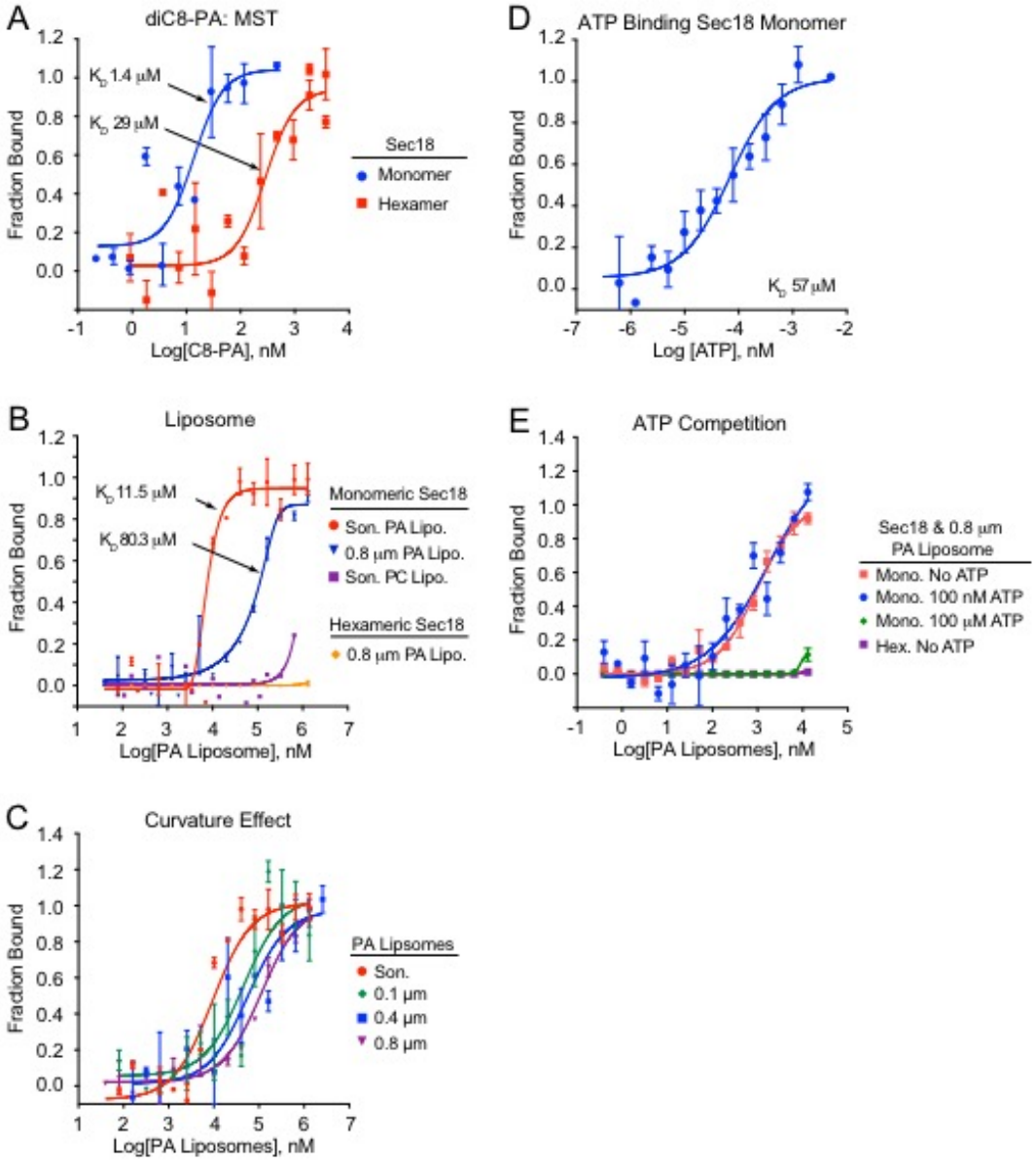

Figure 3.1. Sec18 Hexamer and monomer binding affinity for PA. (A) C8-PA MST measurements were performed using purified Sec18 monomer and hexamer labeled with Ni-NTA Atto-488 dye in the blue channel at 90% LED and High MST using NT.115 Labeled Thermophoresis. Binding affinity was measured using thermophoresis at 15 sec mixing separate reactions of half 100 nM Atto 488 labeled Sec18 monomer and half 1:1 titrations of C8-PA with highest concentration 370 µM according to Graphpad Sigmoidal 4PL curve. **(B)** The K_D of ATP for Sec18 monomer was measured using labeled Sec18 monomer with Ni-NTA Atto 488 dye as in Figure 3.1A with 1:1 titrations of ATP Solution in PBS. **(C)** The K_D of Sec18 monomer and hexamer to sonicated and 800 nm diameter PA liposomes (10% PA, 70% PC, and 20% PE) and

Figure 3.1 (cont.)
PC liposomes (80% PC, 20% PE) was measured using MST as in Figure 3.1A. Concentrations of lipid of 1.3 mM maximum were titrated as in Figure 3.1A for both PA and PC liposomes and affinities for both Sec18 hexamer binding to PA liposomes as well as monomer binding to PC liposomes was not measurable as they did not saturate. **(D)** ATP competition with mSec18 binding to 800 nm PA liposomes was measured as in Figure 3.1A was measured using MST ATP concentrations of 100 nM (D2 saturating) and 100 μM (D1 saturating) and compared to the K_D of monomer and hexamer in the absence of ATP. **(E)** Sec18 monomer affinity for different size of PA liposomes was measured using MST as in Figure 3.1A for sonicated, 100 nm, 400 nm and 800 nm. Curve fitting was performed using Graphad sigmoidal 4PL curve All measurements taken at 15 s thermophoresis using M.O. Affinity Analysis software as in Figure 3.1A.

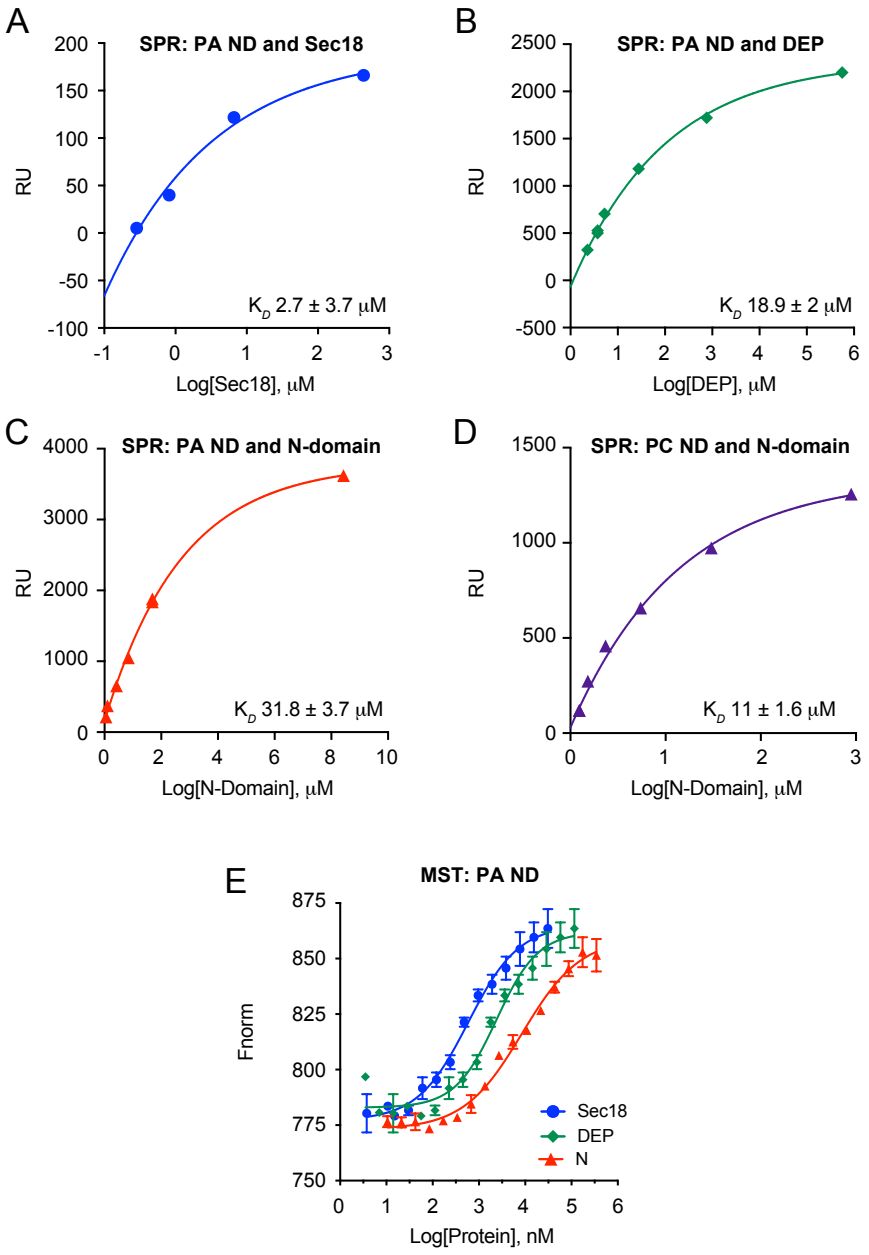

Figure 3.2. Sec18 Binding Affinity Compared to DEP PA Binding Domain for PA Nanodiscs. **(A)** SPR analysis of Sec18 monomer was performed with approximately 2000 RU of 5% PA nanodiscs attached to a Ni-NTA chip using a Biacore 300 Ni-NTA with flowrate 20 μL/s. The steady state fit was exported from BIAevaluate software to GraphPad at 4 seconds before injection stop set at 90 s with disassociation of 120s. **(B)** SPR Analysis of DEP with 5% PA nanodiscs. **(C)** SPR analysis of N domain for Sec18 monomer with 5% PA nanodiscs. **(D)** SPR analysis of PC nanodiscs for Sec18 monomer. **(E)** MST performed with mSec18, DEP, and N-domain with 100 nM Ni-NTA Atto 488 labeled 5% PA nanodiscs using 90% LED and 60% MST. M.O. Affinity analysis software was used and thermophoresis exported at 15 s.

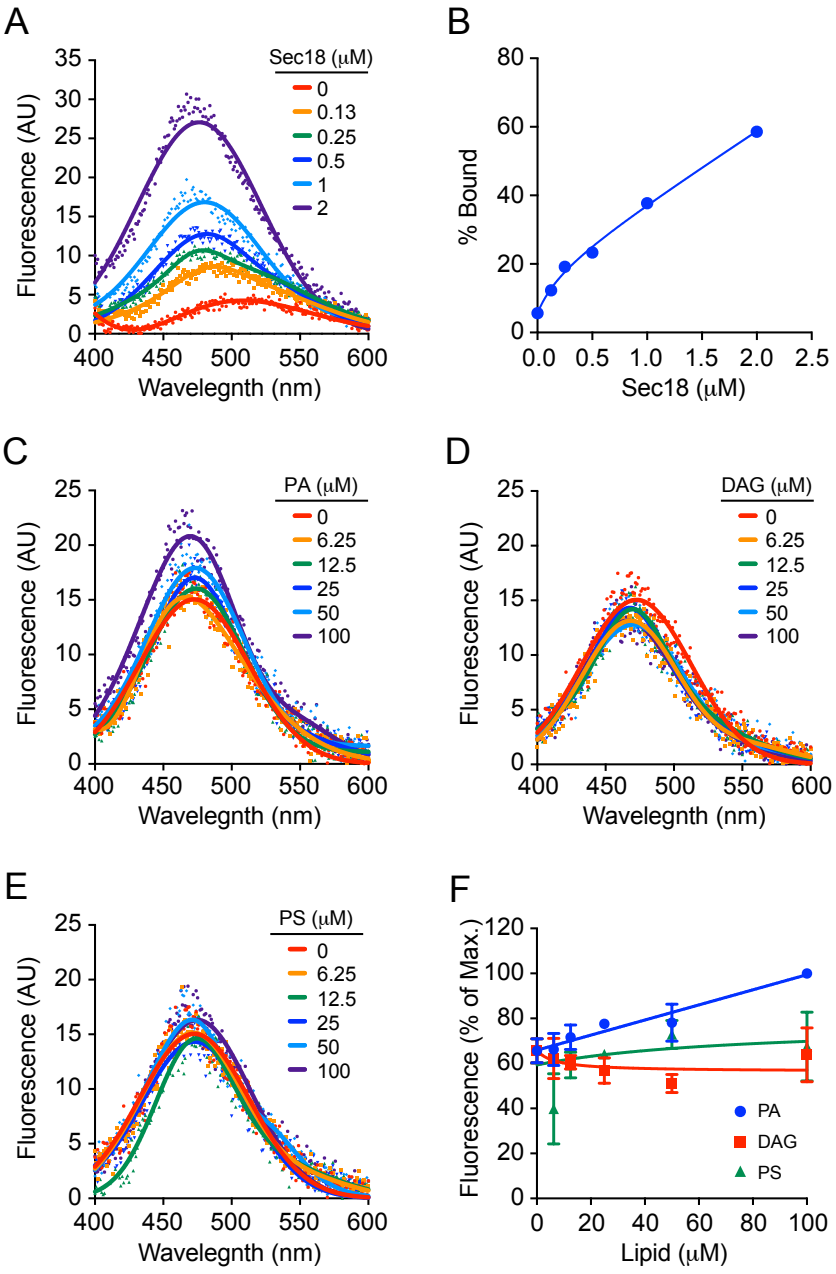

Figure 3.3. Short chain phosphatidic acid alters the binding of 1,8 ANS to Sec18. Increasing concentrations of $Sec18_{His8}$ were incubated with ANS (5 μM) in assay buffer and a representative fluorescence spectrum (ex. 390, em. 400-600 nm) is shown **(A)**. Relative fluorescence at 460 nm **(B)**. $Sec18_{His8}$ (0.5 μM) was incubated with increasing concentrations of short-chain lipids in the presence of ANS (5 μM) and fluorescence spectra were taken (ex. 390, em. 400-600 nm). A representative spectrum for each lipid tested is shown: C8-PA **(C)**, C8-DAG **(D)**, and C8-PS **(E)**. **(F)** Maximum fluorescence for each lipid concentration was normalized against overall maximum fluorescence (100 μM C8-PA) for relative comparison.

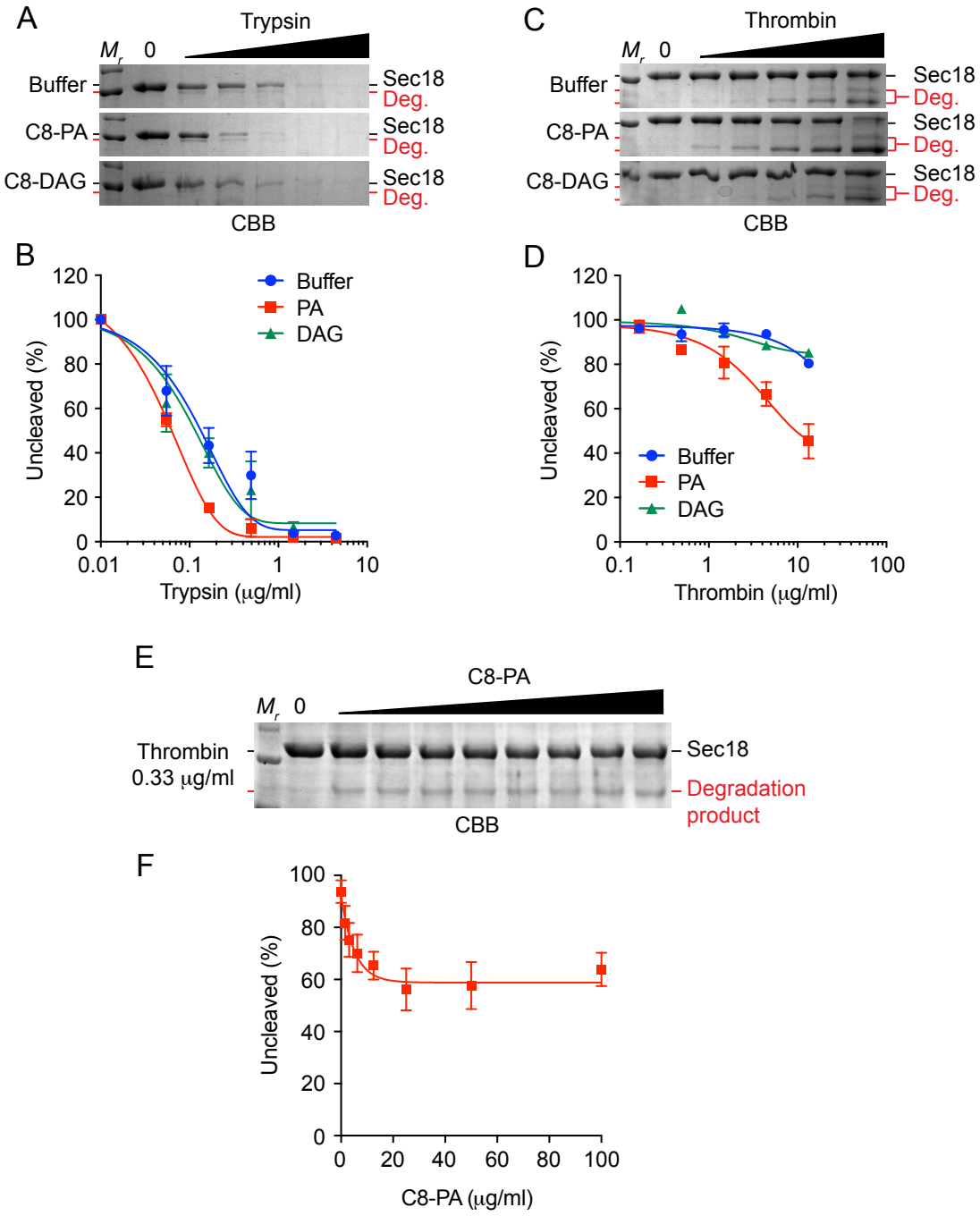

Figure 3.4. Short chain phosphatidic acid alters the proteolytic cleavage profile of Sec18. $Sec18_{His8}$ was incubated with C8-PA (red), C8-DAG (green), or alone (black) before incubation with increasing concentrations of trypsin **(A)** or thrombin **(C)**. Densitometry values of the uncleaved band were measured for each concentration and normalized against the input lane for trypsin **(B)** and thrombin **(D)**. $Sec18_{His8}$ was incubated with increasing concentrations of C8-PA before cleavage by thrombin **(E)**, and normalized densitometry values against the input control are included **(F)**.

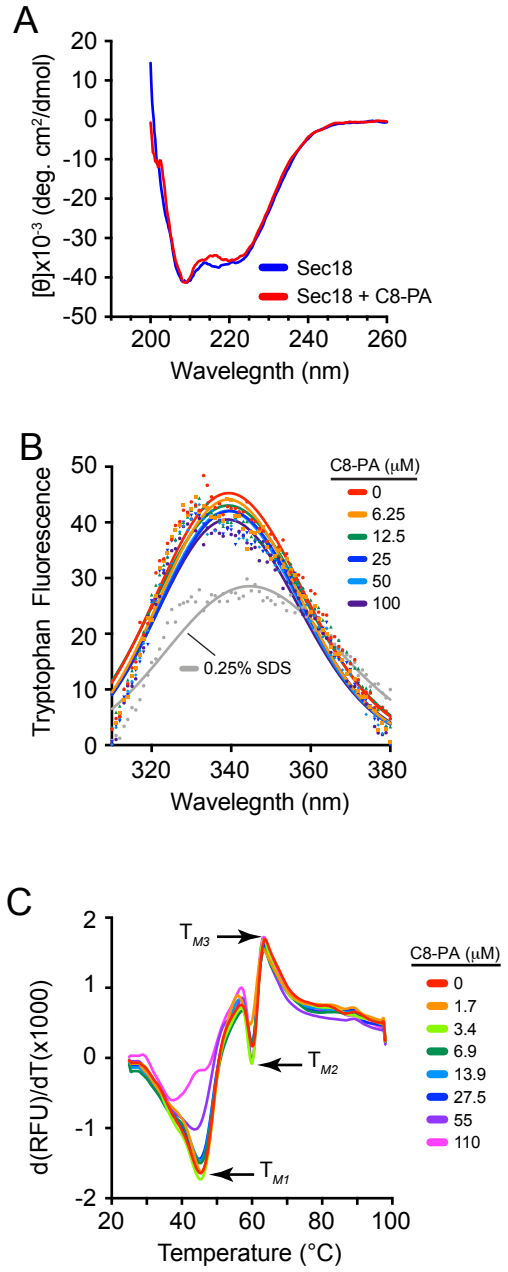

Figure 3.5. Sec18 does not have significantly altered secondary structure in the presence of short chain phosphatidic acid. (A) Circular dichroism spectra were measured (260 to 200 nm, 50 nm min^{-1}) for $Sec18_{His8}$ in the presence and absence of C8-PA (100 μM). **(B)** $Sec18_{His8}$ (500 nM) was incubated with increasing concentrations of C8-PA and fluorescence spectra were measured (ex. 295, em. 300-400 nm). The fluorescence (em. 333 nm) for each concentration tested was normalized against the no lipid control and is shown. **(C)** Differential scanning fluorimetry first derivative melting curves were measured (SYPRO orange: ex. 490, em. 560 nm) for increasing concentrations of C8-PA.

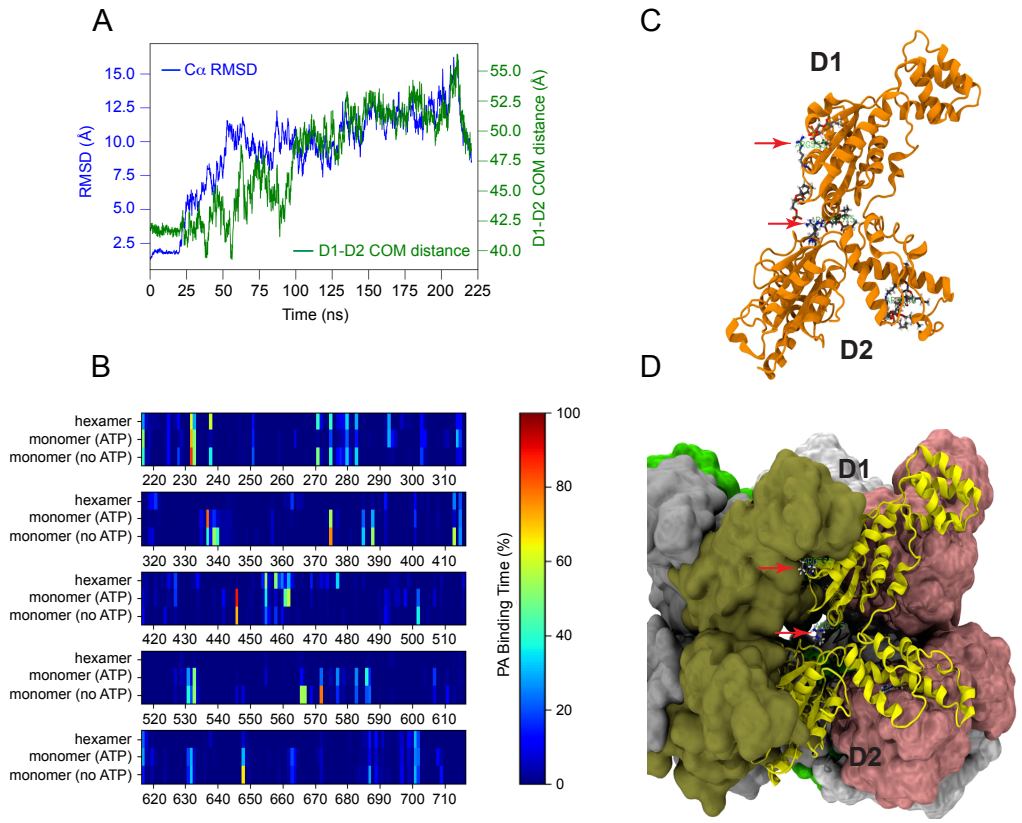

Figure 3.6. Computational Simulations Show Large Scale Conformational Change Between D1 and D2 Subunits of NSF and Indicate Potential PA binding Regions of NSF. (A) D1-D2 monomer undergoes large conformational change during relaxation. In the first 20 ns, D1-D2 monomer was equilibrated with a 0.05 kcal/mol/Å^2 harmonic restraint on protein Cα atoms. Blue: D1-D2 monomer Cα RMSD; green: center of mass distance between D1 and D2 domains. **(B)** Protomer chain A from hexamer cryo-EM structure (PDB: 3J94) was simulated in short-tailed PA solution (119mM, 61 PA molecules in a 95Å x 94Å x120Å water box) for 350 ns with ATP binding and 200 ns without ATP. Binding percentages were measured according to amount of time a PA molecule was within a hydrogen bonding distance from a given amino acid residue of NSF according to heatmap on right side of Figure 3.6C with residues of NSF indicated on the X axis and model flooded on Y axis. Both monomer **(C)** and hexamer **(D)** are shown with key residues from Figure 3.6B indicated on Figure 3.6C monomer and Figure 3.6D hexamer demonstrating region of hexamer where residues of monomer showing high binding are located.

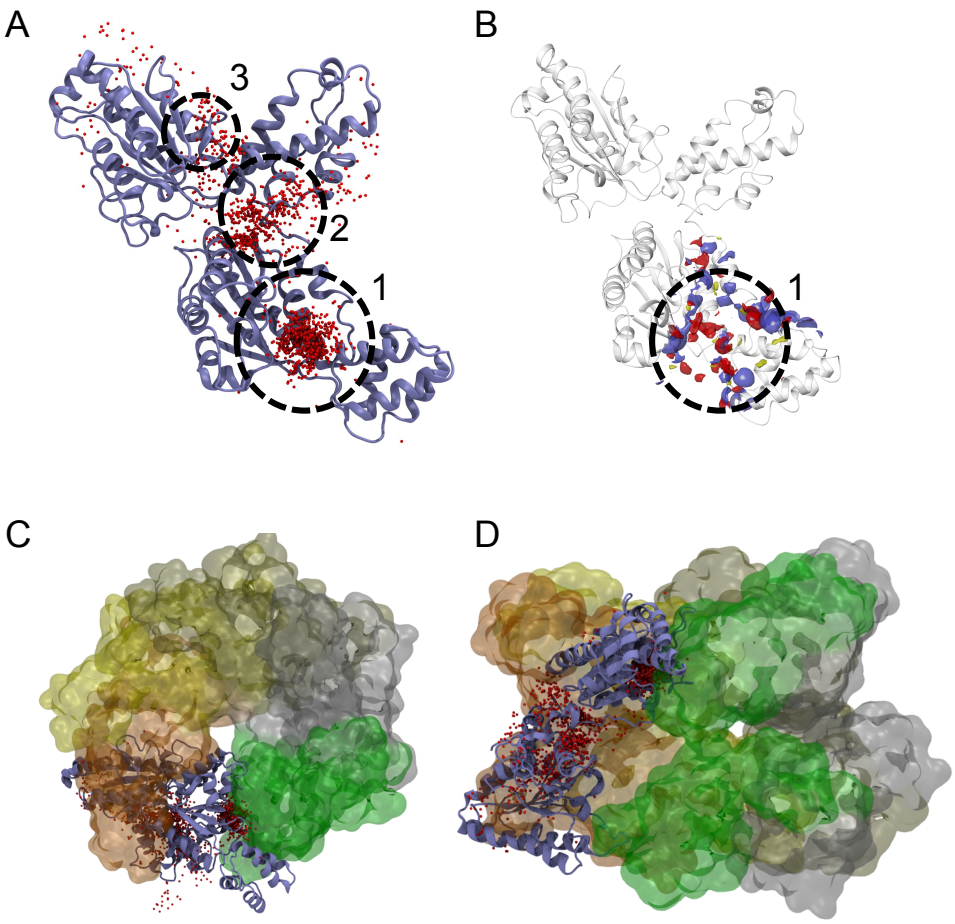

Figure 3.7. Ensemble Molecular Docking and Binding Site Prediction of NSF D1-D2 Monomer. (A) Small red spheres indicate positions on NSF monomer where short chained PA was docked. The circles 1, 2, 3 indicate clusters identified from the top short-chain PA ensemble docking results. **(B)** SiteMap predicted a high affinity binding region of NSF indicated by circle 1, which corresponds to the top ensemble docking cluster from Figure 3.7A where yellow indicates potential hydrophobic binding regions, blue indicates potential acidic binding regions, and red indicates potential basic binding regions on NSF. **(C)** A top down D1-D2 depiction of NSF D1-D2 hexamer is shown indicating clusters as described in Figure 3.7A are shown relative to the hexamer. **(D)** A side-view D1-D2 depiction of NSF D1-D2 hexamer is shown indicating clusters as described in Figure 3.7A are shown relative to the hexamer.

REFERENCES

Beauchamp, K.A., G.R. Bowman, T.J. Lane, L. Maibaum, I.S. Haque, and V.S. Pande. 2011. MSMBuilder2: Modeling conformational dynamics on the picosecond to millisecond scale. *J. Chem. Theory Comput.* doi:10.1021/ct200463m.

Blundell, T.L., A. Sali, A. Israel, N.G. Seidah, S. Jarriault, O. LeBail, C. Brou, C. Bessia, F. Logeat, J. Kimble, A.G. Petcherski, R. Kopan, W.J. Ray, D.J. Pan, X. Tian, A. Griesemer, M.T. Saxena, E.H. Schroeter, J.S. Mumm, J.D. Griffin, S. Artavanis-Tsakonas, R. Lake, S.C. Blacklow, J.C. Aster, L. Wu, J.C. Aster, A.T. Look, S.C. Blacklow, C. Sanchez-Irizarry, L.B. Silverman, J.P. 4th Morris, W. Lee, A.A. Ferrando, A.P. Weng, A. Joutel, T. Gridley, E. Tournier-Lasserve, Z. Li, M. Mericskay, E. Berrou, B. Klonjkowski, L.T. Krebs, J. Maciazek, M. Monet, P. Lacombe, P. Fardoux, V. Domenga, T.-L. Wang, I.-M. Shih, C.G. Eberhart, R.J. Kurman, Z. Zhang, B. Davidson, T.-L. Mao, K. Nakayama, M. Li, J.T. Park, B.-B.S. Zhou, J.C. Aster, Z. Yao, S.C. Blacklow, S. Singh, T. Duensing, R. Martin-Hollister, J. Zheng, G. Histen, L. Vien, T. Fu, S. Scoggin, M. Lu, D.W. Chang, W.R. Gordon, W. Wu, Y. Li, K. Li, L. Bolondi, K.B. Marcu, E. Ramazzotti, S. Pianetti, F. Lago, M. Minguzzi, P. Chieco, L. Gramantieri, C. Giovannini, M.X.G. Ilagan, R. Kopan, T. Walz, S. Artavanis-Tsakonas, H.-Y. Fan, T.C. Middelkoop, R.J. Lake, D.F. Kelly, T.C.G.A.R. Network, Y. Zhang, B. Chang, M. Chen, X. Xu, X. Fan, et al. 1993. Comparative protein modelling by satisfaction of spatial restraints. *J. Mol. Biol.*

Boeddinghaus, C., A.J. Merz, R. Laage, and C. Ungermann. 2002. A cycle of Vam7p release from and PtdIns 3-P-dependent rebinding to the yeast vacuole is required for homotypic vacuole fusion. *J. Cell Biol.* doi:10.1083/jcb.200112098.

Capelluto, D.G.S., X. Zhao, A. Lucas, J.A. Lemkul, S. Xiao, X. Fu, F. Sun, D.R. Bevan, and C. V. Finkielstein. 2014. Biophysical and molecular-dynamics studies of phosphatidic acid binding by the Dvl-2 DEP domain. *Biophys. J.* doi:10.1016/j.bpj.2014.01.032.

Chang, L.F., S. Chen, C.C. Liu, X. Pan, J. Jiang, X.C. Bai, X. Xie, H.W. Wang, and S.F. Sui. 2012. Structural characterization of full-length NSF and 20S particles. *Nat. Struct. Mol. Biol.* doi:10.1038/nsmb.2237.

Darden, T., D. York, and L. Pedersen. 1993. Particle mesh Ewald: An N·log(N) method for Ewald sums in large systems. *J. Chem. Phys.* doi:10.1063/1.464397.

Denisov, I.G., Y. V. Grinkova, A.A. Lazarides, and S.G. Sligar. 2004. Directed Self-Assembly of Monodisperse Phospholipid Bilayer Nanodiscs with Controlled Size. *J. Am. Chem. Soc.* doi:10.1021/ja0393574.

Essmann, U., L. Perera, M.L. Berkowitz, T. Darden, H. Lee, and L.G. Pedersen. 1995. A smooth particle mesh Ewald method. *J. Chem. Phys.* doi:10.1063/1.470117.

Feller, S.E., Y. Zhang, R.W. Pastor, and B.R. Brooks. 1995. Constant pressure molecular dynamics simulation: The Langevin piston method. *J. Chem. Phys.* doi:10.1063/1.470648.

Fleming, K.G., T.M. Hohl, R.C. Yu, S. a Müller, B. Wolpensinger, a Engel, H. Engelhardt, a T. Brünger, T.H. Söllner, and P.I. Hanson. 1998. A revised model for the oligomeric state of the N-ethylmaleimide-sensitive fusion protein, NSF. *J. Biol. Chem.* doi:10.1074/jbc.273.25.15675.

Fratti, R.A., Y. Jun, A.J. Merz, N. Margolis, W. Wickner, and B. Wickner. 2004. Interdependent assembly of specific regulatory lipids and membrane fusion proteins into the vertex ring domain of docked vacuoles. *J. Cell Biol.* doi:10.1083/jcb.200409068.

Friesner, R.A., R.B. Murphy, M.P. Repasky, L.L. Frye, J.R. Greenwood, T.A. Halgren, P.C.

Sanschagrin, and D.T. Mainz. 2006. Extra precision glide: Docking and scoring incorporating a model of hydrophobic enclosure for protein-ligand complexes. *J. Med. Chem.* doi:10.1021/jm051256o.

Halgren, T.A. 2009. Identifying and characterizing binding sites and assessing druggability. *J. Chem. Inf. Model.* doi:10.1021/ci800324m.

Hew, K., S.L. Dahlroth, S. Veerappan, L.X. Pan, T. Cornvik, and P. Nordlund. 2015. Structure of the Varicella Zoster Virus Thymidylate Synthase Establishes Functional and Structural Similarities as the Human Enzyme and Potentiates Itself as a Target of Brivudine. *PLoS One*. doi:10.1371/journal.pone.0143947.

Heyduk, T., and J.C. Lee. 1989. Escherichia coli cAMP receptor protein: evidence for three protein conformational states with different promoter binding affinities. *Biochemistry*. doi:10.1021/bi00443a021.

Huang, J., S. Rauscher, G. Nawrocki, T. Ran, M. Feig, B.L. de Groot, H. Grubmüller, and A.D. MacKerell. 2017. CHARMM36m: an improved force field for folded and intrinsically disordered proteins. *Nat. Methods*. 14:71–73. doi:10.1038/nmeth.4067.

Humphrey, W., A. Dalke, and K. Schulten. 1996. VMD: Visual molecular dynamics. *J. Mol. Graph.* doi:10.1016/0263-7855(96)00018-5.

Jahn, R., T. Lang, and T.C. Südhof. 2003. Membrane fusion. *Cell*. doi:10.1016/S0092-8674(03)00112-0.

Jahn, R., and R.H. Scheller. 2006. SNAREs - Engines for membrane fusion. *Nat. Rev. Mol. Cell Biol.* doi:10.1038/nrm2002.

Jahn, R., and T.C. Südhof. 1999. Membrane Fusion and Exocytosis. *Annu. Rev. Biochem.* doi:10.1146/annurev.biochem.68.1.863.

Jo, S., X. Cheng, S.M. Islam, L. Huang, H. Rui, A. Zhu, H.S. Lee, Y. Qi, W. Han, K. Vanommeslaeghe, A.D. MacKerell, B. Roux, and W. Im. 2014. CHARMM-GUI PDB manipulator for advanced modeling and simulations of proteins containing nonstandard residues. *Adv. Protein Chem. Struct. Biol.* doi:10.1016/bs.apcsb.2014.06.002.

Jun, Y., R.A. Fratti, and W. Wickner. 2004. Diacylglycerol and its formation by phospholipase C regulate Rab- and SNARE-dependent yeast vacuole fusion. *J. Biol. Chem.* doi:10.1074/jbc.M411363200.

Karunakaran, S., and R.A. Fratti. 2013. The Lipid Composition and Physical Properties of the Yeast Vacuole Affect the Hemifusion-Fusion Transition. *Traffic*. doi:10.1111/tra.12064.

Karunakaran, S., T. Sasser, S. Rajalekshmi, and R. a. Fratti. 2012. SNAREs, HOPS and regulatory lipids control the dynamics of vacuolar actin during homotypic fusion in S. cerevisiae. *J. Cell Sci.* doi:10.1242/jcs.091900.

Kato, M., and W. Wickner. 2001. Ergosterol is required for the Sec18/ATP-dependent priming step of homotypic vacuole fusion. *EMBO J.* doi:10.1093/emboj/20.15.4035.

Lapinski, M.M., A. Castro-Forero, A.J. Greiner, R.Y. Ofoli, and G.J. Blanchard. 2007. Comparison of liposomes formed by sonication and extrusion: Rotational and translational diffusion of an embedded chromophore. *Langmuir*. doi:10.1021/la7020963.

Lenzen, C.U., D. Steinmann, S.W. Whiteheart, and W.I. Weis. 1998. Crystal Structure of the Hexamerization Domain of N-ethylmaleimide–Sensitive Fusion Protein. *Cell*. doi:10.1016/S0092-8674(00)81593-7.

Liu, S., K.A. Wilson, T. Rice-stitt, A.M. Neiman, and J.A. Mcnew. 2007. In vitro fusion catalyzed by the sporulation-specific t-sNARE light-chain Spo20p is stimulated by phosphatidic acid. *Traffic*. doi:10.1111/j.1600-0854.2007.00628.x.

Manifava, M., J.W.J.F. Thuring, Z.Y. Lim, L. Packman, A.B. Holmes, and N.T. Ktistakis. 2001. Differential Binding of Traffic-related Proteins to Phosphatidic Acid- or Phosphatidylinositol (4,5)-Bisphosphate-coupled Affinity Reagents. *J. Biol. Chem.* doi:10.1074/jbc.M010308200.

Martyna, G.J., D.J. Tobias, and M.L. Klein. 1994. Constant pressure molecular dynamics algorithms. *J. Chem. Phys.* doi:10.1063/1.467468.

Matveeva, E.A., P. He, and S.W. Whiteheart. 1997. N-Ethylmaleimide-sensitive fusion protein contains high and low affinity ATP-binding sites that are functionally distinct. *J. Biol. Chem.* doi:10.1074/jbc.272.42.26413.

Mayer, A., D. Scheglmann, S. Dove, A. Glatz, W. Wickner, and A. Haas. 2000. Phosphatidylinositol 4,5-Bisphosphate Regulates Two Steps of Homotypic Vacuole Fusion. *Mol. Biol. Cell*. doi:10.1091/mbc.11.3.807.

Mayer, A., W. Wickner, and A. Haas. 1996. Sec18p (NSF)-driven release of Sec17p (α-SNAP) can precede docking and fusion of yeast vacuoles. *Cell*. doi:10.1016/S0092-8674(00)81084-3.

Miner, G.E., M.L. Starr, L.R. Hurst, R.P. Sparks, M. Padolina, and R.A. Fratti. 2016. The central polybasic region of the soluble snare (soluble n-ethylmaleimide-sensitive factor attachment protein receptor) Vam7 affects binding to phosphatidylinositol 3-phosphate by the PX (Phox Homology) domain. *J. Biol. Chem.* doi:10.1074/jbc.M116.725366.

Miyamoto, S., and P.A. Kollman. 1992. Settle: An analytical version of the SHAKE and RATTLE algorithm for rigid water models. *J. Comput. Chem.* doi:10.1002/jcc.540130805.

Nakanishi, H., M. Morishita, C.L. Schwartz, A. Coluccio, J. Engebrecht, and A.M. Neiman. 2006. Phospholipase D and the SNARE Sso1p are necessary for vesicle fusion during

sporulation in yeast. *J. Cell Sci.* doi:10.1242/jcs.02841.

Pande, V.S., K. Beauchamp, and G.R. Bowman. 2010. Everything you wanted to know about Markov State Models but were afraid to ask. *Methods*. doi:10.1016/j.ymeth.2010.06.002.

Phillips, J.C., R. Braun, W. Wang, J. Gumbart, E. Tajkhorshid, E. Villa, C. Chipot, R.D. Skeel, L. Kalé, and K. Schulten. 2005. Scalable molecular dynamics with NAMD. *J. Comput. Chem.* doi:10.1002/jcc.20289.

Putta, P., J. Rankenberg, R.A. Korver, R. van Wijk, T. Munnik, C. Testerink, and E.E. Kooijman. 2016. Phosphatidic acid binding proteins display differential binding as a function of membrane curvature stress and chemical properties. *Biochim. Biophys. Acta - Biomembr.* doi:10.1016/j.bbamem.2016.07.014.

Roberts, R.L., M. a Barbieri, K.M. Pryse, M. Chua, J.H. Morisaki, and P.D. Stahl. 1999. Endosome fusion in living cells overexpressing GFP-rab5. *J. Cell Sci.*

Rogasevskaia, T.P., and J.R. Coorssen. 2015. The role of phospholipase D in regulated exocytosis. *J. Biol. Chem.* doi:10.1074/jbc.M115.681429.

Ryu, J.K., D. Min, S.H. Rah, S.J. Kim, Y. Park, H. Kim, C. Hyeon, H.M. Kim, R. Jahn, and T.Y. Yoon. 2015. Spring-loaded unraveling of a single SNARE complex by NSF in one round of ATP turnover. *Science (80-.).* doi:10.1126/science.aaa5267.

Sasser, T., Q.S. Qiu, S. Karunakaran, M. Padolina, A. Reyes, B. Flood, S. Smith, C. Gonzales, and R.A. Fratti. 2012. Yeast lipin 1 orthologue Pah1p regulates vacuole homeostasis and membrane fusion. *J. Biol. Chem.* doi:10.1074/jbc.M111.317420.

Schreiner, E., L.G. Trabuco, P.L. Freddolino, and K. Schulten. 2011. Stereochemical errors and their implications for molecular dynamics simulations. *BMC Bioinformatics*. doi:10.1186/1471-2105-12-190.

Söllner, T., M.K. Bennett, S.W. Whiteheart, R.H. Scheller, and J.E. Rothman. 1993. A protein assembly-disassembly pathway in vitro that may correspond to sequential steps of synaptic vesicle docking, activation, and fusion. *Cell*. doi:10.1016/0092-8674(93)90376-2.

Sparks, R.P., J.L. Jenkins, G.E. Miner, Y. Wang, W.C. Guida, C.E. Sparks, R.A. Fratti, and J.D. Sparks. 2016. Phosphatidylinositol (3,4,5)-trisphosphate binds to sortilin and competes with neurotensin: Implications for very low density lipoprotein binding. *Biochem. Biophys. Res. Commun.* doi:10.1016/j.bbrc.2016.09.108.

Starr, M.L., L.R. Hurst, and R.A. Fratti. 2016. Phosphatidic Acid Sequesters Sec18p from *cis* -SNARE Complexes to Inhibit Priming. *Traffic*. 17:1091–1109. doi:10.1111/tra.12423.

Stroupe, C., K.M. Collins, R.A. Fratti, and W. Wickner. 2006. Purification of active HOPS complex reveals its affinities for phosphoinositides and the SNARE Vam7p. *EMBO J.* doi:10.1038/sj.emboj.7601051.

Studier, F.W. 2014. Stable expression clones and auto-induction for protein production in E. Coli. *Methods Mol. Biol.* doi:10.1007/978-1-62703-691-7_2.

Trabuco, L.G., E. Villa, K. Mitra, J. Frank, and K. Schulten. 2008. Flexible Fitting of Atomic Structures into Electron Microscopy Maps Using Molecular Dynamics. *Structure*. doi:10.1016/j.str.2008.03.005.

Trott, O., and A. Olson. 2010. AutoDock Vina: inproving the speed and accuracy of docking with a new scoring function, efficient optimization and multithreading. *J. Comput. Chem.* doi:10.1002/jcc.21334.AutoDock.

Tudyka, T., and a Skerra. 1997. Glutathione S-transferase can be used as a C-terminal, enzymatically active dimerization module for a recombinant protease inhibitor, and functionally secreted into the periplasm of Escherichia coli. *Protein Sci.*

doi:10.1002/pro.5560061012.

Vollrath, F., N. Hawkins, D. Porter, C. Holland, and M. Boulet-Audet. 2014. Differential scanning fluorimetry provides high throughput data on silk protein transitions. *Sci. Rep.* doi:10.1038/srep05625.

Wilson, D.W., S.W. Whiteheart, M. Wiedmann, M. Brunner, and J.E. Rothman. 1992. A multisubunit particle implicated in membrane fusion. *J. Cell Biol.* doi:10.1083/jcb.117.3.531.

Yavuz, H., I. Kattan, J.M. Hernandez, O. Hofnagel, A. Witkowska, S. Raunser, P.J. Walla, and R. Jahn. 2018. Arrest of trans-SNARE zippering uncovers loosely and tightly docked intermediates in membrane fusion. *J. Biol. Chem.* doi:10.1074/jbc.RA118.003313.

Yu, R.C., R. Jahn, and A.T. Brunger. 1999. NSF N-terminal domain crystal structure: Models of NSF function. *Mol. Cell*. doi:10.1016/S1097-2765(00)80191-4.

Zhao, M., and A.T. Brunger. 2016. Recent Advances in Deciphering the Structure and Molecular Mechanism of the AAA + ATPase N-Ethylmaleimide-Sensitive Factor (NSF). *J. Mol. Biol.* doi:10.1016/j.jmb.2015.10.026.

Zhao, M., S. Wu, Q. Zhou, S. Vivona, D.J. Cipriano, Y. Cheng, and A.T. Brunger. 2015. Mechanistic insights into the recycling machine of the SNARE complex. *Nature*. doi:10.1038/nature14148.

CHAPTER 4: DELETING THE DAG KINASE Dgk1 AUGMENTS YEAST VACUOLE FUSION THROUGH INCREASED Ypt7 ACTIVITY AND ALTERED MEMBRANE FLUIDITY[2]

ABSTRACT

Diacylglycerol (DAG) is a fusogenic lipid that can be produced through phospholipase C activity on phosphatidylinositol 4,5-bisphosphate [PI(4,5)P_2], or through phosphatidic acid (PA) phosphatase activity. The fusion of *Saccharomyces cerevisiae* vacuoles requires DAG, PA and PI(4,5)P_2, and the production of these lipids is thought to provide temporally specific stoichiometries that are critical for each stage of fusion. Furthermore, DAG and PA can be interconverted by the DAG kinase Dgk1 and the PA phosphatase Pah1. Previously we found that *pah1*Δ vacuoles were fragmented, blocked in SNARE priming and showed arrested endosomal maturation. In other pathways the effects of deleting *PAH1* can be compensated for by additionally deleting *DGK1*, however deleting both genes did not rescue the *pah1*Δ vacuolar defects. Deleting *DGK1* alone caused a marked increase in vacuole fusion that was attributed to elevated DAG levels. This was accompanied by a gain in resistance to the inhibitory effects of PA as well as inhibitors of Ypt7 activity. Together these data show that Dgk1 function can act as

[2] This chapter appeared in its entirety in the journal *Traffic*.
Miner, G. E., Starr, M. L., Hurst, L. R., and Fratti, R. A. (2017). Deleting the DAG kinase Dgk1 augments yeast vacuole fusion through increased Ypt7 activity and altered membrane fluidity. Traffic *18*, 315-329.
This article is reprinted with permission from the publisher and is available from https://onlinelibrary.wiley.com/doi/abs/10.1111/tra.12479
DOI: 10.1111/tra.12479

a negative regulator of vacuole fusion through the production of PA at the cost of depleting DAG and reducing Ypt7 activity.

INTRODUCTION

The movement of vesicles in eukaryotic cells is tightly regulated to prevent the missorting of cargo. Each route of membrane trafficking in the endocytic and secretory pathways is regulated by homologous sets of proteins that are conserved throughout eukarya. The final stage of cargo delivery occurs through the merger of two distinct membranes in a fusion reaction catalyzed by SNARE proteins (Jahn and Scheller, 2006). The fusion reaction pathway can be divided into stages that start with the disassembly of inactive *cis*-SNARE bundles. This process, known as priming, is executed by the SNARE chaperone NSF/Sec18 and its adaptor protein α-SNAP/Sec17 (Mayer et al., 1996). Membranes are subsequently brought into contact by the activity of Rab GTPases and their cognate tethering effectors (Stenmark, 2009). In *Saccharomyces cerevisiae*, vacuolar lysosomes undergo fusion with vesicles from the endocytic pathway, AP-3 coated membranes from the Golgi, autophagosomes, as well as with other vacuoles (Piper et al., 1997; Ishihara et al., 2001; Cabrera et al., 2010; Wickner, 2010). Homotypic vacuole fusion requires the Rab Ypt7 and its effector complex HOPS for tethering (Mayer and Wickner, 1997; Seals et al., 2000). During docking, *trans*-SNARE complexes form between partner membranes leading to the release of luminal Ca^{2+} stores prior to fusion (Merz and Wickner, 2004a). Docked vacuoles become tightly apposed forming a flattened region where they are in contact that is referred to as the boundary domain. The proteins and lipids that drive fusion become enriched at the edge of the boundary termed the vertex ring microdomain (Fratti et al., 2004; Wang et al., 2002, 2003b). Fusion occurs

around the vertex ring leading to the internalization of the boundary membrane and degradation of boundary-localized factors. DAG becomes enriched at the both the vertex and the boundary membrane leading to the potential degradation of this lipid after fusion occurs.

The regulation of membrane trafficking and fusion also involves a group of signaling lipids that play multiple roles in controlling these pathways. Yeast vacuole fusion requires diacylglycerol (DAG), phosphatidic acid (PA), as well as multiple phosphoinositides (PI) and ergosterol (Fratti et al., 2004; Boeddinghaus et al., 2002; Jun et al., 2004; Karunakaran and Fratti, 2013; Kato and Wickner, 2001; Lawrence et al., 2014; Sasser et al., 2012a; Stroupe et al., 2006). During the docking stage of fusion, these lipids accumulate into membrane microdomains that organize the SNAREs, Ypt7, HOPS and actin at the site of fusion (Fratti et al., 2004; Karunakaran and Fratti, 2013). The stoichiometry of these lipids is not static and requires the function of multiple lipid kinases, phosphatases and lipases at different time points to modify lipids to activate (or inactivate) their roles at each fusion stage. For instance, the PI 3-kinase Vps34 produces PI3P allowing the binding of Mon1, HOPS, and the soluble SNARE Vam7 leading to membrane tethering and docking (Lawrence et al., 2014; Stroupe et al., 2006; Cabrera et al., 2014; Cheever et al., 2001; Miner et al., 2016). Similarly, the PA phosphatase Pah1 converts PA to DAG leading to the transfer of PA-bound Sec18 to *cis*-SNARE complexes for priming (Sasser et al., 2012; see Chapter 2).

Pah1 is the yeast Lipin1 orthologue and its activity is required for endoplasmic reticulum and nuclear envelope homeostasis as well as lipid drop formation (Adeyo et al., 2011; Han et al., 2007). In addition, we have found that Pah1 activity is required for endosomal maturation. Deletion of Pah1 leads to the exclusion of Vps34, Mon1, Ypt7 and Vps39 from vacuolar membranes causing

vacuole fragmentation and abolished fusion (Lawrence et al., 2014; Sasser et al., 2012a). Others have shown that the activity of Pah1 can be countered by the DAG kinase of Dgk1 to replenish PA (Han et al., 2008a; b). The morphological defect of the endoplasmic reticulum and nuclear envelope seen in *pah1*Δ cells is reversed by the concomitant deletion of *DGK1*, illustrating the effects of interconverting PA and DAG on organelle homeostasis. DAG produced by Pah1 is used for the synthesis of triacylglycerol and the formation of lipid droplets as well as feeding into the Kennedy pathway for the production of phosphatidylethanolamine and phosphatidylcholine (Adeyo et al., 2011; Karanasios et al., 2010; Choi et al., 2011). DAG is a fusogenic lipid due to the induction of negative curvature and destabilization of lipid bilayers (Das and Rand, 1984; Seddon, 1990). The fusogenicity of DAG is further demonstrated by its ability to promote the fusion of protein-free liposomes (Sánchez-Migallón et al., 1995; Villar et al., 2000). These features are linked to its requirement for efficient vacuole fusion.

In this study we examined the role of Dgk1 in vacuole fusion. We first determined that deleting *DGK1* in *pah1*Δ background strains did not restore the blocked endosomal maturation, fusogenicity, or the vacuole fragmentation phenotype caused by deleting *PAH1* alone. This indicates that Pah1 and Dgk1 functions are not concurrent in vacuole homeostasis unlike their offsetting activities in other pathways. Importantly, the single *dgk1*Δ mutation led to an augmented fusion phenotype. We focused on finding the mechanism for the increased fusion of *dgk1*Δ vacuoles. These vacuoles contained elevated levels of the fusogenic lipid DAG and displayed an enhanced fusion phenotype. This was further characterized with increased resistance to the inhibitory effects of PA and elevated Ypt7-mediated vesicle tethering.

MATERIAL AND METHODS

Reagents

Reagents were dissolved in PS buffer (20 mM PIPES-KOH, pH 6.8, 200 mM sorbitol). Recombinant GST-FYVE, His_6-MTM-1, GST-C1b, His_6-SigD, GST-ENTH, MBP-FAPP1-PH, His_6-DgkB, GST-Vam7 and GST-Vam7^{Q283R}, Gdi1, His_6-Gyp1-46, His_6-Yck3, and Pbi2 were prepared as described and stored in PS buffer with 125 mM KCl (Gillooly, 2000; Taylor et al., 2000; Johnson et al., 2000; Marcus et al., 2001; Rosenthal et al., 1999; DOWLER et al., 2000; Miller et al., 2008; Fratti et al., 2007; Starai et al., 2007; Wang et al., 2003a; Hickey et al., 2009; Slusarewicz et al., 1997). The plasmid for expressing His_6-DgkB was a gift from Dr. C. Rock (St. Jude Children's Research Hospital, Memphis, TN). Antibodies against Sec17, Sec18, Vam3, Nyv1, Vps33, Ypt7 were prepared as described (Mayer et al., 1996; Haas and Wickner, 1996; Nichols et al., 1997; Ungermann et al., 1998; Seals et al., 2000; Mayer and Wickner, 1997). diC8-PA (1,2-dioctanoyl-*sn*-glycero-3-phosphate), diC8-DAG (1,2-diC8-sn-glycerol) and POG/DAG (palmitoyl-2-oleoyl-sn-glycerol) were purchased from Avanti Polar Lipids as chloroform stock solutions and stored at -20ºC. Filipin III was dissolved in DMSO at a stock concentration of 10 mM. Propranolol (Sigma) was dissolved in PS buffer.

Strains

Vacuoles from BJ3505 and DKY6281 were used for fusion assays (Table 4.1) (Haas et al., 1995). Strains lacking *PAH1 or YCK3* were described previously (Sasser et al., 2012a; Haas et al., 1994). *DGK1* was deleted by homologous recombination using PCR products amplified using 5'-DGK1-KO and 3'-DGK1-KO primers with homology flanking the *DGK1* coding sequence (Table 4.2).

The PCR product was transformed into yeast by standard lithium acetate methods and plated on YPD media containing G418 (250 μg/μl) to generate BJ3505 *dgk1*Δ*::kanMX6* (RFY60) and DKY6281 *dgk1*Δ*::kanMX6* (RFY61). *DGK1* was deleted from *pah1*Δ strains using PCR products amplified from pFA6A-hphMX4 and plated on YPD media containing hygromycin to generate RFY62 and RFY63. For complementation of *dgk1*Δ, RFY60 and RFY61 were transformed with pRS416 plasmids encoding *DGK1 or DGK1*^{D177A} inserted between the EcoRI and NotI sites to generate RFY64-67. The *DGK1* open reading frame was cloned using 5'-DGK1 and 3'-DGK1 primers using genomic DNA as a template. Point mutations generated using 5'-DGK1^{D177A} and 3'-DGK1^{D177A} primers. Transformants were selected on complete synthetic media lacking uracil. For cellular distribution analysis, *DGK1* was fused in frame to GFP. DKY6281 was transformed with a PCR product amplified from pFA6a-GFP(S65T)-KanMX6 with homology flanking the stop codon of *DGK1* with 5'-DGK-GFP and 3'DGK-GFP primers. Transformants were plated on YPD medium containing G418 to generate RFY68 (Wach et al., 1997). *PAH1* was deleted from RFY68 using PCR products amplified with 5'-PAH1-KO and 3'-PAH1-KO primers from pAG32 with homology flanking the *PAH1* coding sequence to generate RFY71. For immunoblotting *DGK1* was fused in frame to HA_3. BJ3505 was transformed with a PCR products amplified from pFA6a-3HA-kanMX6 with homology flanking the stop codon to generate RFY69 (Longtine et al., 1998). Using the 5'-YCK3-KO and 3'-YCK3-KO primers *YCK3* was deleted from *dgk1*Δ strains to generate RFY72-73.

Vacuole isolation, cell fractionation, and in vitro vacuole fusion

Vacuoles were isolated as described (Haas et al., 1995). *In vitro* fusion reactions (30 μl) contained 3 μg each of vacuoles from BJ3505 and DKY6281 backgrounds, reaction buffer (20 mM PIPES-

KOH pH 6.8, 200 mM sorbitol, 125 mM KCl, 5 mM $MgCl_2$), ATP regenerating system (1 mM ATP, 0.1 mg/ml creatine kinase, 29 mM creatine phosphate), 10 µM CoA, and 283 nM Pbi2 (Protease B inhibitor). Reactions were incubated at 27°C and Pho8 activity was assayed in 250 mM Tris-Cl, pH 8.5, 0.4% Triton X-100, 10 mM $MgCl_2$, 1 mM *p*-nitrophenylphosphate. Fusion units were measured by determining the *p*-nitrophenolate produced and absorbance was detected at 400 nm.

For Dgk1 localization by immunoblotting, yeast cells were fractionated into a total lysate, a total endomembrane fraction (Membranes), cytosol, endoplasmic reticulum (microsomes), and vacuoles as previously described (Qiu and Fratti, 2010; Sorin et al., 1997). For the total membrane preparation, yeast cells were resuspended in bead buffer (10 mM Tris/HCl, pH 7.4, 0.3 M sorbitol, 0.1 M NaCl, 5 mM $MgCl_2$) containing 1 mM PMSF at a density of 200 A_{600} units/ml. Cells were disrupted with glass beads by vortexing in five 1-min pulses, with intermittent chilling on ice. Lysates were centrifuged in a table-top centrifuge at 100 *g* for 5 min to pellet large debris and the supernatants carefully withdrawn and transferred to ultracentrifuge tubes. The total membrane fraction was collected by centrifugation (100,000 *g*, 1 h, 4°C) and resuspended in PS buffer (20 mM PIPES-KOH, pH 6.8, 200 mM sorbitol). The supernatant was saved as the cytosolic fraction. Endoplasmic reticulum derived microsomes were prepared as described (Grillitsch et al., 2011). Briefly, yeast cells were treated with lyticase to produce spheroplasts as performed for vacuole preparations. Spheroplasts were resuspended in buffer (5 mM MES, pH 5.0, 0.5 mM EDTA, 0.6 M sorbitol, 1 mM PMSF) and centrifuged (20,000 *g*, 0.5 h, 4°C) using a JA-20 rotor. Supernatants were collected and microsomes were pelleted by centrifugation (SW-41 rotor, 60,000 *g*, 0.5 h, 4°C). The pellet was resuspended in 100 µl of buffer.

Quantification of Vacuolar Diacylglycerol by Thin-Layer Chromatography

Lipids were extracted from purified DKY6281 and *dgk1*Δ vacuoles (200 µg protein content) by the method of Bligh and Dyer then dried overnight under vacuum (Bligh and Dyer, 1959). Purified lipids were resuspended in chloroform:methanol (2:1) before being resolved by neutral lipid thin-layer chromatography as previously described (Churchward et al., 2008). Briefly, Whatman Partisil® LK6D Silica Gel Plates (60 Å) were pre-washed with methanol/ethyl acetate (6:4) for 30 minutes. Individual channels were loaded with the indicated amount of diacylglycerol standard (Avanti Lipids) or vacuolar lipids. Plates were run twice with CH_2Cl_2/ethyl acetate/acetone (80:16:4) to 40 and 55 mm then hexanes/ethyl acetate to 68 mm (90:10), 80 mm (95:5), and 90 mm (100:0). Plates were then sprayed with a solution of 10% copper (II) sulfate in 8% phosphoric acid and dried for 10 minutes before charring at 145º C for 10 minutes. Imaging of plates was performed using a BioRad ChemiDoc™ MP Visualization System (605/50 filter, Green Epi illumination). Densitometry values were measured using Image Lab 4.0.1 software.

GST-Vam7 SNARE complex isolation and bypass fusion

SNARE complex isolation was performed as described previously using GST-Vam7 (Miner et al., 2016; Fratti and Wickner, 2007; Fratti et al., 2007). Briefly, 6X fusion reactions were incubated with 85 µg/ml anti-Sec17 IgG to block priming. After 15 min, 2 µM Gyp1-56 or 2 mM propranolol were added to selected reactions and incubated for an additional 5 min before adding 150 nM GST-Vam7. After a total of 90 min, reactions were placed on ice and 30 µl aliquots were removed to measure Pho8 activity. The remaining 150 µl reactions were sedimented (11,000 *g*, 10 min, 4°C), and the supernatants were discarded before extracting vacuoles with solubilization buffer (SB: 20

mM HEPES-KOH, pH 7.4, 100 mM NaCl, 2 mM EDTA, 20% glycerol, 0.5% Triton X-100, 1 mM DTT) with protease inhibitors (1 mM PMSF, 10 µM Pefabloc-SC, 5 µM pepstatin A, and 1 µM leupeptin). Vacuole pellets were overlaid with 100 µl SB and resuspended gently. An additional 100 µl SB was added, gently mixed, and incubated on ice for 20 min. Insoluble debris was sedimented (16,000 *g*, 10 min, 4°C) and 176 µl of supernatants were removed and placed in chilled tubes. Next, 16 µl was removed from each reaction as 10% total samples, mixed with 8 µl of 3X SDS loading buffer and heated (95°C, 5 min). Equilibrated glutathione beads (30 µl) were incubated with the remaining extracts (15 h, 4°C, nutation). Beads were sedimented and washed 5X with 1 ml SB (735 *g*, 2 min, 4°C), and bound material was eluted with 40 µl 1X SDS loading buffer. Protein complexes were examined by Western blotting.

Ca^{2+} efflux assay

Vacuole lumen Ca^{2+} efflux was measured as described (Sasser et al., 2012b). Fusion reactions (2X) contained 20 µg of vacuoles isolated from BJ3505 backgrounds, fusion reaction buffer and the fluorescent Ca^{2+} probe Fluo-4 dextran at 150 nM (Invitrogen). Reaction mixtures were transferred to a black 96-well plate. ATP regenerating system, or buffer was added and reactions were incubated at 27°C while monitoring Fluo-4 fluorescence (λ_{ex}=488 nm; λ_{em}=520 nm).

Lipid mixing

Lipid Mixing assays were conducted using rhodamine B DHPE (Rh-PE; Thermo Fisher) as described.[41] BJ3505 vacuoles (300 µg) were isolated and then incubated in 400 µl of PS buffer containing 150 µM Rh-PE (10 min, 4°C, nutating). Next, 800 µl of 15% Ficoll was added and then transferred to an 11 x 60 mm pollyalomar ultracentrifuge tube, overlaid with 1.2 ml of 8% and 4%,

and 0.5 ml of PS buffer. Labeled vacuoles were isolated by centrifugation (105,200 X *g*, 25 min, 4°C, SW-60 Ti rotor) and recovered from the 0-4% Ficoll interface. Lipid mixing assays (90 µl) contained 2 µg of labeled vacuoles and 16 µg of unlabeled vacuoles in fusion buffer. Reaction mixtures were transferred to a black, half volume 96-well flat-bottom microtiter plate on ice. The plate was transferred to a fluorescence plate reader at 27°C to start the reactions. Measurements were taken every 60 sec for 40 min yielding fluorescence values (λ_{ex}=544 nm; λ_{em}=590 nm) at the onset (F_0) and during the reaction (F_t). After 40 min 0.45% (vol/vol) Triton X-100 was added and the final 10 measurements were averaged to give the value of fluorescence after infinite dilution (F_{TX100}). The relative fluorescence change $\Delta F_t/F_{TX100} = (F_t - F_0)/F_{TX100} - F_0$ was calculated.

Microscopy

Vacuole morphology was monitored by incubating yeast with YPD broth containing the vital dye FM4-64 (Vida and Emr, 1995). Cultures were grown to saturation, diluted to ~0.2 OD_{600} in YPD containing 5 µM FM4-64, grown for 1 h in 30°C shaker, washed with PBS, and resuspended in dye-free YPD to chase the dye for 3 h at 30°C. Cells were washed in PBS, mixed with 0.6% agarose, and mounted on glass slides for observation. Images were acquired using a Zeiss Axio Observer Z1 microscope equipped with an X-Cite 120XL light source, Plan Apochromat 63X oil objective (NA 1.4), and an AxioCam CCD camera.

Statistical analysis

Statistical analysis was calculated using one-way ANOVA or two-tailed paired t-test. *P* values of ≤0.05 were considered significant. The half maximal inhibitory concentrations (IC_{50}) were determined using Origin software (OriginPro 9.1 software, OriginLab).

RESULTS

Vacuole morphology and Dgk1 localization

Vacuole fusion requires the production and turnover of numerous signaling lipids including PA and DAG (Fratti et al., 2004; Jun et al., 2004; Sasser et al., 2012a). Multiple pathways feed into the production and interconversion of these lipids. DAG can be produced by the activity of Plc1 on PI(4,5)P_2 or Pah1 on PA (Flick and Thorner, 1993; Han et al., 2007). PA can be produced by phospholipase D activity on PC or by Dgk1 on DAG (Han et al., 2008a; Waksman et al., 1996). The production of DAG during vacuole fusion is important due to its fusogenic properties (Goñi and Alonso, 1999; Chernomordik and Kozlov, 2003). DAG becomes enriched at the vertex ring and boundary membrane of docked vacuoles and regulates localization of SNAREs, Ypt7 and HOPS to the site of fusion.

We previously found that deletion or inactivation of *PAH1* inhibited endosomal maturation that was characterized by vacuoles that lacked the late endosomal/lysosomal Rab Ypt7, the HOPS subunit Vps39, as well as the PI 3-kinase Vps34 and its product PI3P (Sasser et al., 2012a). The lack of Ypt7 was due to the exclusion of its guanine exchange factor Mon1-Ccz1, which is recruited to membranes in part through its interactions with PI3P (Lawrence et al., 2014; Cabrera et al., 2014). Because deletion of *DGK1* restores the effects of deleting *PAH1* in other pathways we began by testing whether the double deletion would restore the *pah1*Δ vacuolar defects. We first examined whether the double deletion would restore *pah1*Δ vacuole morphology. We found that *dgk1*Δ cells exhibited wild type vacuole morphology (Fig. 4.1A). Curiously, the *dgk1*Δ *pah1*Δ double deletion cells were fragmented in a manner similar to *pah1*Δ cells. Thus, deleting both

enzymes did not rescue the *pah1*Δ vacuole fragmentation phenotype or blocked fusion. This was not in keeping with the effects seen in restoring nuclear/endoplasmic reticulum morphology in other pathways. Quantitation of vacuole fragmentation is shown in Figure 4.1B.

Due to the lack of an effect of deleting *DGK1* on the *pah1*Δ vacuole morphology phenotype we examined if Dgk1 was mislocalized in mutant cells. First, we visualized the distribution of Dgk1-GFP in wild type whole cells. Figure 4.1C shows widefield fluorescent images showing Dgk1-GFP localization in cells stained with FM4-64 to label vacuoles. Dgk1-GFP localized to ribbon-like structures of the endoplasmic reticulum similar to what has been previously reported (Wolinski et al., 2015). We also observed that the Dgk1-GFP ribbons were often adjacent to vacuoles and a fraction of Dgk1-GFP colocalized with FM4-64 suggesting that aside from the endoplasmic reticulum, vacuoles also harbor a portion of the enzyme. Dgk1-GFP localization was next examined in *pah1*Δ cells and we did not detect any appreciable differences in it localization relative to the wild type parent strain. Because some Dgk1-GFP appeared to colocalize with vacuoles we further examined Dgk1 distribution by cell fractionation and immunoblotting. Yeast cells expressing Dgk1-HA were fractionated into crude lysate, cytosol, vacuoles, a total membrane pool as well as microsomes containing endoplasmic reticulum. The blots showed that Dgk1-HA was present in microsomes and vacuoles (Fig. 4.1D). As a control, we probed for Dgk1-HA in the cytosolic fraction and found that this polytopic protein was absent. Ypt7 served as an enrichment marker for vacuoles. Sec61 served as a marker for resident endoplasmic reticulum components. Sec61 was detected in the vacuole fraction indicating that there was some contamination from the endoplasmic reticulum. Although this accounts for the majority of the Dgk1 detected in the vacuole fraction, it should also be noted that the ratio of Dgk1 to Sec61 is greater on vacuoles relative to

the microsome fraction (Fig. 4.1E). Together with the Dgk1-GFP localization it is apparent that a subpopulation of Dgk1 does indeed reside on the vacuolar membrane.

Cells lacking *DGK1* accumulate vacuolar DAG

To determine if deleting *DGK1* would have an effect on vacuolar DAG levels we quantitated this lipid on vacuoles from wild type and *dgk1*Δ cells. Neutral lipids were extracted from wild type and *dgk1*Δ vacuoles and resolved by thin-layer chromatography as described in the Materials and Methods section. Purified DAG was used to generate a standard curve in the first six lanes of the plate (Fig. 4.2A). Three of the five trials run were loaded onto the plate shown. We found that *dgk1*Δ vacuoles consistently contained more DAG than wild type vacuoles. Figure 4.2B shows quantitation of five trials ($p<0.05$). The DAG content of wild type and *dgk1*Δ vacuoles was calculated using a standard curve of pure DAG and plotted as μg of DAG per 150 μg of vacuole protein. These data indicate that vacuoles will accumulate DAG in the absence of Dgk1. However, this does not indicate whether the difference in DAG content is due to Dgk1 activity on the vacuole or whether the lack of DAG kinase activity elsewhere affects the total amount of this lipid trafficked to vacuoles.

The absence of Dgk1 augments vacuole fusion

To further examine the consequence of deleting *DGK1* on vacuole homeostasis we tested fusion efficiency. These experiments showed that *dgk1*Δ vacuole fusion was markedly increased by ~40% relative to wild type (Fig. 4.3A), suggesting that the conversion of DAG to PA by Dgk1 negatively regulates fusion. This is in keeping with the notion that DAG is fusogenic and that Dgk1 activity is needed to reduce unchecked fusion. We next asked if the rate of fusion itself was increased for

*dgk1*Δ vacuoles. The slope of the fusion curve for *dgk1*Δ vacuoles appeared to be steeper in comparison to wild type. However, this appearance could be due to normalizing fusion to the wild type maximum. While this shows the overall increase in total fusion, it does not clearly show the initial rate of fusion. To better visualize the rate of *dgk1*Δ vacuole fusion we re-plotted the data as normalized to its own maximal fusion at the end of 90 min (Fig. 4.3A, red circles). This approach showed that the adjusted *dgk1*Δ fusion curve perfectly overlapped with that of wild type vacuoles, indicating that the rates of fusion were identical and that the augmented fusion of *dgk1*Δ vacuoles was due to other factors. We also asked whether the augmented fusion occurred during different rounds of fusion. To this aim we used a method shown to differentiate the first round of fusion from later events (Merz and Wickner, 2004b). Previously we used this method to determine that deleting *NHX1* only affected the first round of fusion without affecting subsequent fusion cycles (Qiu and Fratti, 2010). To detect the first round of fusion, a 5:1 excess of effector vacuoles (*PEP4 pho8*Δ) was used. For later rounds of fusion reactions used a 4:2 excess of reporter vacuoles (*pep4*Δ *PHO8*). Using this method we found that *dgk1*Δ vacuoles showed enhanced fusion for both early and late rounds of fusion (Fig. 4.3B), suggesting that the effects of deleting *DGK1* was consistent.

Although we have shown that the rate of full fusion and content mixing of *dgk1*Δ vacuoles matches that of wild type, it was possible that the elevated levels of DAG could destabilize the bilayers enough to promote faster hemifusion. Thus, we next measured the mixing of outer leaflet lipids as a reporter for hemifusion (Karunakaran and Fratti, 2013; Reese and Mayer, 2005). Here, a population of vacuoles is loaded with rhodamine conjugated PE (Rh-PE) at levels that quench fluorescence. Rh-PE labeled vacuoles are then incubated with an 8-fold excess of unlabeled vacuoles. Upon lipid mixing of labeled and unlabeled vacuoles the Rh-PE is diluted and the

fluorescence is de-quenched. This approach showed that *dgk1*Δ vacuoles underwent lipid mixing at the same rate versus wild type (Fig. 4.3C). Also shown are the negative controls of excluding ATP or blocking priming with anti-Sec17 antibody. These data suggest that the fusion phenotype of *dgk1*Δ vacuoles was not due to an increased rate of fusion of a set amount of vacuoles but perhaps is a refection that more vacuoles are initially participating in fusion.

Because changes in fusion, as a measure of Pho8 activity, could theoretically be affected indirectly by altered activity of the reporter enzyme itself, we verified that the increased fusion of *dgk1*Δ vacuoles was real by performing a visual assay to measure changes in vacuole diameter (Merz and Wickner, 2004b; Sasser et al., 2012b). Here, vacuole reactions were treated with buffer, anti-Sec18 IgG or propranolol. Both inhibitors potently inhibit fusion at the priming stage (Mayer et al., 1996; Sasser et al., 2012a). Propranolol is a β-adrenergic receptor blocker that also inhibits PA phosphatase activity, which is required for Sec18-mediated SNARE priming to occur (see Chpater 2; Meier et al., 1998). After incubation (90 min, 27°C), fusion reactions were placed on ice and stained with FM4-64 for fluorescence microscopy evaluation. In accord with the content mixing assay, we found that the diameters of *dgk1*Δ vacuoles were significantly larger relative to wild type vacuoles (Fig. 4.3D, $p<0.05$). Incubating reactions on ice as well as treatment with anti-Sec18 or propranolol blocked the increase in vacuole diameter demonstrating that changes in vacuole size were due to fusion.

To determine whether the kinase activity of Dgk1 was linked to the fusion enhancement, *dgk1*Δ strains were complemented with plasmids encoding either wild type *DGK* or the inactivated kinase mutant DGK^{D177A} (Han et al., 2008b). Complementation with p*DGK1* partially restored fusion to

near wild type levels (Fig. 4.3E). The lack of full wild type fusion restoration with complementation was thought to be due to plasmid loss during growth in non-selective medium for vacuole purification. Nevertheless, the difference in fusion between the *dgk1*Δ and complemented vacuoles was statistically significant ($p<0.05$). Moreover, the difference between wild type fusion and the complement was not significant ($p=0.25$). Complementation with the kinase-dead mutant pDGK^{D177A} did not reverse the increased fusion seen with *dgk1*Δ vacuoles (Fig. 4.3F). These data demonstrate that the altered fusion seen with *dgk1*Δ vacuoles was directly due to the kinase activity of Dgk1.

In Figure 4.1A-B we showed that the *dgk1*Δ *pah1*Δ double deletion did not restore the vacuole fragmentation phenotype of *pah1*Δ alone. To further verify effect of deleting *DGK1* on *pah1*Δ vacuole function we tested the mutations in content mixing assays. We found that the *dgk1*Δ*pah1*Δ double deletion strains exhibited attenuated fusion similar to what occurs with the single *PAH1* deletion (Fig. 4.3G). As with the morphological examination of the double deletion strain, we concluded that the activities of these enzymes do not directly counterbalance each other with respect to vacuole homeostasis and fusion. For this reason we focused on the augmented fusion of *dgk1*Δ vacuoles for the remainder of the study.

Changes in fusion could be attributed to a variety of factors including changes in the concentration of regulatory proteins such as SNAREs. Others have shown that increased SNARE levels can enhance vacuole fusion (Starai et al., 2007). Deletion of the ABC transporter Ybt1 and the casein kinase Yck3 has also been shown to increase vacuole fusion through distinct mechanisms (Sasser et al., 2012b; Hickey et al., 2009). To assess if the elevated fusion of *dgk1*Δ vacuoles was due to

changes in the fusion machinery we performed immunoblotting analysis of known regulators. No differences were observed between *dgk1*Δ vacuoles and wild type (Fig. 4.3H). Taken together we conclude that Dgk1 activity suppresses maximal vacuole fusion and that the increased fusion seen with *dgk1*Δ vacuoles was not due to a fault in the reporter systems or caused by increased levels of the core fusion machinery proteins.

DGK1 deletion does not alter SNARE complex formation

Vacuole fusion can be augmented by the increase in the copies of SNAREs or by the improved efficiency of complex formation (Karunakaran and Fratti, 2013; Starai et al., 2007). As seen in Figure 4.3H, the amount of individual SNAREs was unaffected by deleting *DGK1*, however, their effectiveness is not apparent by immunoblotting alone. Thus we examined the efficiency of SNARE complex formation. This assay relies on blocking priming with anti-Sec17 IgG and its bypass by the addition of recombinant GST-Vam7 to restore fusion (Fratti and Wickner, 2007; Fratti et al., 2007). First, we determined if the dosage required for the bypass was different for *dgk1*Δ vacuoles relative to wild type. Figure 4.4A shows the restoration of fusion upon addition of GST-Vam7 at the indicated concentrations. This showed that *dgk1*Δ vacuoles responded to the addition of GST-Vam7 at the same peak of efficacy compared to wild type.

Next, we performed Vam7 bypass experiments to examine the formation of SNARE complexes and HOPS binding. We found that GST-Vam7 interacted with its cognate SNAREs Nyv1 and Vam3 with equal efficiency on either wild type or *dgk1*Δ vacuoles (Fig. 4.4B-C). Hence, it appears that the altered fusion seen with *dgk1*Δ vacuoles was not due to increased SNARE complex formation. To verify that SNARE complexes were similarly active on both vacuole types we

examined the efflux of luminal Ca^{2+} stores that are released upon *trans*-SNARE complex formation (Merz and Wickner, 2004a). Previously we have found that deletion of the ABC transporter Ybt1 strikingly delayed the kinetics of Ca^{2+} efflux, which was linked to increased vacuole fusion.[43] However, there was no difference in the kinetics or amplitude of Ca^{2+} release between *dgk1*Δ and wild type vacuoles (Fig. 4.4D). Together these data indicated that increased fusion of *dgk1*Δ vacuoles was not directly due to altered SNARE complex formation.

Deletion of *DGK1* confers resistance to PA

Previous studies showed that reducing, or blocking, DAG inhibited the enrichment of regulatory lipids at the vertex ring assembly and blocked fusion (Fratti et al., 2004; Jun et al., 2004). We next asked if increasing DAG levels through the deletion of *DGK1* would alter the role of regulatory lipids in fusion. To this aim we examined the effects of blocking regulatory signaling lipids on *dgk1*Δ vacuoles. We found that blocking the function of PI3P, PI4P, $PI(4,5)P_2$, and ergosterol with the ligands FYVE, FappPH, ENTH, and filipin respectively inhibited *dgk1*Δ vacuole fusion indistinguishably from wild type (Fig. 4.5A). There was also no difference when PI3P and $PI(4,5)P_2$ were modified by the phosphatases MTM-1 and SigD, respectively. This indicated that the enhanced fusion phenotype was not due to additional changes in the core fusion machinery or due to off pathway mechanisms. Because Dgk1 activity altered DAG levels on isolated vacuoles we next tested if *dgk1*Δ vacuoles were less sensitive to the DAG ligand C1b. We found that C1b inhibited *dgk1*Δ vacuole fusion at the same concentration needed to block wild type fusion (Fig. 4.5B). This suggests that the change in DAG does not directly affect a protein-lipid interaction such as the binding of Protein kinase C (PKC) to DAG on other membranes (Stahelin et al., 2004). Instead it is likely that the augmented fusion is a result of an indirect effect such as changes in

membrane curvature and fluidity. It is also possible that a population of DAG was inaccessible to C1b by accumulating in the boundary membrane or by translocating across the bilayer (Fratti et al., 2004; Bai and Pagano, 1997).

As is now evident, the conversion of PA to DAG by Pah1 is necessary for vacuolar SNARE priming (see Chapter 2). Increasing PA concentrations through inactivation of Pah1 or through the addition of short-chain PA (diC8-PA) potently blocked fusion by sequestering Sec18 away from SNAREs in a PA-dependent manner. Thus, we asked if the increase in DAG on *dgk1*Δ vacuoles would shift the DAG:PA ratio in a way that would alter the sensitivity of fusion towards PA. To answer this we tested the effect of converting DAG to PA with recombinant His_6-DgkB, the soluble DAG kinase from *Staphylococcus aureus* (Miller et al., 2008). We found that DgkB potently inhibited wild type vacuole fusion as well as fusion by *dgk1*Δ vacuoles (Fig. 4.5C). However, there was a right-shift in the inhibition curves for *dgk1*Δ vacuole fusion that was statistically significant at 130 and 220 μg/ml ($p<0.05$). Although the shift was not large it was consistent with needing more DgkB for the elevated level of DAG at the beginning of the reaction.

To further test the effects of increasing PA on fusion we added diC8-PA to fusion assays. As previously shown, the addition of diC8-PA had a marked inhibitory effect on the fusion of wild type vacuoles (Fig. 4.5D). Importantly, the inhibitory effect of excess PA was clearly reduced with *dgk1*Δ vacuoles. The IC_{50} of diC8-PA on wild type vacuoles was 31.2±5.1 μM whereas the IC_{50} was 122.8±15.2 μM for *dgk1*Δ vacuoles (*$p<0.05$). The increased resistance of *dgk1*Δ vacuole fusion to diC8-PA suggests that the elevated levels of DAG lead to a requirement of more diC8-

PA to fully inhibit fusion. Together these data indicate that the ratio of DAG to PA is a critical component of regulating vacuole fusion.

Augmented *dgk1*Δ vacuole fusion is linked to enhanced Ypt7 activity

To test if the augmented fusion of *dgk1*Δ vacuoles was on pathway and regulated by the known machinery, we tested a panel of inhibitors that targeted the proteins that regulate vacuole fusion. Figure 4.6A shows that antibodies against the SNAREs Nyv1, Vam3, or the HOPS subunit Vps33 inhibited *dgk1*Δ vacuole fusion with similar effects compared to wild type. The relative fusion endpoints for both wild type and *dgk1*Δ vacuoles were normalized to 100% (Fig. 4.6A). Interestingly, *dgk1*Δ vacuole fusion showed reduced sensitivity to anti-Ypt7 IgG. To further examine the change in sensitivity of *dgk1*Δ vacuoles to anti-Ypt7 we performed dose response assays to calculate the IC_{50}. This showed that *dgk1*Δ fusion was significantly less sensitive to anti-Ypt7 with an IC_{50} of 124.9±10.7 μg/ml while the IC_{50} for wild type was 61.2±8.1 μg/ml (Fig. 4.6B, $*p<0.05$). This suggests that Ypt7 could be more active in *dgk1*Δ vacuoles. It is also possible that changes in the membrane curvature and fluidity could allosterically induce conformational changes in Ypt7 leading to decreased binding by the antibody. Based on the effects of anti-Ypt7 IgG we also examined the efficacy of the GTPase activating protein Gyp1 and the Rab-GDP dissociation inhibitor GDI. We found that both proteins had right-shifted inhibition curves with *dgk1*Δ vacuole fusion. Figure 4.6C shows that *dgk1*Δ vacuole were less sensitive to Gyp1-46 with an IC_{50} of 4.17±0.06 μM compared to wild type (IC_{50} = 1.54±0.046 μM, $*p<0.05$). Similarly, *dgk1*Δ vacuole fusion was more resistant to GDI versus wild type. The IC_{50} for GDI with *dgk1*Δ vacuoles was 114.7±8.7 nM, while the IC_{50} with wild type was 209.2±14.1 nM (Fig. 4.6D, $*p<0.05$). Together these data suggest that Ypt7 function is enhanced in *dgk1*Δ vacuoles. That

said, these assays do not distinguish whether *dgk1*Δ vacuoles have increased activity per individual Ypt7 molecule or if there are simply more numerous activated Ypt7 copies per vacuole. Alternatively, it is possible the *dgk1*Δ require less Ypt7 to promote fusion.

The *dgk1*Δ fusion effect is in parallel to the function of Yck3

In addition to the effect of deleting *DGK1* on Ypt7 function shown here, Ungermann et al. found that deleting the type I casein kinase Yck3 resulted in fusion that was resistant to Gdi1 and Gyp7-47.[52] This was linked to augmented vacuole fusion. Yck3 activity reduces fusion by phosphorylating Vps41, Vam3 and Mon1 (Lawrence et al., 2014; LaGrassa and Ungermann, 2005; Brett et al., 2008). The similar phenotypes of elevated fusion and increased Ypt7 activity in both *yck3*Δ and *dgk1*Δ vacuoles led us to ask if they shared a common pathway. We previously reported that the Ypt7 GEF Mon1-Ccz1 was phosphorylated by the casein kinase Yck3 leading to its release from the membrane (Lawrence et al., 2014). Deletion of *YCK3* or mutation of Mon1 phosphorylation sites prevented Mon1 from being released from the membrane during fusion. The influence of Yck3 on fusion is further illustrated through the inhibitory activity of adding exogenous recombinant His_6-Yck3 (Hickey et al., 2009). Together, the data suggest that Dgk1 and Yck3 lie on the same pathway of regulating vacuole fusion.

The experiments in Figure 4.7 begin addressing the connection between Dgk1 and Yck3. First, we immunoblotted for Yck3 on wild type and *dgk1*Δ vacuoles and found that the kinase was present at equal levels on membranes from both strains (Fig. 4.7A-B). This shows that Yck3 does not require Dgk1 for its recruitment to vacuoles. Next we examined if Yck3-dependent Mon1 release occurred on *dgk1*Δ vacuoles. Figure 4.7C shows that Mon1 was released at the same rate on both

sets of vacuoles, indicating that Yck3 function was normal on *dgk1*Δ membranes. Figure 4.7D shows quantitation of Mon1 retention over time. Although Mon1 release was not affected on *dgk1*Δ we went on to test if the addition of recombinant Yck3 would differentially affect the two types of vacuoles. We found that added His_6-Yck3 inhibited the fusion of wild type and *dgk1*Δ vacuoles with identical dose responses (Fig. 4.7E). Thus far, it appears that Yck3 and Dgk1 functions are likely in parallel pathways. To further determine if the underlying mechanisms of the *dgk1*Δ and *yck3*Δ fusion phenotypes are linked, we constructed *yck3*Δ *dgk1*Δ double deletion strains. We hypothesized that if the two functions were in parallel we would observed additive increases in vacuole fusion relative to either *yck3*Δ or *dgk1*Δ single deletions. The lack of further augmented fusion would suggest that the Dgk1 and Yck3 pathways overlap. We found that both *yck3*Δ and *dgk1*Δ single deletions had enhanced fusion as seen previously. Unexpectedly, the double *yck3*Δ *dgk1*Δ double deletion fused to a similar extent the wild type parent strains (Fig. 4.7F, $p>0.05$). The loss of augmented fusion suggests that Yck3 and Dgk1 function in different pathways. Although evidence is lacking, it is not unlikely that the altered function of Ypt7 due to the lack of Dgk1 was negatively affected by the retention of unphosphorylated Mon1 due to the lack of Yck3 resulting in a return to normal overall function. That said, further studies would be required to explore this possibility, which go beyond the scope of this study.

Exogenously added DAG enhances fusion of wild type vacuoles

Because *dgk1*Δ vacuoles contain increased levels of DAG, we next asked if adding the lipid exogenously to wild type vacuoles would alter fusion. Previously we found that while vacuole fusion was inhibited with short chain phosphatidic acid (diC8-PA), fusion was not affected by diC8-DAG (see Chapter 2). The effect of diC8-PA was attributed to the interaction of the PA

headgroup with Sec18 to prevent SNARE priming. DAG on the other hand is directly fusogenic and transmits its effects on membranes through its acyl chains. Thus, the lack of an effect by diC8-DAG was attributed to the inability of short acyl chains to influence membrane curvature or bilayer stability. To better determine the effect of exogenous addition of this lipid we used long chain (16:0, 18:1) DAG to wild type and *dgk1*Δ vacuole fusion reactions. We found that adding DAG enhanced the fusion wild type vacuoles by ~17% at 5 nM while it had no effect on *dgk1*Δ vacuoles (Fig. 4.8A, *p<0.05). Higher levels of DAG did not further enhance fusion (not shown). Although the addition of DAG did not fully mimic the effect of deleting *DGK1*, it does support the notion that DAG levels alone can modulate the efficacy of fusion. Similarly, the addition of 5 nM DAG increased lipid mixing by approximately 20% (Fig. 4.8B, **p<0.01).

The deletion of *DGK1* restores the fusogenicity of mutant Vam7^{Q283R}

In previous studies we found that mutating the ionic zero layer of the Vam7 SNARE motif (Q283R) prevented anti-Sec17 bypass fusion (Fratti et al., 2007; Karunakaran and Wickner, 2013). Fusion reactions containing Vam7^{Q283R} were arrested at a hemifusion intermediate. Fusion could be restored by altering the fluidity and curvature of the vacuole with the cationic amphiphile chlorpromazine. We hypothesized that mutant SNARE complexes containing Vam7^{Q283R} transferred insufficient energy to the membrane to trigger fusion. Thus, the effect of chlorpromazine was thought to be due to lowering the energy barrier for fusion to a level where Vam7^{Q283R} could function. Due to the increased DAG concentration in *dgk1*Δ vacuoles we asked if fluidity and curvature was sufficiently altered to promote Vam7^{Q283R} mediated fusion. Fusion reactions blocked with anti-Sec17 IgG were treated with recombinant Vam7^{Q283R} at the indicated concentrations. We found that Vam7^{Q283R} was able to promote a modest level of fusion in *dgk1*Δ

vacuoles whereas wild type vacuole fusion were unresponsive (Fig. 4.8C, $**p<0.01$). This result is consistent with the notion that the increase in DAG on *dgk1*Δ lowers the energy barrier for fusion in a similar manner to what was seen with chlorpromazine. It is important to consider that exogenous Vam7 rescues anti-Sec17 blocked fusion also bypasses the role of Ypt7 dependent tethering, which requires Sec17 mediated SNARE priming. Thus, the enhanced Ypt7 activity likely did not play a role in this experiment.

DISCUSSION

It has been well established that most membrane fusion is catalyzed by SNARE proteins, yet the interdependence of the fusion machinery and the membrane itself remains unclear. Among the lipids that compose the membrane is a group that is subject to modification by specific kinases, phosphatases, and lipases to regulate membrane trafficking. The most studied of these lipids are the phosphoinositides that can be differentially phosphorylated on their inositol head groups to yield a panel of bioactive molecules that help orchestrate the fusion machinery through direct interactions with protein ligands. Specific PIs are necessary at various stages of fusion. For instance, vacuole fusion requires $PI(4,5)P_2$ during priming as well as after docking (Collins et al., 2005; Mayer et al., 2000). $PI(4,5)P_2$ is turned over by Plc1 to yield IP_3 and DAG, a fusogenic lipid required for vacuole content mixing (Jun et al., 2004). DAG can also be produced through the activity of the PA phosphatase Pah1, a pathway that is complemented by the activity of Dgk1 on DAG to restore PA levels (Han et al., 2008b, 2006). PA plays important roles in various membrane trafficking pathways including sporulation, mitochondrial fusion, and Glut4 trafficking (Choi et al., 2006; Nakanishi et al., 2006; Vicogne et al., 2006). Like DAG, PA induces negative curvature

(Kooijman and Burger, 2009). However the monophosphoester head group of PA adds a negative charge to the membrane that can play a role in binding proteins, including NSF/Sec18 (Matveeva et al., 2001; see Chapter 2). Moreover, Pah1 activity is required during Sec18-mediated priming (Sasser et al., 2012a; see Chapter 2). Deletion of Pah1 leads to broad cellular defects including the enlargement of the endoplasmic reticulum and nuclear membranes, blocked lipid droplet synthesis, and inhibited endosomal maturation(Lawrence et al., 2014; Sasser et al., 2012a; Adeyo et al., 2011; Han et al., 2007).

In other pathways, such as lipid droplet formation, the effects caused by deleting *PAH1* can be countered by concurrent deletion of *DGK1* illustrating that the interconversion of PA and DAG by Pah1 and Dgk1 respectively can negate the effects of inactivating one of the enzymes (Adeyo et al., 2011; Han et al., 2008a). Importantly, it shows that the balance struck by these two enzymes is consistent during the homeostasis of some pathways. Unlike other pathways deleting *DGK1* had no effect on the *pah1*Δ vacuolar phenotype (Fig. 4.9). This suggested one of two things. First, it is likely that the defect seen in *pah1*Δ vacuoles was not simply due to a steady-state imbalance of PA and DAG. It is possible that the PA:DAG ratio varies throughout the fusion pathway. For example, Pah1 activity is needed during priming, indicating that a reduction of PA and increase in DAG is necessary (Sasser et al., 2012a). However, inhibiting Pah1 activity after priming has no effect on fusion, demonstrating that PA levels no longer need to be reduced. Our previous findings show that DAG does not play a role during priming but is instead required after the formation of *trans*-SNARE complexes (Jun et al., 2004; Karunakaran and Fratti, 2013; Fratti and Wickner, 2007; Fratti et al., 2007). This leads us to propose that the activities of Dgk1 and Pah1 are separated temporally on the fusion pathway making it unlikely to balance activities at any time. A second

possibility is that DAG generated by Pah1 is fed into lipid synthesis pathways to generate phosphatidylethanolamine and phosphatidylcholine through the Kennedy pathway, or into the formation of triacylglycerol for storage (Adeyo et al., 2011; Kennedy and Weiss, 1956). However, the latter is unlikely as lipid synthesis occurs at the endoplasmic reticulum and not the vacuole. Nevertheless, changes in lipid synthesis can propagate throughout the cell via membrane trafficking.

Although both PA and DAG are essential for vacuole fusion, their exact function remains to be fully elucidated. DAG is a fusogenic lipid due in part to its intrinsic negative curvature in a membrane and ability to destabilize lipid bilayers and even trigger the fusion of protein-free vesicles (Das and Rand, 1984; Seddon, 1990; Sánchez-Migallón et al., 1995; Villar et al., 2000). DAG can also bind fusion regulators such as protein kinase C (PKC) through its C1 domain (Dries and Newton, 2008; Johnson et al., 2000). PKC has been shown to affect membrane fusion by several pathways including the phosphorylation of NSF to regulate neurotransmitter release, or phosphorylating the SNARE Syntaxin4 to control thrombin release from platelets (Matveeva et al., 2001; Chung et al., 2000). That said, it has not been determined whether PKC activity occurs on isolated vacuoles.

Another potential reason for the enhanced fusion of *dgk1*Δ vacuoles is that skewing the lipid balance to have less PA versus DAG can have an effect on priming. In a separate study we found that PA binds Sec18 to prevent *cis*-SNARE complex association (see Chapter 2). Conversion of PA to DAG by Pah1 releases Sec18 allowing it to engage *cis*-SNARE bundles. An excess of PA or inhibiting Pah1 activity results in the retention of Sec18 on PA domains. Thus we theorized that

the converse could occur in the absence of Dgk1 and a likely reduced pool of PA would facilitate the recruitment of Sec18 to *cis*-SNARE complexes and lead to more efficient priming. Enhanced priming could result in a functional increase in active SNAREs and would be in keeping with other studies showing that overexpression of SNAREs augments vacuole fusion. In our hands however, we did not observe a difference in priming activity on *dgk1*Δ vacuoles (not shown). Thus, we conclude that the effects of deleting *DGK1* are mostly due to the physical changes caused by elevated DAG. This notion is consistent with bilayer destabilization by the non-lamellar lipid DAG and lowering the energy barrier needed for SNAREs to trigger fusion.

One of the striking findings of this study was that fusion showed decreased sensitivity to reagents that target Ypt7 activity. Our results showed that fusion gained varying levels of resistance to anti-Ypt7 antibody, the GAP Gyp1-46, and GDI. One interpretation of these results is that Ypt7 is more active on *dgk1*Δ vacuoles and that increased activity would manifest in augmented tethering. Even though measuring tethering efficiency is difficult to quantitate using light microscopy, we propose a model where the lipid composition of the vacuole modulates Rab activity. Alternatively, these results could reflect a reduced need of Ypt7 for *dgk1*Δ vacuole fusion.

How would an increase in DAG levels affect Ypt7 function? To date there is no direct evidence of membrane fluidity affecting Rab proteins. One can imagine that the membrane affects the rotation or angle of insertion of the Ypt7 lipid anchor leading to an altered conformational state that strengthens its interactions with the HOPS complex, or a yet to be identified binding partner. Alternatively, the increase in DAG could lead to the enhanced recruitment of a Rab interacting protein. For example, in mammalian renal cortical tubule and mesangial cells the production of

DAG promotes the interactions of hmunc13 with Rab34 (Speight and Silverman, 2005). This was due to the DAG recruitment of hmunc13 to membranes containing Rab34. The latter is unlikely here as the IC_{50} of C1b was unaltered on *dgk1*Δ vacuoles, suggesting that there was no change in competition for a protein ligand. Therefore, we favor a model where the physical properties of the membrane modulate Ypt7 activity. Although evidence linking Rab activity to the physical properties of a membrane is lacking, there are some clues that come from cholesterol storage defects. For instance, cholesterol accumulation prevents the mammalian Ypt7 homologue Rab7 from recruiting its effector protein RILP (Huynh et al., 2008). This is linked with the inhibition of fusion between lysosomes and phagosomes and is likely due to decreased membrane fluidity caused by the increase in cholesterol as seen Niemann-Pick type C disease cells (Koike et al., 1998). Decreased fluidity due to excess cholesterol in Niemann-Pick type C disease cells has also been shown to reduce the ability of GDI to extract Rab7 (Lebrand et al., 2002). The authors subsequently drew the conclusion cholesterol plays a role in the Rab7 cycle. These studies are in keeping with our proposed model where membrane fluidity modulates Rab activity.

In summary, our observations indicate that the PA-to-DAG ratio, regulated in part by the non-concurrent, yet complementary functions of Pah1 and Dgk1, can modulate vacuole fusion. The effects of increased DAG in the absence of Dgk1 led to improved Ypt7 activity as shown by the increased resistance to Gyp1-46, GDI and anti-Ypt7 antibody. Finally, the changes in the physical properties of *dgk1*Δ vacuole membranes restored the ability of $Vam7^{Q283R}$ to stimulate fusion.

FIGURES AND TABLES

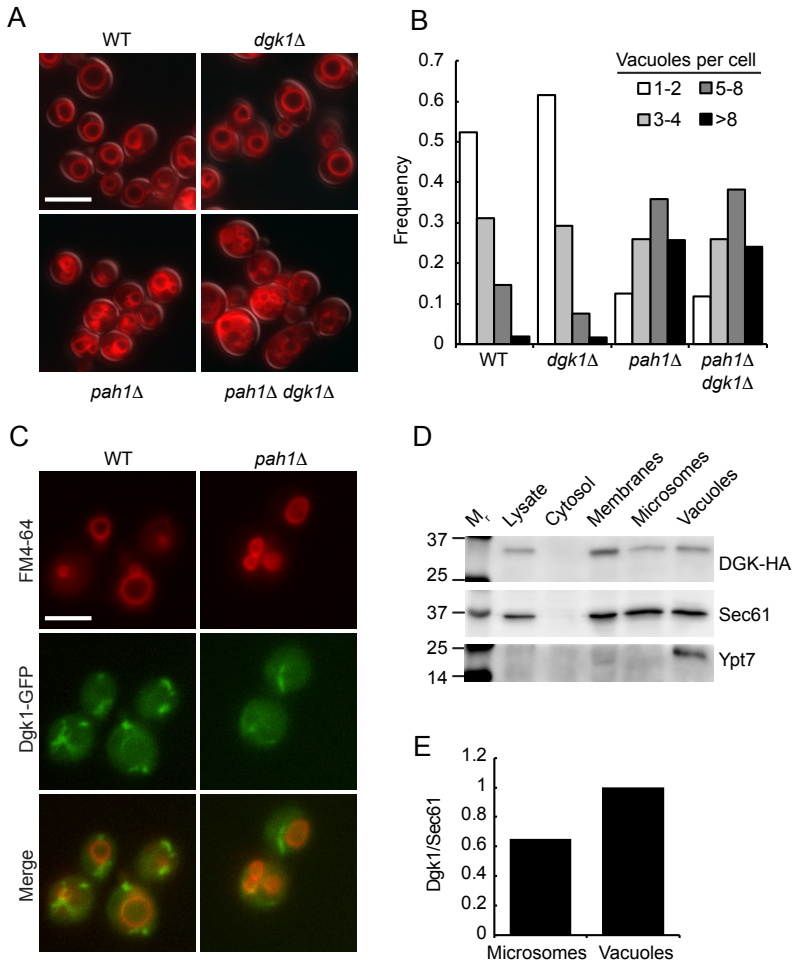

Figure 4.1. Dgk1 is localized to the vacuole. (A) Vacuole morphology was examined using wild type, *dgk1*Δ, *pah1*Δ, and *dgk1*Δ *pah1*Δ yeast. Cells were incubated with 5 μM FM4-64 to label vacuoles. (B) Quantitation of vacuole fragmentation. The number of vacuoles per cell was determined for each strain (n>300 cells per strain). Cells with 8 or more vacuoles were combined into one population. (C) Dgk1-GFP expression in wild type and *pah1*Δ strains were double labeled with FM4-64 and used for fluorescence microscopy. (D) Immunoblotting of Dgk1-HA_3 distribution in 10 μg samples of whole cell lysates, cytosol, vacuoles, endoplasmic reticulum and total membrane fraction using anti-HA antibody. Ypt7 and Sec61 were probed for as a controls for vacuole or endoplasmic reticulum enrichment. (E) Western blot analysis. Shown is the vacuolar enrichment of Dgk1 on vacuoles relative to contaminating membranes from the endoplasmic reticulum. Using densitometry, the relative amount of vacuolar Dgk1 was measured as a ratio to the amount of Sec61 in the vacuolar preparation and set to 1. The Dgk1/Sec61 ratio was also determined for the microsomal fraction in comparison to the vacuolar ratio. Densitometry was determined using BioRad ChimiDoc XRS+ System. Bar, 5μm.

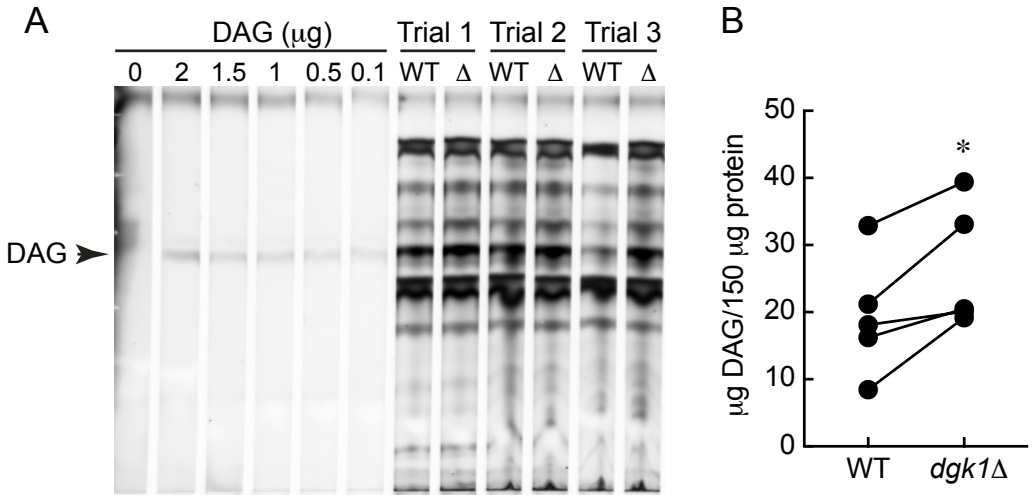

Figure 4.2. DAG vacuolar content. (A) Neutral lipids were extracted from wild type and *dgk1*Δ vacuoles and resolved by thin layer chromatography. Lipids were visualized by charring with copper (II) sulfate. (B) Quantitation of DAG from wild type and *dgk1*Δ vacuoles (150 μg of by protein). * $P<0.05$ (two-tailed paired t-test). n=5.

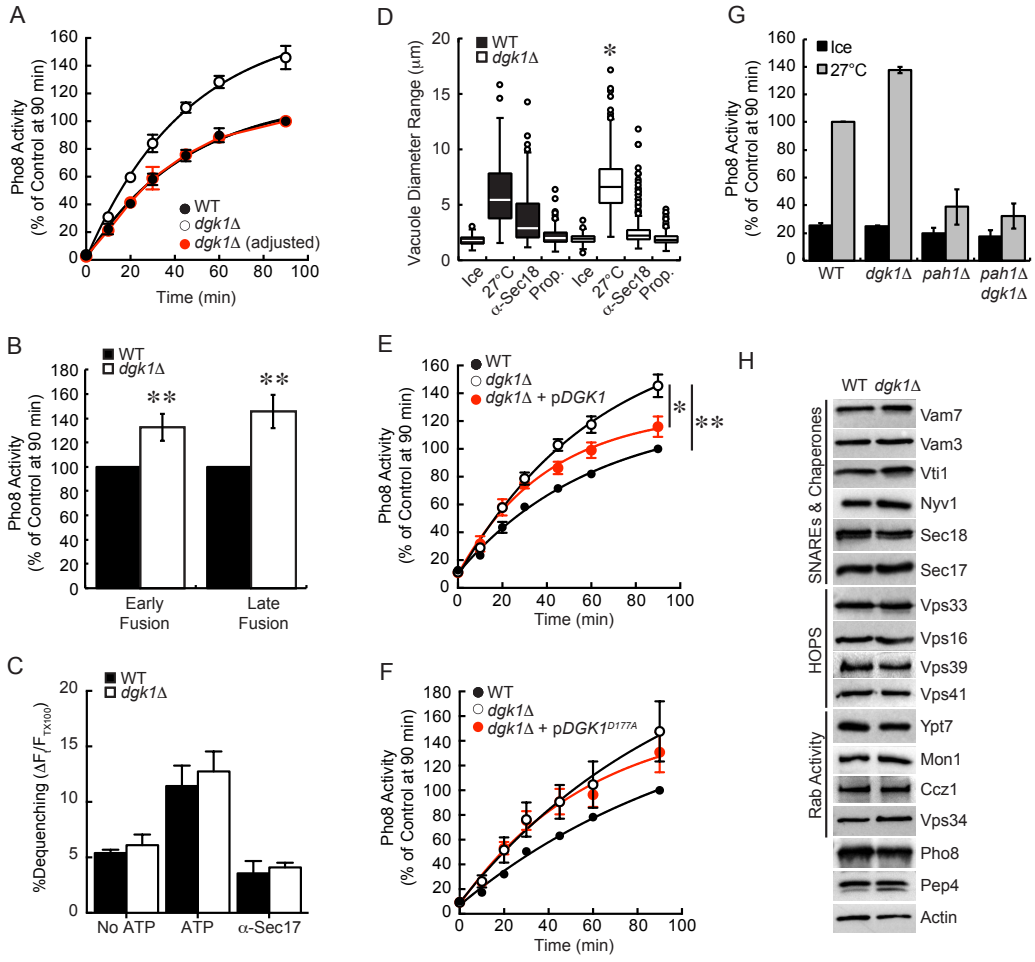

Figure 4.3. Dgk1 suppresses vacuole fusion. (A) Fusion reactions were performed using wild type and *dgk1*Δ vacuoles. Reactions were incubated at 27°C for the indicated times and assayed for Pho8 activity. The red trace represents *dgk1*Δ fusion when normalized to its own maximum. This reveals the rate of *dgk1*Δ vacuole fusion versus wild type. (B) The ratio of effector and reporter vacuoles were altered to show early versus late rounds of fusion. To show early rounds of fusion an excess of effector vacuoles (5 μg *PEP4 pho8*Δ) were incubated with 1 μg of reporter vacuoles (*pep4*Δ *PHO8*). To show late rounds of fusion, an excess of reporter vacuoles (4 μg *pep4*Δ *PHO8*) were incubated with 2 μg of effector vacuoles (*PEP4 pho8*Δ). (C) Lipid mixing assay were performed with wild type or *dgk1*Δ vacuoles. Reporter vacuoles (2 μg) labeled with Rh-PE were incubated with 16 μg of unlabeled vacuoles. Fluorescence (λ_{ex}=544 nm; λ_{em}=590 nm) was measured every 60 sec for 40 min. Shown is the average lipid mixing at 40 min. (D) Measurement of vacuole diameters after incubation (27°C, 90 min). Fusion reactions were treated with PS buffer, 12 μg/ml anti-Sec18, or 2 mM propranolol (Prop.). Measurements were plotted as a box plot representing median vacuoles with upper and lower quartile values. The lines extending from the boxes represent the minimum and maximum vacuoles in the data set. Outliers are displayed as points. (E-F) Fusion assays were performed with vacuoles from wild type, *dgk1*Δ, or *dgk1*Δ strains complemented with p*DGK1* or p*DGK1*^{D177A}. (G) Endpoint fusion efficiency was

Figure 4.3 (cont.)
compared between wild type, *dgk1*Δ, *pah1*Δ, and *pah1*Δ *dgk1*Δ vacuoles. (H) Analysis of fusion components. Vacuoles were isolated from wild type BJ3505 and RFY17 (BJ3505 *dgk1*Δ) (5 μg protein) and immunoblotted with antibodies against the indicated proteins. To examine the effect of deleting *DGK1* on Pep4 trafficking, vacuoles were examined from DKY6281 and RFY18 (DKY6281 *dgk1*Δ). Error bars represent S.E.M. (n≥3). **p*<0.05, ***p*<0.01 (one-way ANOVA).

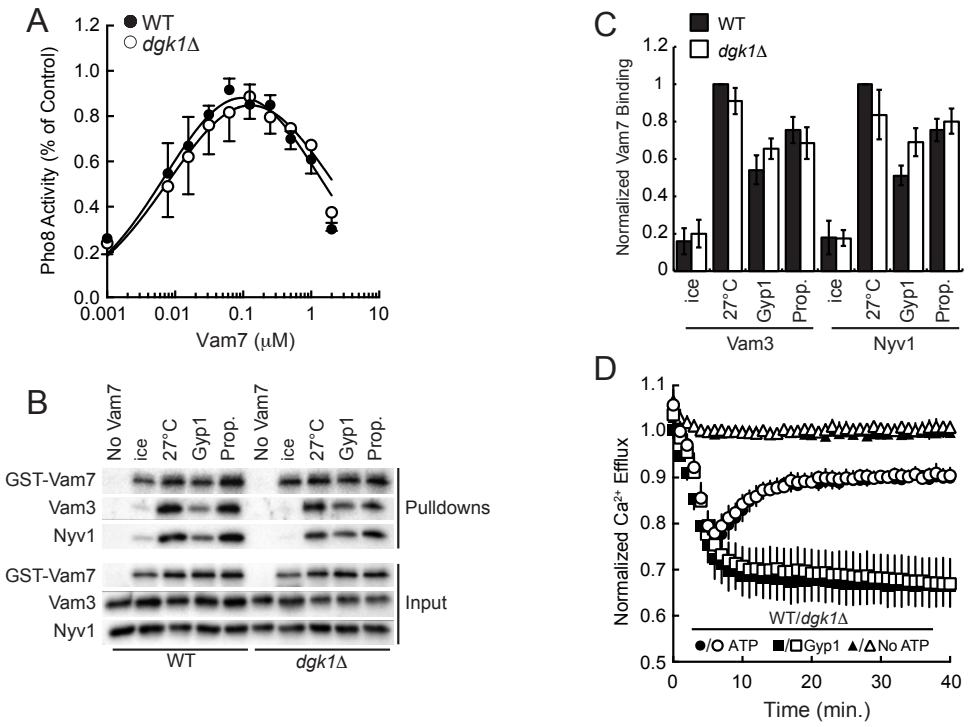

Figure 4.4. SNARE complex formation and Ca^{2+} efflux are not affected on *dgk1*Δ vacuoles. (A) Anti-Sec17 IgG bypass fusion. Fusion reactions were treated with anti-Sec17 IgG to block the priming stage of fusion. Recombinant GST-Vam7 was added at the indicated concentrations to stimulate fusion. (B) SNARE complex formation as described in the Materials and Methods section. (C) Quantitation of three GST-Vam7 pulldown assays. Protein band intensities were normalized to wild type at 27°C without inhibitors. (n=3). (D) Fusion reactions (2X) were prepared with 20 μg of wild type or *dgk1*Δ vacuoles in the presence of 150 nM low affinity Fluo-4 dextran in the presence or absence of ATP. A subset of reactions was treated with 2 μM Gyp1-46 to inhibit Ypt7 activity and block Ca^{2+} efflux. Fluo-4 fluorescence was normalized to the average fluorescence of wild type vacuoles without ATP. Error bars represent S.E.M. (n=3).

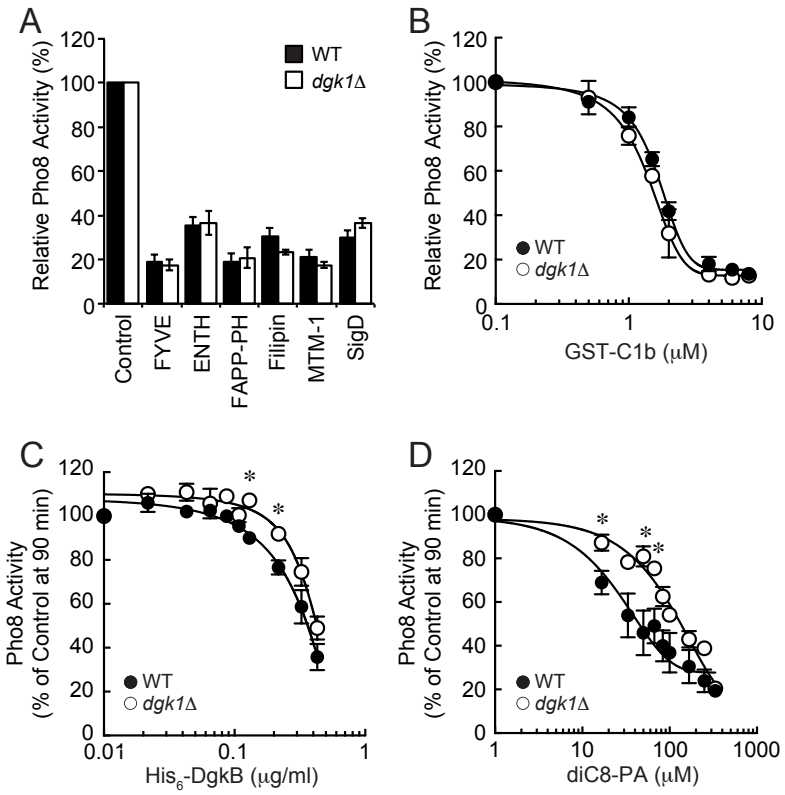

Figure 4.5. Deletion of *DGK1* confers resistance to PA (A) Fusion reactions were performed using wild type or *dgk1*Δ vacuoles. Fusion reactions containing wild type or *dgk1*Δ vacuoles treated with PS buffer, 2 μM GST-FYVE, 20 μM GST-ENTH, 10 μM MBP-FappPH, 20 μM Filipin, 1 μM His_6-MTM1 or 1.2 μM SigD. (B-D) Dose response curves of GST-C1b, His_6-DgkB and diC8-PA at the indicated concentrations. Error bars represent S.E.M. (n=3). * $p<0.05$ (one-way ANOVA).

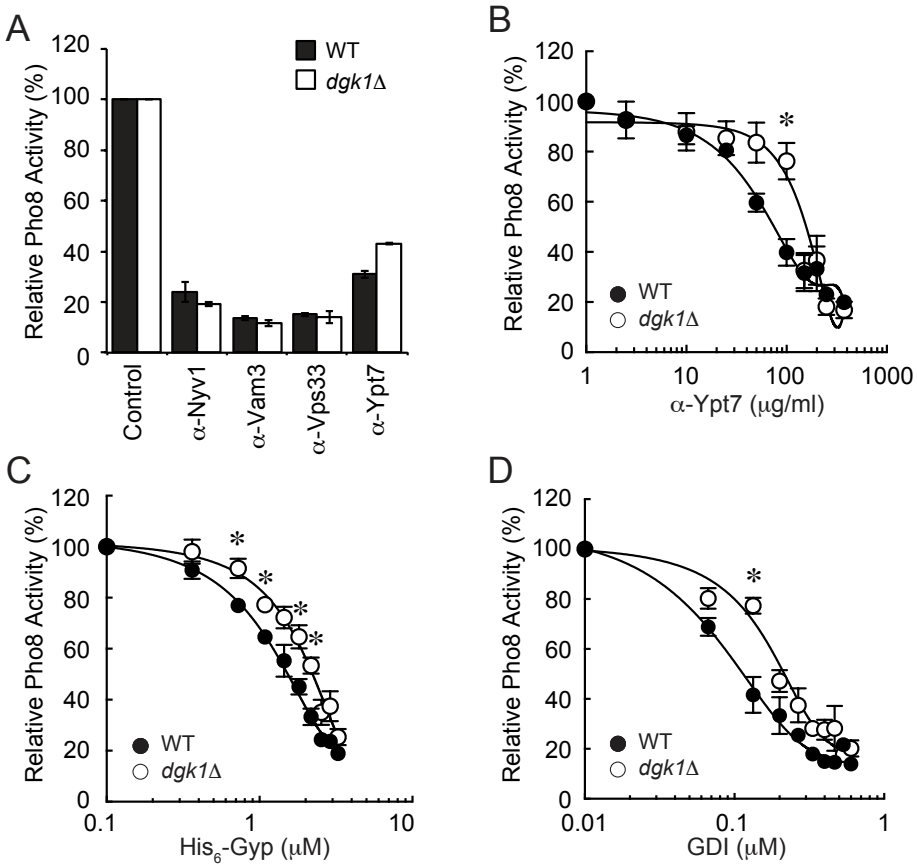

Figure 4.6. The augmented fusion of *dgk1*Δ vacuoles is linked to Ypt7 function. (A) Fusion reactions were performed using wild type or *dgk1*Δ vacuoles. Individually, reactions were treated with PS buffer (Control), or antibodies against Nyv1 (17 μg/ml), Vam3 (27 μg/ml), Vps33 (5 μg/ml) or Ypt7 (8 μg/ml). (B-D) Dose response curves of anti-Ypt7 IgG (B), Gyp1-46 (C), and GDI (D). Reactions containing wild type of *dgk1*Δ vacuoles were incubated for 90 min at 27°C and tested for fusion. Error bars represent S.E.M. (n=3). **P*<0.05 (one-way ANOVA).

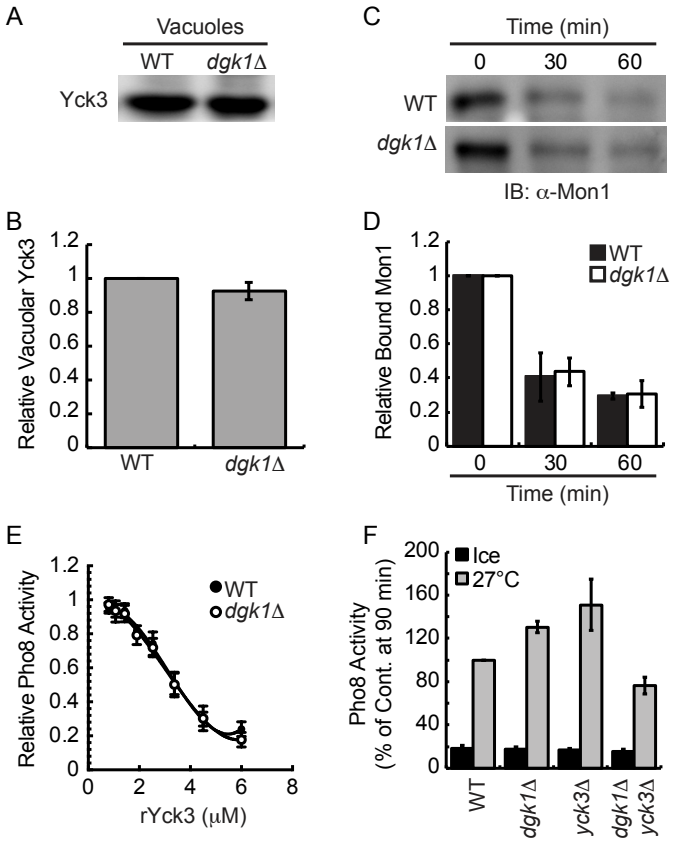

Figure 4.7. The *dgk1*Δ fusion effect is in parallel to the function of Yck3. (A-B) Immunoblotting and quantitation of Yck3 content on vacuoles from wild type and *dgk1*Δ cells. (C) Immunoblotting of Mon1 release from vacuoles during the fusion reaction. Fusion reactions were incubated for 0, 30, or 60 min after which membranes (bound) and supernatants (unbound) were separated by centrifugation (13,000 *g*, 15 min, 4°C). (D) Quantitation of bound Mon1 at the indicated times. (E) Fusion reactions containing were treated with indicated concentrations of recombinant His_6-Yck3. (F) Fusion of wild type, *dgk1*Δ, *yck3*Δ and *dgk1*Δ/*yck3*Δ vacuoles. Fusion reactions were incubated for 90 min at 27°C. Error bars represent S.E.M. (n=3).

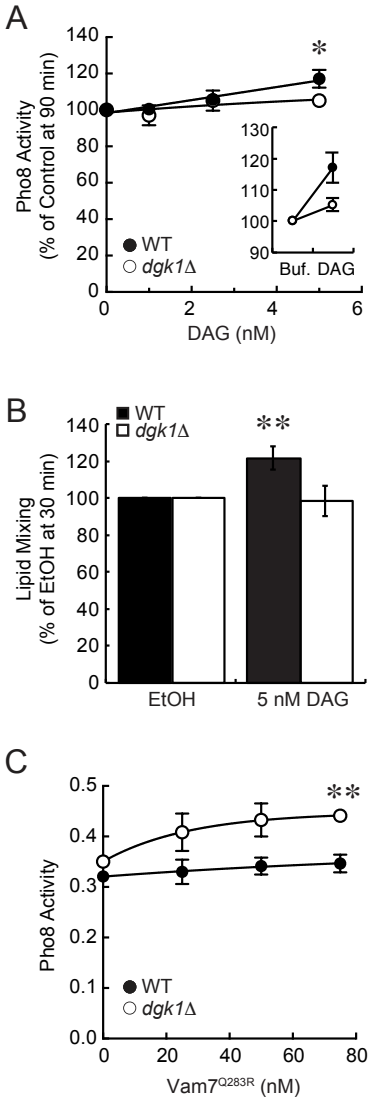

Figure 4.8. Fusion of *dgk1*Δ vacuoles and resistance to diC8-PA. (A) Exogenous addition of DAG at the indicated concentrations to fusion reactions containing wild type or *dgk1*Δ vacuoles. Inset shows the direct comparison of 5 nM DAG and buffer with an equivalent volume of carrier (EtOH). (B) Lipid mixing using wild type and *dgk1*Δ vacuoles in the presence of 5 nM DAG or buffer with an equivalent volume of EtOH. (C) Anti-Sec17 IgG bypass fusion reactions using wild type or *dgk1*Δ vacuoles. Individual fusion reactions were treated with recombinant GST-Vam7^{Q283R} to stimulate fusion. Fusion reactions were incubated for 90 min at 27°C. Error bars represent S.E.M. (n=3). *p<0.05, **p<0.01 (one-way ANOVA).

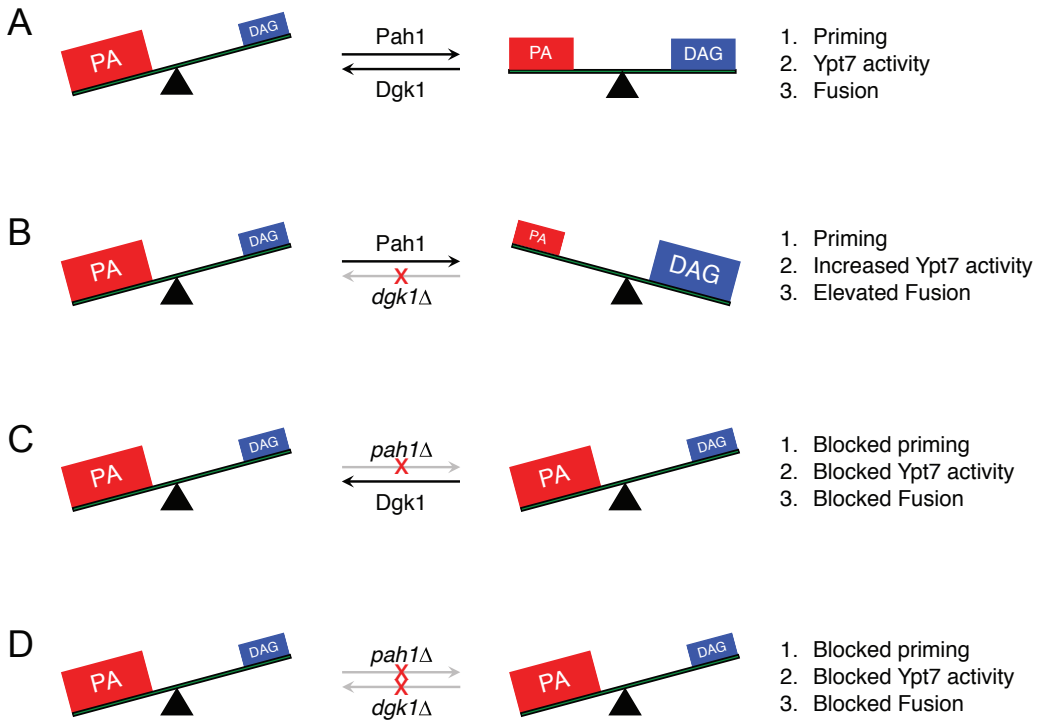

Figure 4.9. Schematic of role of PA and DAG production and modification on vacuole fusion. (A) Wild type fusion (*PAH1 DGK1*) leads to a reduction of PA by Pah1 and increase in DAG at the start of the pathway to promote SNARE priming, Ypt7 activation and support fusion. (B) In the absence of Dgk1 there is an accumulation of DAG leading to increased Ypt7 activity and augmented fusion. (C) In the absence of Pah1 high PA levels are maintained that sequester Sec18 from SNARE complexes and preventing priming. Consequently, Ypt7 activity is blocked and fusion is abrogated. (D) The double deletion of *PAH1* and *DGK1* does not restore fusion and phenocopies the *pah1*Δ single deletion.

Table 4.1. Yeast strains used in this study

Strain	Genotype	Source
BJ3505	*MAT*a *pep4::HIS3 prb1-Δ1.6R his3–200 lys2–801 trp1Δ101 (gal3) ura3–52 gal2 can1*	[90]
DKY6281	*MATα pho8::TRP1* leu2*–3 leu 2–112 ura3–52 his3-Δ200 trp1-Δ901 lys2–801*	[82]
RFY17	BJ3505, *pah1Δ::kanMX6*	[19]
RFY18	DKY6281, *pahΔ::kanMX6*	[19]
CHY53	BJ3505, *yck3Δ::hphMX4*	[46]
CHY54	DKY6281, *yck3Δ::hphMX4*	[46]
RFY60	BJ3505, *dgk1Δ::hphMX4*	This study
RFY61	DKY6281, *dgk1Δ::hphMX4*	This study
RFY62	RFY17, *dgk1Δ:: hphMX4*	This study
RFY63	RFY18, *dgk1Δ:: hphMX4*	This study
RFY64	RFY60, *pRS416-DGK1*	This study
RFY65	RFY61, *pRS416-DGK1*	This study
RFY66	RFY60, *pRS416-DGK1^{D177A}*	This study
RFY67	RFY61, *pRS416-DGK1^{D177A}*	This study
RFY68	BJ3505, *DGK1::GFP-kanMX6*	This study
RFY69	BJ3505, *DGK1::3XHA-kanMX6*	This study
RFY71	RFY68, *pah1Δ:: hphMX4*	This study
RFY72	RFY60, *yck3Δ:: kanMX6*	This study
RFY73	RFY61, *yck3Δ:: kanMX6*	This study

Table 4.2. Primers used in this study

Oligonucleotide	Sequence
5'-DGK1-KO	5'-GTCGTAGAGCAGTTGAACATTACGTAAACAGATATCTACGAT AGGCCACTAGTGGATCTG–3'
3'-DGK1-KO	5'-GAGGTGCTGGATCGTTAACCACAGATAAACTGAATCGCGCTC AGCTGAAGCTTCGTACGC–3'
5'-DGK1	5'-GTACTCGAATTCCTCTTACAAGAGACCATC-3'
3'-DGK1	5'-GTACTCGCGGCCGCGCGCTTGTTGGCACATAT-3'
5'-DGK1^{D177A}	5'-TTGGTCCGCTACAGCCGCCGCAACTATTGGAAGAAAGTAT-3'
3'-DGK1^{D177A}	5'-CGGCTGTAGCGGACCAACTTAGCAAAAATAACGATATTAAGG-3'
5'-DGK1-GFP/HA	5'-ATCACTTTTTATGAACGCAGTAATCAAAACATTCAAGAAACGGAT CCCCGGGTTAATTAA-3'
3'-DGK1-GFP/HA	5'-CGAAGAATATAAAACACTCCTGTTTTTGGTATATATGCTTGAATT CGAGCTCGTTTAAAC-3'
5'-PAH1-KO	5'-ACAGGGAAGAAATTACTGAAGATAGACACATCGGTCGATTCTGTT TAGCTTGCCTTGTCC-3'
3'-PAH1-KO	5'-AGTATGGATCGTTATAAATAATATTCGGCTACAAGAATCTGACAC TGGATGGCGGCGTTA-3'

REFERENCES

Adeyo, O., P.J. Horn, S.K. Lee, D.D. Binns, A. Chandrahas, K.D. Chapman, and J.M. Goodman. 2011. The yeast lipin orthologue Pah1p is important for biogenesis of lipid droplets. *J. Cell Biol.* doi:10.1083/jcb.201010111.

Bai, J., and R.E. Pagano. 1997. Measurement of spontaneous transfer and transbilayer movement of BODIPY- labeled lipids in lipid vesicles. *Biochemistry*. doi:10.1021/bi970145r.

Bligh, E.G., and W.J. Dyer. 1959. A RAPID METHOD OF TOTAL LIPID EXTRACTION AND PURIFICATION. *Can. J. Biochem. Physiol.* doi:10.1139/o59-099.

Boeddinghaus, C., A.J. Merz, R. Laage, and C. Ungermann. 2002. A cycle of Vam7p release from and PtdIns 3-P-dependent rebinding to the yeast vacuole is required for homotypic vacuole fusion. *J. Cell Biol.* doi:10.1083/jcb.200112098.

Brett, C.L., R.L. Plemel, B.T. Lobinger, M. Vignali, S. Fields, and A.J. Merz. 2008. Efficient termination of vacuolar Rab GTPase signaling requires coordinated action by a GAP and a protein kinase. *J. Cell Biol.* doi:10.1083/jcb.200801001.

Cabrera, M., L. Langemeyer, M. Mari, R. Rethmeier, I. Orban, A. Perz, C. Bröcker, J. Griffith, D. Klose, H.J. Steinhoff, F. Reggiori, S. Engelbrecht-Vandré, and C. Ungermann. 2010. Phosphorylation of a membrane curvature-sensing motif switches function of the HOPS subunit Vps41 in membrane tethering. *J. Cell Biol.* doi:10.1083/jcb.201004092.

Cabrera, M., M. Nordmann, A. Perz, D. Schmedt, A. Gerondopoulos, F. Barr, J. Piehler, S. Engelbrecht-Vandre, and C. Ungermann. 2014. The Mon1-Ccz1 GEF activates the Rab7 GTPase Ypt7 via a longin-fold-Rab interface and association with PI3P-positive membranes. *J. Cell Sci.* doi:10.1242/jcs.140921.

Cheever, M.L., T.K. Sato, T. De Beer, T.G. Kutateladze, S.D. Emr, and M. Overduin. 2001. Phox domain interaction with Ptdlns(3)P targets the Vam7 t-SNARE to vacuole membranes. *Nat. Cell Biol.* doi:10.1038/35083000.

Chernomordik, L. V., and M.M. Kozlov. 2003. Protein-Lipid Interplay in Fusion and Fission of Biological Membranes. *Annu. Rev. Biochem.* doi:10.1146/annurev.biochem.72.121801.161504.

Choi, H.S., W.M. Su, J.M. Morgan, G.S. Han, Z. Xu, E. Karanasios, S. Siniossoglou, and G.M. Carman. 2011. Phosphorylation of phosphatidate phosphatase regulates its membrane association and physiological functions in Saccharomyces cerevisiae: Identification of SER602, THR723, and SER744as the sites phosphorylated by CDC28 (CDK1)-encoded cyclin-dependent kinas. *J. Biol. Chem.* doi:10.1074/jbc.M110.155598.

Choi, S.Y., P. Huang, G.M. Jenkins, D.C. Chan, J. Schiller, and M.A. Frohman. 2006. A common lipid links Mfn-mediated mitochondrial fusion and SNARE-regulated exocytosis. *Nat. Cell Biol.* doi:10.1038/ncb1487.

Chung, S.H., J. Polgar, and G.L. Reed. 2000. Protein kinase C phosphorylation of syntaxin 4 in thrombin-activated human platelets. *J. Biol. Chem.* 275:25286–91. doi:10.1074/jbc.M004204200.

Churchward, M.A., T. Rogasevskaia, D.M. Brandman, H. Khosravani, P. Nava, J.K. Atkinson, and J.R. Coorssen. 2008. Specific lipids supply critical negative spontaneous curvature-an essential component of native Ca2+-triggered membrane fusion. *Biophys. J.* doi:10.1529/biophysj.107.123984.

Collins, K.M., N.L. Thorngren, R.A. Fratti, and W.T. Wickner. 2005. Sec17p and HOPS, in distinct SNARE complexes, mediate SNARE complex disruption or assembly for fusion.

EMBO J. doi:10.1038/sj.emboj.7600658.

Das, S., and R.P. Rand. 1984. Diacylglycerol causes major structural transitions in phospholipid bilayer membranes. *Biochem. Biophys. Res. Commun.* doi:10.1021/bi00358a022.

Dowler, S., R.A. Currie, D.G. Campbell, M. Deak, G. Kular, C.P. Downes, and D.R. Alessi. 2000. Identification of pleckstrin-homology-domain-containing proteins with novel phosphoinositide-binding specificities. *Biochem. J.* doi:10.1042/bj3510019.

Dries, D.R., and A.C. Newton. 2008. Kinetic analysis of the interaction of the C1 domain of protein kinase C with lipid membranes by stopped-flow spectroscopy. *J. Biol. Chem.* doi:10.1074/jbc.M709943200.

Flick, J.S., and J. Thorner. 1993. Genetic and biochemical characterization of a phosphatidylinositol-specific phospholipase C in Saccharomyces cerevisiae. *Mol. Cell. Biol.* doi:10.1128/MCB.13.9.5861.Updated.

Fratti, R.A., K.M. Collins, C.M. Hickey, and W. Wickner. 2007. Stringent 3Q·1R composition of the SNARE 0-layer can be bypassed for fusion by compensatory SNARE mutation or by lipid bilayer modification. *J. Biol. Chem.* doi:10.1074/jbc.M700971200.

Fratti, R.A., Y. Jun, A.J. Merz, N. Margolis, W. Wickner, and B. Wickner. 2004. Interdependent assembly of specific regulatory lipids and membrane fusion proteins into the vertex ring domain of docked vacuoles. *J. Cell Biol.* doi:10.1083/jcb.200409068.

Fratti, R.A., and W. Wickner. 2007. Distinct targeting and fusion functions of the PX and SNARE domains of yeast vacuolar Vam7p. *J. Biol. Chem.* doi:10.1074/jbc.M700584200.

Gillooly, D.J. 2000. Localization of phosphatidylinositol 3-phosphate in yeast and mammalian cells. *EMBO J.* doi:10.1093/emboj/19.17.4577.

Goñi, F.M., and A. Alonso. 1999. Structure and functional properties of diacylglycerols in

membranes. *Prog. Lipid Res.* doi:10.1016/S0163-7827(98)00021-6.

Grillitsch, K., M. Connerth, H. Köfeler, T.N. Arrey, B. Rietschel, B. Wagner, M. Karas, and G. Daum. 2011. Lipid particles/droplets of the yeast Saccharomyces cerevisiae revisited: Lipidome meets Proteome. *Biochim. Biophys. Acta - Mol. Cell Biol. Lipids*. doi:10.1016/j.bbalip.2011.07.015.

Haas, a, and W. Wickner. 1996. Homotypic vacuole fusion requires Sec17p (yeast alpha-SNAP) and Sec18p (yeast NSF). *EMBO J.*

Haas, A., B. Conradt, and W. Wickner. 1994. G-protein ligands inhibit in vitro reactions of vacuole inheritance. *J. Cell Biol.* doi:10.1083/jcb.126.1.87.

Haas, A., D. Scheglmann, T. Lazar, D. Gallwitz, and W. Wickner. 1995. The GTPase Ypt7p of Saccharomyces cerevisiae is required on both partner vacuoles for the homotypic fusion step of vacuole inheritance. *EMBO J.*

Han, G.S., L. O'Hara, G.M. Carman, and S. Siniossoglou. 2008a. An unconventional diacylglycerol kinase that regulates phospholipid synthesis and nuclear membrane growth. *J. Biol. Chem.* doi:10.1074/jbc.M802903200.

Han, G.S., L. O'Hara, S. Siniossoglou, and G.M. Carman. 2008b. Characterization of the yeast DGK1-encoded CTP-dependent diacylglycerol kinase. *J. Biol. Chem.* doi:10.1074/jbc.M802866200.

Han, G.S., S. Siniossoglou, and G.M. Carman. 2007. The cellular functions of the yeast lipin homolog Pah1p are dependent on its phosphatidate phosphatase activity. *J. Biol. Chem.* doi:10.1074/jbc.M705777200.

Han, G.S., W.I. Wu, and G.M. Carman. 2006. The Saccharomyces cerevisiae lipin homolog is a Mg2+-dependent phosphatidate phosphatase enzyme. *J. Biol. Chem.*

doi:10.1074/jbc.M600425200.

Hickey, C.M., C. Stroupe, and W. Wickner. 2009. The major role of the Rab Ypt7p in vacuole fusion is supporting HOPS membrane association. *J. Biol. Chem.* doi:10.1074/jbc.M109.000737.

Huynh, K.K., E. Gershenzon, and S. Grinstein. 2008. Cholesterol accumulation by macrophages impairs phagosome maturation. *J. Biol. Chem.* doi:10.1074/jbc.M806232200.

Ishihara, N., M. Hamasaki, S. Yokota, K. Suzuki, Y. Kamada, A. Kihara, T. Yoshimori, T. Noda, and Y. Ohsumi. 2001. Autophagosome requires specific early Sec proteins for its formation and NSF/SNARE for vacuolar fusion. *Mol. Biol. Cell*. doi:10.1091/MBC.12.11.3690.

Jahn, R., and R.H. Scheller. 2006. SNAREs - Engines for membrane fusion. *Nat. Rev. Mol. Cell Biol.* doi:10.1038/nrm2002.

Johnson, J.E., J. Giorgione, and A.C. Newton. 2000. The C1 and C2 domains of protein kinase C are independent membrane targeting modules, with specificity for phosphatidylserine conferred by the C1 domain. *Biochemistry*. doi:10.1021/bi000902c.

Jun, Y., R.A. Fratti, and W. Wickner. 2004. Diacylglycerol and its formation by phospholipase C regulate Rab- and SNARE-dependent yeast vacuole fusion. *J. Biol. Chem.* doi:10.1074/jbc.M411363200.

Karanasios, E., G.-S. Han, Z. Xu, G.M. Carman, and S. Siniossoglou. 2010. A phosphorylation-regulated amphipathic helix controls the membrane translocation and function of the yeast phosphatidate phosphatase. *Proc. Natl. Acad. Sci.* doi:10.1073/pnas.1007974107.

Karunakaran, S., and R.A. Fratti. 2013. The Lipid Composition and Physical Properties of the Yeast Vacuole Affect the Hemifusion-Fusion Transition. *Traffic*. doi:10.1111/tra.12064.

Karunakaran, V., and W. Wickner. 2013. Fusion proteins and select lipids cooperate as

membrane receptors for the soluble N-Ethylmaleimide-sensitive factor attachment protein receptor (SNARE) Vam7p. *J. Biol. Chem.* doi:10.1074/jbc.M113.484410.

Kato, M., and W. Wickner. 2001. Ergosterol is required for the Sec18/ATP-dependent priming step of homotypic vacuole fusion. *EMBO J.* doi:10.1093/emboj/20.15.4035.

Kennedy, E.P., and S.B. Weiss. 1956. The function of cytidine coenzymes in the biosynthesis of phospholipides. *J. Biol. Chem.*

Koike, T., G. Ishida, M. Taniguchi, K. Higaki, Y. Ayaki, M. Saito, Y. Sakakihara, M. Iwamori, and K. Ohno. 1998. Decreased membrane fluidity and unsaturated fatty acids in Niemann-Pick disease type C fibroblasts. *Biochim. Biophys. Acta*. doi:10.1016/S0925-4439(98)00019-2.

Kooijman, E.E., and K.N.J. Burger. 2009. Biophysics and function of phosphatidic acid: a molecular perspective. *Biochim Biophys Acta*. doi:S1388-1981(09)00093-6 [pii]\r10.1016/j.bbalip.2009.04.001.

LaGrassa, T.J., and C. Ungermann. 2005. The vacuolar kinase Yck3 maintains organelle fragmentation by regulating the HOPS tethering complex. *J. Cell Biol.* doi:10.1083/jcb.200407141.

Lawrence, G., C.C. Brown, B.A. Flood, S. Karunakaran, M. Cabrera, M. Nordmann, C. Ungermann, and R.A. Fratti. 2014. Dynamic association of the PI3P-interacting Mon1-Ccz1 GEF with vacuoles is controlled through its phosphorylation by the type 1 casein kinase Yck3. *Mol. Biol. Cell*. doi:10.1091/mbc.E13-08-0460.

Lebrand, C., M. Corti, H. Goodson, P. Cosson, V. Cavalli, N. Mayran, J. Fauré, and J. Gruenberg. 2002. Late endosome motility depends on lipids via the small GTPase Rab7. *EMBO J.* doi:10.1093/emboj/21.6.1289.

Longtine, M.S., A. McKenzie, D.J. Demarini, N.G. Shah, A. Wach, A. Brachat, P. Philippsen, and J.R. Pringle. 1998. Additional modules for versatile and economical PCR-based gene deletion and modification in Saccharomyces cerevisiae. *Yeast*. doi:10.1002/(SICI)1097-0061(199807)14:10<953::AID-YEA293>3.0.CO;2-U.

Marcus, S.L., M.R. Wenk, O. Steele-Mortimer, and B.B. Finlay. 2001. A synaptojanin-homologous region of Salmonella typhimurium SigD is essential for inositol phosphatase activity and Akt activation. *FEBS Lett.* doi:10.1016/S0014-5793(01)02356-0.

Matveeva, E.A., S.W. Whiteheart, T.C. Vanaman, and J.T. Slevin. 2001. Phosphorylation of the N-Ethylmaleimide-sensitive Factor Is Associated with Depolarization-dependent Neurotransmitter Release from Synaptosomes. *J. Biol. Chem.* doi:10.1074/jbc.M007394200.

Mayer, A., D. Scheglmann, S. Dove, A. Glatz, W. Wickner, and A. Haas. 2000. Phosphatidylinositol 4,5-Bisphosphate Regulates Two Steps of Homotypic Vacuole Fusion. *Mol. Biol. Cell*. doi:10.1091/mbc.11.3.807.

Mayer, A., and W. Wickner. 1997. Docking of yeast vacuoles is catalyzed by the ras-like GTPase Ypt7p after symmetric priming by Sec18p (NSF). *J. Cell Biol.* doi:10.1083/jcb.136.2.307.

Mayer, A., W. Wickner, and A. Haas. 1996. Sec18p (NSF)-driven release of Sec17p (α-SNAP) can precede docking and fusion of yeast vacuoles. *Cell*. doi:10.1016/S0092-8674(00)81084-3.

Meier, K.E., K.C. Gause, a E. Wisehart-Johnson, a C. Gore, E.L. Finley, L.G. Jones, C.D. Bradshaw, a F. McNair, and K.M. Ella. 1998. Effects of propranolol on phosphatidate phosphohydrolase and mitogen-activated protein kinase activities in A7r5 vascular smooth

muscle cells. *Cell. Signal.*

Merz, A.J., and W.T. Wickner. 2004a. Trans-SNARE interactions elicit Ca2+ efflux from the yeast vacuole lumen. *J. Cell Biol.* doi:10.1083/jcb.200310105.

Merz, A.J., and W.T. Wickner. 2004b. Resolution of organelle docking and fusion kinetics in a cell-free assay. *Proc. Natl. Acad. Sci. U. S. A.* doi:10.1073/pnas.0404583101.

Miller, D.J., A. Jerga, C.O. Rock, and S.W. White. 2008. Analysis of the Staphylococcus aureus DgkB Structure Reveals a Common Catalytic Mechanism for the Soluble Diacylglycerol Kinases. *Structure*. doi:10.1016/j.str.2008.03.019.

Miner, G.E., M.L. Starr, L.R. Hurst, R.P. Sparks, M. Padolina, and R.A. Fratti. 2016. The central polybasic region of the soluble snare (soluble n-ethylmaleimide-sensitive factor attachment protein receptor) Vam7 affects binding to phosphatidylinositol 3-phosphate by the PX (Phox Homology) domain. *J. Biol. Chem.* doi:10.1074/jbc.M116.725366.

Nakanishi, H., M. Morishita, C.L. Schwartz, A. Coluccio, J. Engebrecht, and A.M. Neiman. 2006. Phospholipase D and the SNARE Sso1p are necessary for vesicle fusion during sporulation in yeast. *J. Cell Sci.* doi:10.1242/jcs.02841.

Nichols, B.J., C. Ungermann, H.R.B. Pelham, W.T. Wickner, and A. Haas. 1997. Homotypic vacuolar fusion mediated by t- and v-SNAREs. *Nature*. doi:10.1038/387199a0.

Piper, R.C., N.J. Bryant, and T.H. Stevens. 1997. The membrane protein alkaline phosphatase is delivered to the vacuole by a route that is distinct from the VPS-dependent pathway. *J. Cell Biol.* doi:10.1083/jcb.138.3.531.

Qiu, Q.-S., and R.A. Fratti. 2010. The Na+/H+ exchanger Nhx1p regulates the initiation of Saccharomyces cerevisiae vacuole fusion. *J. Cell Sci.* doi:10.1242/jcs.067637.

Reese, C., and A. Mayer. 2005. Transition from hemifusion to pore opening is rate limiting for

vacuole membrane fusion. *J. Cell Biol.* doi:10.1083/jcb.200510018.

Rosenthal, J.A., H. Chen, V.I. Slepnev, L. Pellegrini, A.E. Salcini, P.P. Di Fiore, and P. De Camilli. 1999. The epsins define a family of proteins that interact with components of the clathrin coat and contain a new protein module. *J. Biol. Chem.* doi:10.1074/jbc.274.48.33959.

Sánchez-Migallón, M.P., F.J. Aranda, and J.C. Gómez-Fernández. 1995. The dissimilar effect of diacylglycerols on Ca(2+)-induced phosphatidylserine vesicle fusion. *Biophys. J.* 68:558–66. doi:10.1016/S0006-3495(95)80217-1.

Sasser, T., Q.S. Qiu, S. Karunakaran, M. Padolina, A. Reyes, B. Flood, S. Smith, C. Gonzales, and R.A. Fratti. 2012a. Yeast lipin 1 orthologue Pah1p regulates vacuole homeostasis and membrane fusion. *J. Biol. Chem.* doi:10.1074/jbc.M111.317420.

Sasser, T.L., M. Padolina, and R.A. Fratti. 2012b. The yeast vacuolar ABC transporter Ybt1p regulates membrane fusion through Ca^{2+} transport modulation. *Biochem. J.* doi:10.1042/BJ20120847.

Seals, D.F., G. Eitzen, N. Margolis, W.T. Wickner, and A. Price. 2000. A Ypt/Rab effector complex containing the Sec1 homolog Vps33p is required for homotypic vacuole fusion. *Proc. Natl. Acad. Sci.* doi:10.1073/pnas.97.17.9402.

Seddon, J.M. 1990. An Inverse Face-Centered Cubic Phase Formed by Diacylglycerol-Phosphatidylcholine Mixtures. *Biochemistry*. doi:10.1021/bi00486a031.

Slusarewicz, P., Z. Xu, K. Seefeld, A. Haas, and W.T. Wickner. 1997. I2B is a small cytosolic protein that participates in vacuole fusion. *Proc. Natl. Acad. Sci. U. S. A.* doi:10.1073/pnas.94.11.5582.

Sorin, A., G. Rosas, and R. Rao. 1997. PMR1, a Ca2+-ATPase in yeast Golgi, has properties

distinct from sarco/endoplasmic reticulum and plasma membrane calcium pumps. *J. Biol. Chem.* doi:10.1074/jbc.272.15.9895.

Speight, P., and M. Silverman. 2005. Diacylglycerol-activated Hmunc13 serves as an effector of the GTPase Rab34. *Traffic*. doi:10.1111/j.1600-0854.2005.00321.x.

Stahelin, R. V, M. a Digman, M. Medkova, B. Ananthanarayanan, J.D. Rafter, H.R. Melowic, and W. Cho. 2004. Mechanism of diacylglycerol-induced membrane targeting and activation of protein kinase Cdelta. *J. Biol. Chem.* doi:10.1074/jbc.M403191200.

Starai, V.J., Y. Jun, and W. Wickner. 2007. Excess vacuolar SNAREs drive lysis and Rab bypass fusion. *Proc. Natl. Acad. Sci.* doi:10.1073/pnas.0704741104.

Stenmark, H. 2009. Rab GTPases as coordinators of vesicle traffic. *Nat. Rev. Mol. Cell Biol.* doi:10.1038/nrm2728.

Stroupe, C., K.M. Collins, R.A. Fratti, and W. Wickner. 2006. Purification of active HOPS complex reveals its affinities for phosphoinositides and the SNARE Vam7p. *EMBO J.* doi:10.1038/sj.emboj.7601051.

Taylor, G.S., T. Maehama, and J.E. Dixon. 2000. Myotubularin, a protein tyrosine phosphatase mutated in myotubular myopathy, dephosphorylates the lipid second messenger, phosphatidylinositol 3-phosphate. *Proc. Natl. Acad. Sci. U. S. A.* doi:10.1073/pnas.160255697.

Ungermann, C., B.J. Nichols, H.R.B. Pelham, and W. Wickner. 1998. A vacuolar v-t-SNARE complex, the predominant form in vivo and on isolated vacuoles, is disassembled and activated for docking and fusion. *J. Cell Biol.* doi:10.1083/jcb.140.1.61.

Vicogne, J., D. Vollenweider, J.R. Smith, P. Huang, M.A. Frohman, and J.E. Pessin. 2006. Asymmetric phospholipid distribution drives in vitro reconstituted SNARE-dependent

membrane fusion. *Proc. Natl. Acad. Sci. U. S. A.* doi:10.1073/pnas.0606881103.

Vida, T.A., and S.D. Emr. 1995. A new vital stain for visualizing vacuolar membrane dynamics and endocytosis in yeast. *J. Cell Biol.* doi:10.1083/jcb.128.5.779.

Villar, A. V., A. Alonso, and F.M. Goni. 2000. Leaky vesicle fusion induced by phosphatidylinositol-specific phospholipase C: Observation of mixing of vesicular inner monolayers. *Biochemistry*. doi:10.1021/bi992515c.

Wach, A., A. Brachat, C. Alberti-Segui, C. Rebischung, and P. Philippsen. 1997. Heterologous HIS3 marker and GFP reporter modules for PCR-targeting in Saccharomyces cerevisiae. *Yeast*. doi:10.1002/(SICI)1097-0061(19970915)13:11<1065::AID-YEA159>3.0.CO;2-K.

Waksman, M., Y. Eli, M. Liscovitch, and J.E. Gerst. 1996. Identification and characterization of a gene encoding phospholipase D activity in yeast. *J. Biol. Chem.* doi:10.1074/JBC.271.5.2361.

Wang, C.W., P.E. Stromhaug, E.J. Kauffman, L.S. Weisman, and D.J. Klionsky. 2003a. Yeast homotypic vacuole fusion requires the Ccz1-Mon1 complex during the tethering/docking stage. *J. Cell Biol.* doi:10.1083/jcb.200308071.

Wang, L., A.J. Merz, K.M. Collins, and W. Wickner. 2003b. Hierarchy of protein assembly at the vertex ring domain for yeast vacuole docking and fusion. *J. Cell Biol.* doi:10.1083/jcb.200209095.

Wang, L., E.S. Seeley, W. Wickner, and A.J. Merz. 2002. Vacuole fusion at a ring of vertex docking sites leaves membrane fragments within the organelle. *Cell*. doi:10.1016/S0092-8674(02)00632-3.

Wickner, W. 2010. Membrane Fusion: Five Lipids, Four SNAREs, Three Chaperones, Two Nucleotides, and a Rab, All Dancing in a Ring on Yeast Vacuoles. *Annu. Rev. Cell Dev.*

Biol. doi:10.1146/annurev-cellbio-100109-104131.

Wolinski, H., H.F. Hofbauer, K. Hellauer, A. Cristobal-Sarramian, D. Kolb, M. Radulovic, O.L. Knittelfelder, G.N. Rechberger, and S.D. Kohlwein. 2015. Seipin is involved in the regulation of phosphatidic acid metabolism at a subdomain of the nuclear envelope in yeast. *Biochim. Biophys. Acta - Mol. Cell Biol. Lipids*. doi:10.1016/j.bbalip.2015.08.003.

CHAPTER 5: GENERAL DISCUSSION

All eukaryotes utilize SNARE dependent membrane fusion to traffic cargo between organelles. The membrane fusion process is cyclic, so once it has occurred it can repeat to allow for additional cargo transport and delivery. Fusion occurs across the well-defined stages of priming, tethering, docking, and fusion. The process has been studied for decades and many of its key players have been thoroughly classified. However, studies have mostly focused on the protein machinery involved in fusion. It is now clear membrane lipids also serve important roles across the fusion stages and are now receiving more attention. In the research including in this dissertation, I have presented evidence of fusion regulation by the membrane lipids diacylglycerol (DAG) and phosphatidic acid (PA). In this work, the following have been shown: (i) increased diacylglycerol levels at the vacuole membrane increases fusion; (ii) phosphatidic acid regulates the activation of *cis*-SNAREs by the SNARE chaperone Sec18; (iii) phosphatidic acid binding to Sec18 affects the protein's overall architecture.

Dgk1 is a negative regulator of vacuole fusion

In Chapter 4, we found that Dgk1 is a negative regulator of vacuole fusion. Deletion of Dgk1 led to a significant increase in measured fusion which interestingly appeared to be independent of the rate of fusion. Inhibition of vacuoles lacking Dgk1 with a panel of traditional inhibitors showed that the increased fusion is still blocked and fusion still proceeds through the known, canonical pathway. However, a shift in sensitivity to fusion inhibition was observed with *dgk1*Δ vacuoles when dioctanoyl-PA (diC8-PA) or inhibitors against the Rab Ypt7 were used. When Dgk1 was removed from vacuoles, membrane levels of the regulatory lipid DAG were confirmed to be

increased. Furthermore, addition of exogenous DAG to wild type vacuoles increased their levels of fusion. These results taken together suggest that DAG directly promotes vacuole fusion. This is not surprising as DAG has previously been shown to be a fusogenic lipid that localizes to the vacuole vertex domain immediately before the final fusion stage occurs (Jun et al., 2004; Fratti et al., 2004). DAG is also a neutral lipid that supports non-bilayer structure formation in membranes which is a required component for membrane compartments to completely fuse (Zick et al., 2014). It is also not unexpected that *dgk1*Δ vacuoles have decreased sensitivity to addition of exogenous diC8-PA since they should contain decreased levels of endogenous membrane PA. What is more surprising is the decreased sensitivity to Ypt7 inhibitors that *dgk1*Δ vacuoles show. This shift seen could be for two distinct reasons. First, increased membrane DAG could promote increased activation of Ypt7. Second, increased membrane DAG could decrease the requirement for Ypt7 in the vacuole fusion process.

Activation of Ypt7 is dependent on the nucleotide exchange factor Mon1-Ccz1 (Nordmann et al., 2010). This activation is required for Ypt7 to facilitate tethering of vacuoles. It is known that the Mon1-Ccz1 complex relies on the regulatory lipid phosphatidylinositol 3-phosphate (PI3P) for its association with vacuole membranes. Our work with *dgk1*Δ vacuoles suggests that increased DAG, or perhaps decreased PA, at the vacuole may influence the activity of Mon1-Ccz1. Activation of Ypt7 by Mon1-Ccz1 is stimulated by some anionic lipid species including PI3P and phosphatidylserine (PS), however this activity has not been measured on membranes containing PA (Cabrera et al., 2014). It is possible that PA interferes with a specific activation of Mon1-Ccz1 activity by PI3P at the vacuole vertex ring. Future work utilizing reconstituted proteolipsomes

(RPLs) could isolate the effects specific lipids have on Mon1-Ccz1 activity and thus the downstream tethering activity of Ypt7.

The primary function of Ypt7 is to tether vacuoles via associations with the homotypic vacuole fusion and protein sorting (HOPS) complex (Hickey et al., 2009). Interestingly, HOPS alone can tether two membranes and is considered the primary agent in tethering (Hickey and Wickner, 2010). Furthermore, HOPS can carry out tethering via associations with acidic lipids even in the absence of Ypt7 (Orr et al., 2015). On *dgk1*Δ vacuoles we expect a decrease in PA and a corresponding increase in DAG. PA is an acidic lipid so it is possible the effect we saw in Chapter 4 was due to a decrease in HOPS-PA interactions. Decreased HOPS-PA interactions could lead to an increase in Ypt7-HOPS complexes formed which could decrease sensitivity to Ypt7 inhibitors. This model, however, does not adequately explain why *dgk1*Δ vacuoles have higher fusion than wild type in the absence of all inhibitors. It seems more likely that a decrease in sensitivity to Ypt7 inhibition would be due to an increase in Ypt7 effectiveness. Ypt7 is lipid anchored to vacuole membranes when in its active state (Seabra, 1998; Vetter and Wittinghofer, 2001). The increased DAG levels in *dgk1*Δ vacuole membranes may alter membrane fluidity which could affect Ypt7 activity via its prenylation anchor. Future work addressing this possibility using RPLs could isolate the potential effects membrane lipid dynamics have on lipid anchored protein function.

Phosphatidic acid regulates the priming stage of vacuole fusion

In Chapter 2, we showed that the regulatory lipid PA blocks Sec18 activity on inactive SNAREs during the priming stage of vacuole fusion. Sec18 was shown to be a PA binding protein, and higher levels of PA at the vacuole led to decreased priming. We proposed that this may be due to

a decrease in the mobility of PA-bound Sec18 which was not effectively recruited to *cis*-SNAREs. The fact that Sec18 directly interacted with PA was not unexpected since previous work had shown that mammalian NSF, its homologue, is a PA-binding protein (Manifava et al., 2001). What is perhaps less intuitive is the fact that PA inhibits a stage in the fusion cascade. Previous studies had shown that PA is a required lipid for vacuole fusion to occur (Mima and Wickner, 2009). Why then would it completely block the necessary function of a chaperone whose activity is required for the appropriate progression of fusion? We did not isolate the exact function of PA in the work presented in Chapter 2, but our observations combined with previous work suggest that PA may be preventing Sec18 from being too active. The well-known primary role of Sec18 is to reactivate inactive SNAREs after they have been used in a round of fusion. A secondary role of Sec18 that has more recently been explored is one that prevents SNAREs from pairing incorrectly. When SNAREs form *trans*-complexes, occasionally they do not properly associate and are blocked by chaperone proteins (Starai et al., 2008). Sec17 and Sec18 are recruited to these inactive SNAREs, during docking, to reactivate them. However, if this step becomes unregulated or occurs in the presence of excess Sec18, all SNARE complexes are disassembled whether active or inactive and fusion cannot proceed (Ungermann et al., 1998; Rohde et al., 2003; Mima et al., 2008; Stroupe et al., 2009). In the cell, this proofreading process is tightly controlled by Vps33, a subunit of the HOPS complex (Lobingier et al., 2014; Schwartz et al., 2017). HOPS assists with the tethering of vacuoles in a Ypt7 dependent manner while also preventing Sec18 association with active, properly formed *trans*-SNARE complexes during docking. Taken together, our work combined with that from other labs suggests PA at the vacuole membrane may temporally regulate Sec18.

Our most current model suggests that Sec18 exists on the membrane in an inactive PA-bound state which may be the result of a PA-dependent membrane recruitment step. When inactive *cis*-SNAREs form, PA is largely converted to DAG by Pah1, and Sec18 transitions from a PA-bound state to a SNARE-bound state where it carries out its priming function. After priming, Sec18 is either inactivated by an increase in membrane PA levels or by a release from the membrane. During docking, Sec18 is recruited back to the membrane in a PA dependent manner where its activity is suppressed by PA and Vps33 until HOPS dissociation and priming-associated Pah1 activity. This model could be addressed in future experiments using RPLs. By varying PA levels in RPLs, Sec18 membrane association, Sec18 recruitment to SNAREs, and overall fusion can all be tested with an exclusive dependence on change in PA levels.. This could highlight whether PA acts alone in the regulation we have described, or if it works in concert with another fusion factor found at the vacuole. Experiments could also test whether *cis*-SNAREs act as an activator for Pah1 activity. Additionally, future work describing the effect PA binding has on Sec18 architecture could elucidate some of the finer mechanistic details of this regulation (discussed below).

Phosphatidic acid binding alters the architecture of Sec18

In Chapter 2, we showed regulation of the SNARE chaperone Sec18 by the regulatory vacuole lipid PA. This regulation was shown at the organelle level rather than at the protein level. To further describe how PA may regulate the priming stage of vacuole fusion we wanted to also address its specific effects on the structure of Sec18. In Chapter 3, we show that PA binding to Sec18 significantly alters the protein's conformation and this effect may prevent hexamerization of Sec18 to its active state. These results are in line with our previous data that showed Sec18 recruitment is decreased when PA levels at the vacuole membrane are increased. When Sec18, or

its mammalian homolog NSF, binds to inactive SNAREs, it does so as a homohexamer (Fleming et al., 1998). Our most recent data suggests that formation of the Sec18 hexamer is blocked by PA which locks the protein in a conformation that shields key residues necessary for hexamerization. This data provides an additional level of detail to our current model. While it still appears that increased PA levels block Sec18 recruitment to *cis*-SNAREs, we believe it may do so by stabilizing an inactive monomeric state of the protein. Moving forward it would be beneficial to acquire structural data of Sec18 in a PA-bound state. In the past, this would have been impossible to achieve as the Sec18 hexamer is very large. However, with the recent increase in electron cryomicroscopy capabilities, structural information about many larger proteins has been gained. This includes the structure of the Sec18 homolog NSF (Zhao et al., 2015). Future work will be aimed at solving a Sec18-PA structure to gain even greater detail of the mechanism of PA regulation of Sec18 at the vacuole.

Summary

The research included in this dissertation provides evidence of previously undiscovered lipid regulation of the stages of vacuole fusion. Evidence is provided for the regulation of Ypt7-dependent tethering by DAG or PA levels in the membrane. Extensive work looking at the effects of PA at the vacuole suggests a regulatory mechanism in which PA specifically regulates Sec18 priming activity at the vacuole by decreasing its association with *cis*-SNAREs. This regulation of Sec18 by PA appears to be through a direct interaction that alters the overall architecture of the protein. Questions remain including the effects other lipids or lipid modifications may have on the different stages of fusion. This work provides a baseline level of understanding and approach

which can be added to and utilized for further understanding of the roles regulatory lipids play in mediating yeast vacuole fusion.

REFERENCES

Cabrera, M., M. Nordmann, A. Perz, D. Schmedt, A. Gerondopoulos, F. Barr, J. Piehler, S. Engelbrecht-Vandre, and C. Ungermann. 2014. The Mon1-Ccz1 GEF activates the Rab7 GTPase Ypt7 via a longin-fold-Rab interface and association with PI3P-positive membranes. *J. Cell Sci.* doi:10.1242/jcs.140921.

Fleming, K.G., T.M. Hohl, R.C. Yu, S. a Müller, B. Wolpensinger, a Engel, H. Engelhardt, a T. Brünger, T.H. Söllner, and P.I. Hanson. 1998. A revised model for the oligomeric state of the N-ethylmaleimide-sensitive fusion protein, NSF. *J. Biol. Chem.* doi:10.1074/jbc.273.25.15675.

Fratti, R.A., Y. Jun, A.J. Merz, N. Margolis, W. Wickner, and B. Wickner. 2004. Interdependent assembly of specific regulatory lipids and membrane fusion proteins into the vertex ring domain of docked vacuoles. *J. Cell Biol.* doi:10.1083/jcb.200409068.

Hickey, C.M., C. Stroupe, and W. Wickner. 2009. The major role of the Rab Ypt7p in vacuole fusion is supporting HOPS membrane association. *J. Biol. Chem.* doi:10.1074/jbc.M109.000737.

Hickey, C.M., and W. Wickner. 2010. HOPS Initiates Vacuole Docking by Tethering Membranes before trans-SNARE Complex Assembly. *Mol. Biol. Cell*. doi:10.1091/mbc.E10-01-0044.

Jun, Y., R.A. Fratti, and W. Wickner. 2004. Diacylglycerol and its formation by phospholipase C regulate Rab- and SNARE-dependent yeast vacuole fusion. *J. Biol. Chem.* doi:10.1074/jbc.M411363200.

Lobingier, B.T., D.P. Nickerson, S.Y. Lo, and A.J. Merz. 2014. SM proteins Sly1 and Vps33 co-

assemble with Sec17 and SNARE complexes to oppose SNARE disassembly by Sec18. *Elife*. doi:10.7554/eLife.02272.

Manifava, M., J.W.J.F. Thuring, Z.Y. Lim, L. Packman, A.B. Holmes, and N.T. Ktistakis. 2001. Differential Binding of Traffic-related Proteins to Phosphatidic Acid- or Phosphatidylinositol (4,5)-Bisphosphate-coupled Affinity Reagents. *J. Biol. Chem.* doi:10.1074/jbc.M010308200.

Mima, J., C.M. Hickey, H. Xu, Y. Jun, and W. Wickner. 2008. Reconstituted membrane fusion requires regulatory lipids, SNAREs and synergistic SNARE chaperones. *EMBO J.* doi:10.1038/emboj.2008.139.

Mima, J., and W. Wickner. 2009. Complex lipid requirements for SNARE-and SNARE chaperone-dependent membrane fusion. *J. Biol. Chem.* doi:10.1074/jbc.M109.010223.

Nordmann, M., M. Cabrera, A. Perz, C. Bröcker, C. Ostrowicz, S. Engelbrecht-Vandré, and C. Ungermann. 2010. The Mon1-Ccz1 complex is the GEF of the late endosomal Rab7 homolog Ypt7. *Curr. Biol.* doi:10.1016/j.cub.2010.08.002.

Orr, A., W. Wickner, S.F. Rusin, A.N. Kettenbach, and M. Zick. 2015. Yeast vacuolar HOPS, regulated by its kinase, exploits affinities for acidic lipids and Rab:GTP for membrane binding and to catalyze tethering and fusion. *Mol. Biol. Cell*. doi:10.1091/mbc.E14-08-1298.

Rohde, J., L. Dietrich, D. Langosch, and C. Ungermann. 2003. The transmembrane domain of Vam3 affects the composition of cis- and trans-SNARE complexes to promote homotypic vacuole fusion. *J. Biol. Chem.* doi:10.1074/jbc.M209522200.

Schwartz, M.L., D.P. Nickerson, B.T. Lobingier, R.L. Plemel, M. Duan, C.G. Angers, M. Zick, and A.J. Merz. 2017. Sec17 (α-SNAP) and an SM-tethering complex regulate the outcome

of SNARE zippering in vitro and in vivo. *Elife*. doi:10.7554/eLife.27396.

Seabra, M.C. 1998. Membrane association and targeting of prenylated Ras-like GTPases. *Cell. Signal.* doi:10.1016/S0898-6568(97)00120-4.

Starai, V.J., C.M. Hickey, and W. Wickner. 2008. HOPS Proofreads the trans-SNARE Complex for Yeast Vacuole Fusion. *Mol. Biol. Cell*. doi:10.1091/mbc.E08-01-0077.

Stroupe, C., C.M. Hickey, J. Mima, A.S. Burfeind, and W. Wickner. 2009. Minimal membrane docking requirements revealed by reconstitution of Rab GTPase-dependent membrane fusion from purified components. *Proc. Natl. Acad. Sci.* doi:10.1073/pnas.0903801106.

Ungermann, C., K. Sato, and W. Wickner. 1998. Defining the functions of trans-SNARE pairs. *Nature*. doi:10.1038/25069.

Vetter, I.R., and A. Wittinghofer. 2001. The guanine nucleotide-binding switch in three dimensions. *Science (80-.).* doi:10.1126/science.1062023.

Zhao, M., S. Wu, Q. Zhou, S. Vivona, D.J. Cipriano, Y. Cheng, and A.T. Brunger. 2015. Mechanistic insights into the recycling machine of the SNARE complex. *Nature*. doi:10.1038/nature14148.

Zick, M., C. Stroupe, A. Orr, D. Douville, and W.T. Wickner. 2014. Membranes linked by trans-SNARE complexes require lipids prone to non-bilayer structure for progression to fusion. *Elife*. doi:10.7554/eLife.01879.